uOttawa

L'Université canadienne
Canada's university

Poly(Sodium Acrylate)-Based Antibacterial Nanocomposite Materials

Samaneh Khanlari

Thesis submitted to the
Faculty of Graduate and Postdoctoral Studies
in partial fulfillment of the requirements
for the degree of

Doctorate in Philosophy in
Chemical Engineering

Department of Chemical and Biological Engineering

Faculty of Engineering

UNIVERSITY OF OTTAWA

Abstract

Polymer-based bioadhesives for sutureless surgery provide a promising alternative to conventional suturing. In this project, a new poly(sodium acrylate)-based nanocomposite with antibacterial properties was developed.

Poly(sodium acrylate), was prepared using a redox solution polymerization at room temperature; this polymer served as a basis for a nanocomposite bioadhesive material using silver nanoparticles. In-situ polymerization was chosen as a nanocomposite synthesizing method and three methods were applied to quantify the distribution and loadings of nanofiller in the polymer matrices. These included the Voronoi Diagram, Euclidean Minimum Spanning Tree (EMST) method and pixel counting. Results showed that pixel counting combined with the EMST method would be most appropriate for nanocomposite morphology quantification.

Real-time monitoring of the in-situ polymerization of poly(sodium acrylate)-based nanocomposite was investigated using in-line Attenuated Total Reflectance/Fourier Transform infrared (ATR-FTIR) technique. The ATR-FTIR spectroscopy method was shown to be valid in reaction conversion monitoring using a partial least squares (PLS) multivariate calibration method and the results were consistent with the data from off-line water removal gravimetric monitoring technique.

Finally, a second, more degradable polymer (i.e., gelatin and poly(vinyl alcohol)) was used to modify the degradation rate and hydrophilicity of the nanocomposite bioadhesive. Biodegradation, cytotoxicity and antibacterial activity of the synthesized nanocomposites were examined as well as the adhesion strength of the nanocomposite bioadhesives. Results showed that the nanocomposites are fairly biocompatible and possess excellent antibacterial properties to make them suitable for out-clinic surgeries such as may be necessary in the aftermath of natural disasters.

In conclusion this was the first biocompatible biodegradable antibacterial nanocomposite bioadhesive synthesized. It is expected that in the future, they may serve as a substitute for well-known sutures especially in out-clinic first aids.

Résumé

Les bioadhésifs à base de polymères pour la chirurgie de suture fournissent une alternative prometteuse à la suture conventionnelle. Dans ce projet, un nouveau matériel nano composé à base de poly(acrylate de sodium) avec des propriétés antibactériennes a été développé.

Le poly(acrylate de sodium) a été préparé en utilisant une polymérisation en solution par initiation réduction-oxidation à température ambiante; ce polymère a servi de base pour un matériel nano composé bioadhésif en utilisant des nanoparticules d'argent. La polymérisation en situ a été choisie comme méthode de synthèse de matériaux nano composés et trois méthodes ont été appliquées pour quantifier la répartition des nano matériaux dans des matrices de polymères. Il sagit notamment du diagramme de Voronoï, la méthode Euclidian Minimum Spanning Tree (EMST) et comptage de pixels. Les résultats ont démontré que le comptage de pixels combiné avec la méthode d'EMST serait le plus approprié pour la quantification de la morphologie des matériaux nano composés.

La surveillance en temps réel, en ligne, de la polymérisation en situ de nano composé à base de poly(acrylate de sodium) a été étudiée à l'aide d'une technique en ligne de réflectance totale atténuée Transforme de Fourier infrarouge (ATR-FTIR). La méthode de la spectroscopie ATR-FTIR s'est avérée valable pour la surveillance de la conversion de la réaction.

Enfin, un second polymère, et plus dégradable (par exemple, la gélatine et le poly(alcool vinylique)) a été utilisé pour modifier la vitesse de dégradation et l'hydrophilie du bioadhésif nano composé. La biodégradation, la cytotoxicité et l'activité antibactérienne des matériaux nano composés synthétisés ont été examinées, ainsi que la force d'adhérence des bioadhésifs. Les résultats ont démontré que les matériaux nano composés sont assez biocompatibles et possèdent d'excellentes propriétés antibactériennes pour les rendres aptes pour les chirurgies hors clinique comme cela peut être nécessaire à la suite de catastrophes naturelles.

En conclusion nous avons synthétisé le premier bioadhésif nano composé biodégradable et biocompatible antibactérien. Il est prévu que dans l'avenir, ces

bioadhésifs pourront servir de substitut pour les sutures bien connus en particulier dans les premières aides-clinique.

To My Parents,

who were my first teachers,

and being their daughter was my first honour:

My mother for her unconditional, everlasting love and encouragement

and

My father for his belief in me and endless support.

Statement of Contributions of Collaborators

I hereby declare that I am the sole author of this thesis. I performed all polymerization and nanocomposite synthesis experiments, polymer and nanocomposite characterization and data analysis unless otherwise indicated. Dr. Jian Tang assisted with the biocompatibility (MTT) test, Ms. Tara Kelly operated the x-ray diffractometer, Dr. Yun Liu operated the scanning electron microscope and Mr. Amin Gheibi assisted with the image processing methods and associated Matlab coding.

My thesis supervisor, Prof. Marc A. Dubé, provided me with an excellent collaboration throughout this work with discussions, support and editorial comments for all of my written work.

Samaneh Khanlari _____ 2015

Acknowledgments

I would first like to acknowledge my supervisor, Dr. Marc A. Dubé, for allowing me to work on this project, and for his guidance, mentorship, and his continuous support over the duration of my doctoral studies. I have learnt so much as a result of this wonderful experience that led me to achieve this paramount achievement of my life.

I am indebted to a number of people who provided immense help throughout this project. I would like to acknowledge with gratitude Stéphane Roberge, Louis Tremblay and Dr. Esther Trevino for invaluable training and technical advice.

I am grateful to all of the friends I have met during my graduate studies who provided me with both research insight and light-hearted relief.

Finally, I would like to thank my parents who constantly inspired and humbled me with their unwavering patience, kindness, wisdom, and my siblings for their encouragement, love and joy throughout my life. My special thanks go to my dear husband, for his love, devotion, support and scientific discussions.

Samaneh Khanlari

February 2015

Table of Contents

List of Figures

Chapter 2

Chapter 3

Chapter 4

Chapter 5

Chapter 6

Chapter 7

Chapter 8

List of Tables

Chapter 2

Chapter 3

Chapter 4

Chapter 5

Chapter 6

Chapter 7

Appendices

Nomenclature

Ge	Gelatin
g	Gram/ grams
h	Hour/ hours
T_g	Glass to rubber transition [ºC]
KDS	Potassium disulfite
$\bar{M}_n$	Number average molecular weight[g mol^{-1}]
$\bar{M}_w$	Weight average molecular weight [g mol^{-1}]
NaA	Sodium acrylate
NaOH	Sodium hydroxide
pH	-Log[H^+]
PNaA	Poly(sodium acrylate)
T	Temperature [ºC]
t	Time
x	Conversion [mol. %]

List of Abbreviations

AA	Acrylic acid
AAm	Acrylamide
AAP	Acetaminophen
AFM	Atomic force microscopy
AMP	Aminopyrine
APS	Ammonium persulfate
ATR-FTIR	Attenuated total reflection-fourier transform infrared
BMA	Butyl methacrylate
CAGR	Compound annual growth rate
CLD	Crosslink density
DDW	Distilled deionized water
DEAP	Diethoxyacetophenone
DSC	Differential scanning calorimetry
EA	Ethyl acrylate
EG	Ethylene glycol
EGDMA	Ethylene glycol dimethacrylate
ELP	Elastin-like polypeptide
EMST	Euclidean minimum spanning tree
GPC	Gel permeation chromatography
HA	Hydroxy apatite
HIV	Human immunodeficiency virus
HPMCAM	Hydroxypropyl methylcellulose acetate maleate
HT	Hydrotalcite
IPN	Interpenetrating polymer network
LB	Lysogeny broth
MAA	Methacrylic acid
MMA	Methyl methacrylate
NIPAAm	N-isopropylacrylamide
NC	Nanoclay

NS	Nanosilver
OD	Optical density
PAA	Poly(acrylic acid)
PAE	Poly(β-amino ester)
PBS	Phosphate buffer saline
PCL	Poly(caprolactone)
PDI	Poly dispersity index
PEG	Poly(ethylene glycol)
PEO	Poly(ethylene oxide)
PLGA	Poly(lactic-*co*-glycolic acid)
PLS	Partial least squares
PRESS	Predicted residual error sum of squares
PSA	Presser sensitive adhesives
PVA	Poly(vinyl alcohol)
PVP	Poly(vinyl pyrrolidone)
RMSEC	Root mean squared error of calibration
SD	Standard deviation
SEM	Scanning electron microscopy
TEM	Transmission electron microscopy
UV	Ultraviolet
VCA	Video contact angle
XRD	X-ray diffraction

Chapter 1: Introduction

1.1 Project Background

Natural disasters typically result in a hazard overwhelming a highly vulnerable community, leading to high levels of injury, disease and mortality. Even the most developed countries are vulnerable to natural disasters, such as Hurricane Katrina in the United States in 2005 and the Great Eastern Japan Earthquake and tsunami in 2011. Global population growth, poverty, land shortages and urbanization in many countries have increased the number of people living in areas prone to natural disasters and this multiplies the impact on public health [1]. Over the past decades, the incidence and magnitude of natural disasters has grown and over 300 natural disasters occur yearly around the world, affecting millions and costing billions of dollars[2]. Natural catastrophes can lead to outbreaks of infectious disease aside from damaging and destroying infrastructure[3]. In such instances, immediate surgery may not be possible and alternatives to suturing to join damaged tissues that ensure prevention of infection and encourage healing are needed. Materials such as polymeric bioadhesives are well suited for such cases [4]. Although suturing remains the most common method for closing wounds, topical skin adhesives are increasingly being used by health professionals to replace sutures, staples and adhesive strips in the fields of trauma, plastic and other surgeries, emergency medicine and pediatrics [5].

Bioadhesion may be defined as the state in which two materials, at least one of which is biological in nature, are held together for extended periods of time by interfacial forces [6, 7] and it is used for many hard- and soft-tissue applications [8]. Bioadhesives

have some advantages compared with traditional suturing. They provide a needle-free method of wound closure and do not require local anesthetics. They can accomplish other tasks, such as haemostasis (i.e., cessation of bleeding) and the ability to seal air leakages. Another advantage of bioadhesives is the fact that they usually provide excellent cosmetic results [5, 9]. Tissue adhesives also present the potential to serve as drug delivery systems and can be engineered for slow, localized release of medications, such as pain treatment drugs, antibiotics, chemotherapy treatment or as a vehicle to growth factors and actual cell lines to assist in healing, namely, in poor healing tissues like cartilage [10]. Although the cost of tissue adhesives is higher than conventional sutures, follow-up visits for suture removal are not needed, reducing medical service time during the wound check visit [9].

Silver nanoparticles (nanosilver) are clusters of silver atoms that range in diameter from 1 to 100 nm, contain 20–15,000 silver atoms, and are attracting interest as long-term antibacterial, antimicrobial and antifungal agents for applications in medicine. No side effects or toxicity on human cells and tissues were observed when using biomaterials based on metallic nanosilver in clinical trials [11, 12]. Due to its strong antibacterial activity, nanosilver coatings are used on various textiles and as coatings on certain implants. Furthermore, nanosilver is used for the treatment of wounds and burns and is marketed as a water disinfectant and room spray. Nanosilver has shown accelerated burn healing[13]. Thus, in recent years, the use of nanosilver has become more widespread in medical and related applications [14], for example, in antimicrobial polypropylene (PP) based sutures[15], antibacterial chitin-based wound dressings[16], burn dressings[13], and bone cement[14].

The anti-microbial mechanism for nanosilver can be explained as follows: Generally, Ag^+ metal ions destroy or pass through the microorganism's membrane and bond to the −SH group of cellular enzymes. The consequent critical decrease of enzymatic activity causes the microorganisms' metabolism to change and inhibits their growth, up to the cell's death. The Ag^+ metal ions also catalyze the production of oxygen radicals that oxidize the molecular structure of bacteria. The antibacterial-antimicrobial-antifungal mechanism of silver nanoparticles has been attributed to the presence of water and oxygen. Elemental silver particles are released in the form of silver ions. The formation of active oxygen occurs according to the chemical reaction:

$$H_2O + \frac{1}{2}O_2 \xrightarrow{Silver\ Ions} H_2O_2 \rightarrow H_2O + (\dot{O}) \tag{1.1}$$

Such a mechanism does not need any direct contact between the anti-microbial agent and the bacteria, because the produced active oxygen (oxygen radical) diffuses from the nanocomposite to the surrounding environment. Therefore, the Ag^+ metal ions inhibit the multiplication of microorganisms. Bacteria are not permanently exposed to oxygen radicals and thus, the ionic additive does not seem to facilitate the selection of resistant strains [17].

Another mechanism for the antibacterial activity of nanosilver proposed by Kumar and Munstedt states that the silver cation, Ag^+, binds strongly to electron releasing groups in biological molecules containing sulfur, oxygen, or nitrogen, present in bacteria. This may result in defects of the cytoplasm membrane or its detachment from

the cell, and as a result, DNA molecules become condensed and lose their ability to replicate [18].

Li et al. observed that the surface of *Staphylococcus aureus* grown on a polymer membrane was smoother than that grown on polymer/nanosilver media [19]. This morphological change of bacterial growth implies that nanosilver may affect the structure of the bacterial membrane, thereby causing the defunctionalisation of the bacteria. Ni et al. demonstrated similar morphological results for bacteria exposed to polymeric materials containing $AgNO_3$ (0.12 mol/L)[19]. The purpose of using $AgNO_3$ rather than silver nanoparticles was to increase the compatibility between the phases as metallic silver is insoluble in water, but metallic salts such as silver nitrate ($AgNO_3$) and silver chloride (AgCl) are soluble in water [20].

Many different methods have been developed for the incorporation of silver nanoparticles into a polymer matrix. In one approach, the monomer is polymerized with metal ions (e.g., Ag^+, NO_3^-) introduced either before or after polymerization. These metal ions located in the polymer matrix are made to dissociate, either chemically, thermally, or by ultraviolet (UV) irradiation. The dissociated ions (e.g., Ag+), then agglomerate to form nanoparticles (e.g., nanosilver). In another approach, the metal nanoparticles (e.g., nanosilver) are synthesized first, and sometimes their surface is organically compatibilized. The nanoparticles are then dispersed into a polymer solution or monomer that is then polymerized [21]. In order to have a stable nanocomposite, both the metal nanoparticle and the polymer matrix must be compatible from the points of view of their polarity/non-polarity and hydrophobicity/hydrophilicity.

In this study, nanosilver was synthesized prior to addition to the monomer mixture and then polymerized (this is often referred to as in situ polymerization[11]).

1.2 Research Objectives

Commercially available bioadhesives normally do not exhibit antibacterial properties although products such as Dermabond™ provide a mechanical barrier to bacterial attack. The main objective for this project is to synthesize an antibacterial bioadhesive from a poly(sodium-acrylate)-based nanocomposite material using nanosilver. The hypotheses to be tested in order to achieve the main objective are shown below:

1. High conversion poly(sodium acrylate) can be synthesized via redox initiated solution polymerization to achieve a molecular weight appropriate for bioadhesion.
2. In-situ polymerization can be used to synthesize evenly distributed nanocomposites using nanosilver.
3. Degradation rate is tunable by IPN formation using a more degradable polymer as a second component.

In order to test these hypotheses, the following objectives were established:

Part 1: pH sensitivity of acrylic acid polymerization

To achieve the primary objective of this research, a screening study on sodium acrylate (NaA) redox solution polymerization was conducted using different extents of acrylic acid (AA) neutralization at similar experimental conditions. The knowledge obtained

served as a basis for the production of poly(sodium acrylate) (PNaA)-based nanocomposites.

Part 2: Nanofiller incorporation into the synthesized polymer and its effect on polymerization and product properties.

The synthesis of PNaA-based nanocomposites with different nanosilver loadings was studied. Different nanocomposite properties necessary for bioadhesive applications were tested.

Part 3: Nanocomposite homogeneity quantification.

Because of the importance of nanofiller distribution throughout the sample, three different quantitative methods were proposed to assess the homogeneity of nanofiller distribution quantitatively.

Part 4: IR monitoring of nanocomposite formation.

The use of on-line monitoring of the reaction progress (conversion) using attenuated total reflectance Fourier transform infrared (ATR-FTIR) spectroscopy was investigated. The results were compared to conversion data from an off-line water removal gravimetric method.

Part 5: Bioadhesive property studies.

The antibacterial properties and biocompatibility of the synthesized nanocomposites containing different nanofiller loadings were assessed. Degradation rate of the polymer

was tuned using an interpenetrating polymer network (IPN) approach. Finally, the adhesion strength of the nanocomposite bioadhesives was tested.

1.3 Thesis Structure

This thesis is divided into eight chapters which include the introduction (Chap. 1), a review on bioadhesives (Chap. 2), a concluding chapter (Chap. 8) and five chapters (3-7) representing each of the objectives outlined above. The reader will note that this thesis is presented as a series of journal articles; each of Chapters 2-7 corresponds to an independent publication that has been (or will be) submitted to a refereed scientific journal. With this in mind, the reader can expect to find some overlap in information in the introductory and experimental sections of the various chapters. The chapters are:

Chapter 2: Bioadhesives: A Review, S. Khanlari and M. A. Dubé, *Macromol. React. Eng.*, Volume 7, Issue 11, 573-587, 2013.

This chapter provides a comprehensive review on bioadhesives, bioadhesion mechanisms, bioadhesives used in sutureless surgery (tissue adhesives) and those used in drug delivery.

Chapter 3: Effect of pH on Poly(acrylic acid) Solution Polymerization, S. Khanlari and M. A. Dubé, *J. Macromol. Sci. – Pure Appl. Chem.*, Volume 52, Issue 8, 587-592, 2015.

This chapter presents the results of the redox solution polymerization of acrylic acid at different pH. The acrylic acid was neutralized to different extents by means of sodium

hydroxide solutions. The polymers synthesized at different pH were compared in terms of conversion, molecular weight and glass transition temperature (T_g). The result of this chapter was to identify a pH at which the polymer should be synthesized.

Chapter 4: *In situ* Poly(sodium acrylate)-based Nanocomposite Formation by Redox-Initiated Solution Polymerization, S. Khanlari and M. A. Dubé, *Polym. Eng. Sci.*, Volume 55, Issue 6, 1230–1236, 2015.

This chapter summarizes the results of experiments performed to synthesize and characterize the poly(sodium acrylate) nanocomposite polymer.

Chapter 5: Image Processing Techniques for Nanocomposite Distribution Quantification, S. Khanlari, A. Gheibi and M. A. Dubé (to be submitted).

The distribution of the nanoparticles in the polymer matrix will have important effects on the nanocomposite properties. In this chapter, three different quantitative methods are proposed to quantify the distribution of the nanoparticles in the polymer matrix.

Chapter 6: Reaction Monitoring of in-Situ Formation of Poly(sodium acrylate) Based Nanocomposites Using ATR-FTIR Spectroscopy, S. Khanlari and M. A. Dubé, *Ind. Eng. Chem. Res.*, Volume 54, 5598−5603, 2015.

The ability of on-line monitoring of monomer conversion for nanocomposite production was studied.

Chapter 7: Bioactivity of Nanocomposites synthesized as Bioadhesive, S. Khanlari, M.A. Dubé, J. Tang and K. Kirkwood (to be submitted).

In this chapter, the effect of a second, more degradable polymer on the degradation rate was investigated. Antibacterial activity and biocompatibility of the nanocomposites synthesized were also assessed. Finally, the adhesion strength of the nanocomposites was measured.

Chapter 8: General Discussion and Conclusions

This final chapter presents a general discussion relating all aspects of the thesis. A summary of several possible ways for achieving the thesis objectives is provided.

Appendix A.

The codes used for image processing (the Voronoi method, the Euclidean Minimum Spanning Tree method and the pixel counting method) shown in Chapter 5 are presented.

Appendix B.

Details of the polymerization kinetics from Chapter 3 are shown.

1.4 References

[1] K. K. Isidore, S. Aljundi, T. Kamigaki, K. Hammad and H. Oshitani, *Preventing and Controlling Infectious Diseases After Natural Disasters*, United Nationa University, On line Report, **2012**, http://unu.edu/publications/articles/preventing-and-controlling-infectious-diseases-after-natural-disasters.html#info, Accessed Feb. 24th 2015.

[2] A. S. Prasad, and L.H. Francescutti, *Natural Disasters*, in Reference Module in Biomedical Sciences. **2014**, Elsevier.

[3] J. Ambrosioni, D. Lew, and I. Uçkay, *Infectious Diseases and Infection Control After Natural Disasters*, International Journal of Infectious Diseases, **2010**, 14, Supplement *1(0)*: 1-16.

[4] S. Khanlari, and M. A. Dubé, *Bioadhesives: A Review*, Macromolecular Reaction Engineering, **2013**, *7(11)*: 573-587.

[5] P. Ferreira, J. F. Coelho, M. H. Gil, *Development of a New Photocrosslinkable Biodegradable Bioadhesive*, International Journal of Pharmaceutics, **2008**, *352*: 172-181.

[6] S. K. Roy and B. Prabhakar, *Bioadhesive Polymeric Platforms for Transmucosal Drug Delivery Systems – a Review*, Tropical Journal of Pharmaceutical Research, **2010**, *9(1)*: 91-104.

[7] J. D.Smart, T*he Basics and Underlying Mechanisms of Mucoadhesion*, Advanced Drug Delivery Reviews, **2005**, *57*: 1556-1568.

[8] W. F. Lee, Y. C. Chen, *Effect of Hydrotalcite on the Physical Properties and Drug-Release Behavior of Nanocomposite Hydrogels Based on Poly[Acrylic Acid-co-Poly(Ethylene Glycol) Methyl Ether Acrylate] Gels*, Journal of Applied Polymer Science, **2004**, *94*: 692-699.

[9] D. F. Aukerman, W. J. Sebastianelli, and J. Nashelsky, *How Does Tissue Adhesive Compare with Suturing for Superficial Lacerations?* Journal of Family Practice, **2005**, *54*: 378-378.

[10] C. D. Hoemann, J. Sun, A. Le´gare, M. D. McKee, and M. D. Buschmann, *Tissue Engineering of Cartilage Using an Injectable and Adhesive Chitosan-based Cell-delivery Vehicle*, OsteoArthritis and Cartilage, **2005**, *13*: 318-329.

[11] P. A.Zapata, L. Tamayo, M. Paez, E. Cerda, I. Azocar, and F. M. Rabagliati, *Nanocomposites Based on Polyethylene and Nanosilver Particles Produced by Metallocenic "in Situ" Polymerization: Synthesis, Characterization, and Antimicrobial Behavior*, European Polymer Journal, **2011**, *47(8)*: 1541-1549.

[12] D.C. Tien, C. Y. Liao, J. C. Huang, K. H. Tseng, J. K. Lung, T.T. Tsung, W. S. Kao, T. H. Tsai, T.W. Cheng, B. S. Yu, H. M. Lin, and L. Stobinski, *Novel Technique for Preparing a Nano-Silver Water Suspension by the Arc-Discharge Method*, Reviews on Advanced Materials Science, **2008**, *18*: 750-756.

[13] Y. Huang, X. Li, Z. Liao, G. Zhang, Q. Liu, J. Tang, Y. Peng, X. Liu, and Q. Luo, *A Randomized Comparative Trial Between Acticoat and SD-Ag in the Treatment of Residual Burn Wounds*, Including Safety Analysis, Burns, **2007**, *33*: 161-166.

[14] X. Chen, and H. J. Schluesener, *Nanosilver: A Nanoproduct in Medical Application*, Toxicology Letters, **2008**, *176(1)*: 1-12.

[15] S. Saxena, A. R. Ray, A. Kapil, G. Pavon-Djavid, D. Letourneur, B. Gupta, and A. M. Pelle, *Development of a New Polypropylene-Based Suture: Plasma Grafting, Surface Treatment, Characterization, and Biocompatibility Studies*, Macromolecular Bioscience, **2011**, *11*: 373-382.

[16] P. T. S. Kumar, S. Abhilash, K. Manzoor, S. V. Nair, H. Tamura, and R. Jayakumar, *Preparation and Characterization of Novel b-Chitin/Nanosilver Composite Scaffolds for Wound Dressing Applications*, Carbohydrate Polymers, **2010**, *80*: 761-767.

[17] R. Dastjerdi, and M. Montazer, *A Review on the Application of Inorganic Nano-Structured Materials in the Modification of Textiles: Focus on Anti-Microbial Properties*, Colloids and Surfaces B: Biointerfaces, **2010**, *79(1)*: 5-18.

[18] R. Kumar, and H. Münstedt, *Silver Ion Release from Antimicrobial Polyamide/Silver Composites,* Biomaterials, **2005**, *26(14)*: 2081-2088.

[19] Z. Ni, Z. Wang, L. Sun, B. Li, and Y. Zhao, *Synthesis of Poly Acrylic Acid Modified Silver Nanoparticles and their Antimicrobial Activities,* Materials Science and Engineering: C, **2014**, *41(0)*: 249-254.

[20] S. W. P. Wijnhoven, W. J. G. M. Peijnburg, C. A. Herberts, W. I. Hagens, A.G. Oomen, E. H.W. Heugens, B. Roszek, J. Bisschops, I. Gosens, D. V. De Meent, S. Dekkers, W. H. De Jong, M. V. Zijverden, A. N. J. A. M. Sips, and R. E. Geertsma, *Nano-silver, a Review of Available Data and Knowledge Gaps in Human and Environmental Risk Assessment,* Nanotoxicology, **2009**, *3*: 109-138.

[21] T. Hasell, L. Lagonigro, A. C. Peacock, S. Yoda, P. D. Brown, P. J. A. Sazio, and S. M. Howdle, *Silver Nanoparticle Impregnated Polycarbonate Substrates for Surface Enhanced Raman Spectroscopy*, Advanced Functional Materials, **2008**, *18*: 1265–1271.

Chapter 2: Bioadhesives: A Review

S. Khanlari and M. A. Dubé, *Macromolecular Reaction Engineering* (2013), Volume 7, Issue 11, pages 573–587.

Abstract: Bioadhesives are high molecular weight, biocompatible, biodegradable polymers used to join two surfaces where at least one of them is a living tissue. Bioadhesives are used for two main purposes, first as a replacement for surgical sutures and second as a substitute for traditional drug dosage systems. There are several considerations and issues associated with the use of biopolymers in suture-less surgery as well as in drug delivery systems. Herein is presented a review of bioadhesives; the focus being on the adhesive properties. Bioadhesives for tissue joining are considered first, along with their main characteristics and advantages. That is followed by a discussion on the use of bioadhesives as drug carriers for efficient drug delivery.

2.1 Introduction

Bioadhesion may be defined as the state in which two materials, at least one of which is biological in nature, are held together for extended periods of time by interfacial forces [1, 2]. Bioadhesives are used for many hard- and soft-tissue applications [3] as well as for reinforcing fragile tissues in treatment and assisting in haemostasis (i.e., cessation of blood flow) [4].

The term “bioadhesion” was first used in the 1970s to describe phenomena related to the ability of some synthetic and biological macromolecules and hydrocolloids to adhere to biological tissues. Nonetheless, polymeric adhesives were used in a biological

context well before that time. An extension to the bioadhesive concept, that of combining adhesion with drug delivery, was introduced in 1947 when gum tragacanth (a viscous, odourless, tasteless, water-soluble mixture of polysaccharides obtained from the sap of several species of Middle Eastern legumes) was mixed with dental adhesive powder. The aim was to deliver penicillin into the oral mucosa. This later became "Orabase", a formulation used to treat mouth ulcers. This product is available as a paste which will stick to the wet surfaces of the mouth and form a protective film over the mouth ulcer. "Orabase" paste contains polymers such as gelatin, pectin and carboxymethyl cellulose [5]. Thus, bioadhesives may perform several functions such as the protection of tissues (e.g., in the event of a wound), the prevention of fluid escape (e.g., blood), suture replacement, and drug delivery.

Herein, we review the materials and methods used in bioadhesive synthesis and recent advances in bioadhesive technologies.

2.2 Adhesion Mechanism

Bioadhesion only differs from conventional adhesion from the point of view of the requirements and properties of the substrate(s) being joined; it is governed by interfacial phenomena [1]. By adhesion, we refer to the molecular attraction between the contacting surfaces of two solid or liquid phases. This can be classified by both chemical mechanisms (e.g., electrostatic theory and adsorption theory) and physical mechanisms (e.g., wetting, and interpenetration or diffusion). In other words, adhesion relates to the ability of the adhesive to flow, to wet the substrate and maintain certain physicochemical intermolecular forces [6]. The mechanisms of bioadhesion are often classified as shown

in Table 2.1. The overall mechanism of adhesion can be summarized as follows: the adhesive is made to wet each of two objects and intermolecular, physico-chemical, attractive forces maintain the bond between the two objects.

Table 2.1 Bioadhesion mechanisms [2, 7].

Bioadhesion Mechanism
Electrostatic: Electrostatic forces between the tissue and the bioadhesive material.
Wetting: Ability of the bioadhesive to spread and develop intimate contact with the target tissue.
Adsorption: Surface forces resulting in physical bonding between the tissue and the bioadhesive.
Diffusion: Results in physical entanglements of the tissue and the bioadhesive's flexible polymer chains.
Mechanical: Interlocking of the bioadhesive into irregularities on the rough surface of the tissue.

The electrostatic mechanism of bioadhesion involves the formation of a double layer of electric charge at the interface of the bioadhesive/living tissue. The strength of adhesion is due to the attractive forces between this electrical double-layer.

Wetting theory uses interfacial tensions to predict the ability of the bioadhesive to spread on and contact the target surface. Thus, the surface energy of both the bioadhesive and the living tissue are important. High quality wetting implies that the contact angle

between the bioadhesive and the tissue is at or very close to zero. Using the wetting theory it is possible to calculate a spreading coefficient and predict bonding strength.

Adsorption theory states that the bonding strength between the bioadhesive and the tissue arises from van der Waals interactions and hydrogen bonds. Among the proposed theories for adhesion, adsorption theory is the most widely accepted. Diffusion theory describes how interpenetration and entanglement of the bioadhesive polymer chain into the living tissue produces semi-permanent bonds. Finally, in the mechanical theory of bioadhesion, a mechanical interlocking of polymer chains and the living tissue is considered, while diffusion through the living tissue is not.

The quality of an adhesive is typically evaluated by assessing two different physical forces: adhesion and cohesion. The adhesive strength refers to the intermolecular forces maintaining the bond between the substrate and the adhesive whereas the cohesive strength refers to the internal strength of the adhesive or its ability to withstand shear stresses [8]. Two important factors that influence adhesion and cohesion include the adhesive crosslink density and the degree of penetration into the tissue [4]. Crosslinks provide the adhesive with greater cohesive (gel) strength, which permits it to withstand shear forces. The degree of penetration into the tissue is a function of the parameters noted in Table 2.1 and thus a stronger electrostatic double layer, better tissue surface wetting, greater adsorption, higher diffusion and more mechanical interlocking all result in better adhesion. Some of these are also a function of the polymer molecular weight and glass transition temperature (T_g). Too low a molecular weight may result in a polymer that cannot achieve appropriate mechanical entanglements and too high a molecular weight may prevent adequate diffusion and surface wetting. The T_g dictates how well the

polymer may flow to achieve appropriate surface wetting, diffusion, etc. An application temperature above the adhesive's T_g is required.

Manipulation of the molecular weight is of course achieved by the usual means such as the reaction conditions (e.g., temperature), the initiator concentration, solvent (if used) concentration, and the addition of chain transfer agents. Crosslinkers are of course used to influence the crosslink density. Copolymer composition has a direct effect on the T_g. As discussed later, the performance of an adhesive joint is normally evaluated using tack, peel strength and shear strength measurements.

Often, an increase in adhesive strength beyond a certain level may come at the expense of the cohesive strength of the adhesive and vice-versa. Some interesting ideas on overcoming this have been reported [9, 10]. Qie and Dubé [9] produced butyl acrylate/methyl methacrylate/hydroxyethyl methacrylate/acrylic acid emulsion latexes that showed remarkable improvements to shear strength without compromising tack. The resulting adhesive films were heated after casting to influence the creation of a continuous gel structure. Thus, tack and peel strength (adhesive strength) were preserved while simultaneously increasing the shear strength (cohesive strength) of the adhesive. In another approach, miniemulsion polymerization was used to create multimodal particle size and molecular weight distributions in a single reaction vessel to control adhesive properties without the need for post-reaction blending. The adhesives were produced using 2-ethylhexyl acrylate/methyl methacrylate. The performance of unimodal particle size and molecular weight distribution miniemulsion-based PSA films were compared to that from conventional emulsion polymerizations and then, compared to the multimodal

miniemulsion case. Results showed remarkable control and improvements to the adhesive properties [10].

2.3 Adhesive Strength Measurement

Along with hydrophilicity, biocompatibility, blood compatibility, toxicity and biodegradability, adhesive strength is a critical property for a bioadhesive to be used as an ideal tissue adhesive. This property which is defined as the force required to detach two tissue sections with the test bioadhesive sandwiched between them should be the same as the mechanical strength of the target tissue to be bonded; it is determined using a tensile tester. The force detection system consists of a precise load cell and the bonding strength is determined with a constant speed of 30 mm/min and the force required to either fracture the adhesive bond or detach the bioadhesive from the tissue is recorded as the critical measure of bioadhesive strength [11]. At the end of the test, there are three different possibilities for the specimen's failure point, the bioadhesive thickness, the tissue, and bioadhesive-tissue intersection. If the specimen is torn from the glue thickness, the energy consumed is considered to have been mostly used to tear the adhesive which means the cohesive strength is less than needed, but if the specimen is torn from the tissue, it implies that the mechanical strength of the bioadhesive is higher than that of the tissue. Finally, if the specimen is detached at the bioadhesive-tissue intersection, one can conclude that bonding strength of the bioadhesive is less than expected.

2.4 Biocompatibility

Biocompatibility refers to the ability of a material to perform its desired function *in vivo*, without any undesirable local or systemic effects in the host. Generally, a candidate biomaterial must possess two important characteristics. It must be firstly biochemically compatible, i.e., non-toxic, non-irritant, non-allergenic and non-carcinogenic; secondly, it must be mechanically compatible with surrounding tissues. Biocompatibility also depends on the location of the application of the biomaterial. For example, a material that is biocompatible for bone replacement may not necessarily be biocompatible in a direct blood contact application [12].

An assessment of biocompatibility usually involves two common tests: haemocompatibility and cytotoxicity. Haemocompatibility is the compatibility of a material with blood. Events that determine haemocompatibility often occur at the molecular level and can influence inflammatory processes [13]. Cytotoxicity is defined as the cell-killing ability of a compound and is assessed by immersing the synthetic biomaterial in a cell-culture and determining the amount of viable cells under controlled conditions [14].

Drug delivery systems provide stability to the drug being administered. Many drugs are unstable *in vivo* thus, by encapsulating the drug, it is protected from degradation. In addition, by delivering the drug at a slow but more consistent rate, one is capable of having a dose that is within the targeted, optimal range in contrast to the case where direct dosing (e.g., intravenously) would occur and frequent dosing intervals would be required. Due to the development of these sustained release systems, it is possible to administer unstable drugs once a week to once a year that in the past required daily

dosing. Studies have shown superior effectiveness of these systems over conventional methods of treatment [15].

2.5 Tissue Adhesives

Although suturing remains the most common method for closing wounds, topical skin tissue bioadhesives are increasingly being used by health professionals to replace sutures, staples and adhesive strips in the fields of trauma, plastic and other surgeries, emergency medicine and pediatrics [5, 16]. The use of traditional suturing methods allows for the thorough closure of wounds but bioadhesives do present several advantages [17]. Bioadhesives can enhance tissue repair and wound healing while reducing operative risks [16]. They do not require local anaesthetics and provide a pain-free (i.e., needle-free) wound closure while completely avoiding the risk of needle-stick injury to the surgeon [17]. Other roles such as preventing the escape of fluids from the wound (e.g., haemostasis), protecting the wound from further infection and the possibility of drug-delivery are also noted [16]. The potential for drug-delivery opens the door to slow, localized release of medication for antibiotic pain-treatment and the encouragement of cell-growth [18]. Bioadhesives also usually provide excellent cosmetic results [5, 19] and, because suture removal is not required, medical service time is reduced [17, 19].

Commercial biomedical adhesives can be sourced from both natural and synthetic starting materials. These materials are described later. Surgical adhesives must exhibit several important properties and satisfy many clinical requirements [20]:

- Adhesion – Obviously, the surgical adhesive must hold the two sides of the tissue together and remain present without additional support until the wound has

sufficiently healed. It should then, in the case of internal applications, degrade to non-toxic, biocompatible products.

- Curing environment – The adhesive should ideally present the ability to cure, if necessary, in a moist environment [5].
- Flowability – Adhesives generally require a certain ability to flow. Flowability of bioadhesive, which refers specifically to the movement of the polymer chains, is important because it controls the extent of interpenetration between the polymers and mucosal/epithelial surfaces.
- Hydrophilicity – Polymers that are hydrophilic in nature are preferred as they are able to form strong adhesive bonds with living tissues, which are composed of large amounts of water.
- Hydrogen bonding – Hydrogen bonding between entangled polymer chains, along with the other parameters affecting flowability of the adhesive, provides a minimum required cohesive strength. Cohesive strength refers to the ability of the adhesive molecules to remain interconnected. A minimum cohesive strength exists when failure of the adhesive bond occurs between the adhesive and substrate rather than due to the adhesive's internal forces. Therefore, the presence of strong hydrogen-bonding groups such as ¯OH and ¯COOH is preferable. For most bioadhesive polymers, there is one ¯OH or ¯COOH group per monomer and the number per molecule depends on the number-average molecular weight.
- High molecular weight – Polymers with a high molecular weight, typically in the range of 100,000 Daltons, are desirable because they provide a higher degree of entanglement.

- Surface tension (or wettability) – For any adhesive to adhere to a substrate, one fundamental thermodynamic requirement has to be satisfied first: the measured surface energy of the adhesive must be equal to or less than that of the adherent. Unless this condition is satisfied, a material cannot adhere to the substrate. Low surface tensions are needed to spread the bioadhesive polymer onto the tissue surface.
- Crosslinking – Most references mention the necessity of crosslink formation after application in order to increase mechanical strength [5, 21].

2.6 Market Share

Greater than 12 million traumatic wounds are treated yearly in hospital emergency departments across the United States. Given an average cost of ~$20 per wound, greater than ~$250 million is spent annually on suturing kits alone. Despite the greater material cost of adhesives compared to sutures, when the equipment, health care workers' time and follow-up visits are accounted for, the use of bioadhesives becomes more cost-effective. Nonetheless, 60% of wound closure methods are still via sutures, staples and other mechanical methods [22]. On the other hand, alternative technologies which include bioadhesives represent an estimated future global market potential of $38 billion by 2017, as illustrated in Figure 2.1 [23]. It should be noted that while the predicted shifts in percent market share are small, these are percentages of a $5 billion global market and are thus, significant.

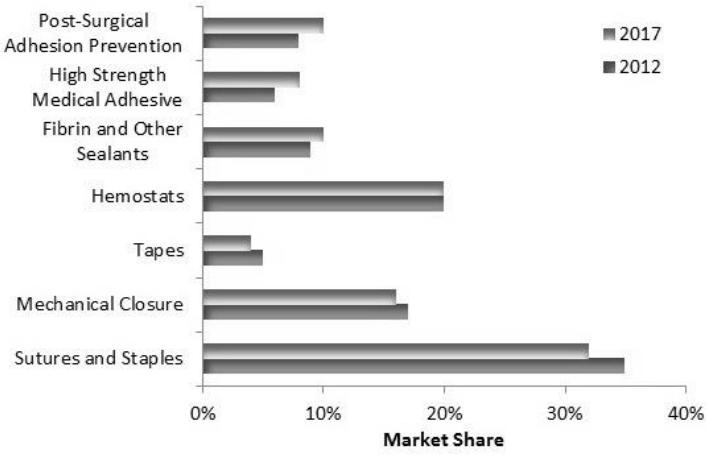

Figure 2.1 Market share of bioadhesives and other wound closure methods, 2012 vs. 2017 [23].

2.7 Materials Used

Bioadhesives used in tissue adhesive applications should fulfill both mechanical and biomedical requirements. It is difficult to design a tissue adhesive which exhibits biocompatibility, biodegradation, sufficient adhesive strength, acceptable cosmetic results, haemostatic properties, at a reasonable cost and ease of application, while being broadly applicable to different tissues and healing rates. Thus, a number of natural (i.e., biologically derived) and synthetic components have been employed in the development of bioadhesives.

Bioadhesives are sourced from both natural and synthetic polymer resources. Fibrin-based (natural) and cyanoacrylate (synthetic) bioadhesives are two well-known materials used in the past. Fibrin glue was the most successful tissue adhesive up until the early 1990s. It has many advantages over cyanoacrylates in terms of its biocompatibility, biodegradation and haemostatic properties [24]. However, fibrin-based adhesives do

present several problems such as immunogenicity (i.e., the provocation of an immune response in the body) and the risk of blood transmission of diseases, for example, the human immunodeficiency virus (HIV) and Hepatitis C. On the other hand, cyanoacrylate adhesives degrade in aqueous media to produce formaldehyde, which may cause inflammation, and have been reported as potential carcinogens [5]. Furthermore, both fibrin glue and cyanoacrylates work best when applied to a dry surgical field, which greatly restricts their applications for wet tissue adhesion and haemostasis required in many internal organ surgeries.

Fibrin-based adhesives have been shown to improve the success of skin grafts, especially when associated with difficult grafting sites or sites associated with unavoidable movement. However, their bonding strength is relatively weak and their degradation rate is faster than time expected for wound healing. Thus, they have predominantly been used to stop bleeding from organs such as the spleen or the liver. In general, bioadhesives often have the shortcoming of inadequate bonding strength in a watery milieu, which is the most critical characteristic required of bioadhesives. The trade-off between adhesive strength and biocompatibility also continues to be a major challenge [16].

Cyanoacrylate adhesives are synthesized by polycondensation of cyanoacetate and formaldehyde [25]. They encourage rapid wound healing. Tremendous bonding strength and the ability to adhere to wet surfaces have expanded their use in medical applications. However, when polymerized in direct contact with living tissue, the starting materials (cyanoacetate and formaldehyde) cause excessive inflammation and tissue necrosis [26]. Some commercial examples of cyanoacrylate based tissue adhesives include

Dermabond® and Histoacryl® [27]. The advent of numerous renewable or "green" polymers may also hold interesting promise as bioadhesive starting materials [28]. Table 2.2 lists other biomaterials used in tissue adhesive applications. While all of the materials shown in Table 2.2 exhibit good biocompatibility, their use as bioadhesive materials has provided varying degrees of success. Of the natural materials employed, biopolymers such as fibrin glue, collagen and gelatin have exhibited haemorrhage control properties; a property which has not been demonstrated in synthetic tissue adhesives. Another concern lies with the degradation products of these bioadhesives. For example, cyanoacrylate adhesives are used for cosmetic surgeries but the effect of their degradation products on living tissues is not clear. On the other hand, the degradation products of the natural bioadhesives are usually biocompatible.

Table 2.2 Materials used in tissue adhesives.

Polymer Type	Material	Description
Natural	Fibrin Glue [24]	Fibrous protein tissue adhesive from human blood plasma, which mimics the physiological coagulation cascade and polymerizes to form blood clots.
	Rice Starch [29]	Rice starch-based bioadhesives were prepared by dissolving the material in water at 60°C. Bioadhesion was tested for topical use.
	Collagen [30]	Collagen-based adhesives are mentioned as a new class of tissue glues.
	Gelatin [31]	Gelatin-based bioadhesives crosslinked with formaldehyde and/or glutaraldehyde were examined for cytotoxicity, flexibility and bonding strength.
	Chitosan [32, 33]	Chitosan nanoparticle bioadhesives were prepared and

		evaluated for adhesion, swelling, drug delivery, entrapment efficiency and loading capacity.
	Pectin [34]	Pectin-based bioadhesives were prepared and tested for bioadhesion, swelling and erosion.
	Dextran [32]	Dextran was used as the second component of a two-component bioadhesive system as a bone adhesive. In vitro cell testing demonstrated excellent biocompatibility.
	Carboxymethyl cellulose (CMC) [35, 36]	CMC-based bioadhesive patches were used for drug delivery and were evaluated for moisture absorption capacity, tensile strength and percent elongation. In vitro release patterns of these patches also were analyzed.
Synthetic	Cyanoacrylates [26]	Solvent-free, instantaneous and very strong adhesives that cure immediately at room temperature.
	Polyacrylic acid (PAA) [37]	Micro- and nano-particle PAA bioadhesives were synthesized via inverse emulsion polymerization and yielded excellent bioadhesive properties in an in vitro assay.
	Polycaprolactone (PCL) [5]	UV-crosslinked PCL bioadhesives were prepared. Biodegradation in human plasma and haemocompatibility were evaluated.
	Polyvinyl alcohol (PVA) [38]	Bioadhesives based on PVA were used and swelling ratio was investigated.
	Polyethylene glycol (PEG) [39, 40]	Ethylene glycol was used as both a polymer (PEG) and comonomer for bioadhesive preparation. Hardness, compressibility, adhesion, cohesion and rheological properties of PEG-based bioadhesives were examined. EG was also used as a comonomer and these hydrogel copolymers showed strong bioadhesion.

All of the polymers listed in Table 2.2 are biocompatible, biodegradable and hydrophilic. As noted in section 2.3, a number of necessary criteria exist for a biopolymer to be applied as a bioadhesive. Dextran, rice starch, collagen, chitosan, polyvinyl alchohol and polyethylene glycol all possess –OH groups in their chemical structure, polyacrylic acid has a –COOH group, and pectin and carboxymethylcellulose have both groups. The polymers listed as synthetic bioadhesives can be synthesized at molecular weights which result in appropriate flowability. There are several methods for crosslink formation in polymers. For polymers with the ability to crystallize, crystalline regions can act as crosslinks [41]. Rice starch [42], poly(caprolactone) [43], poly(vinyl alchohol) [41, 44], and poly(ethylene glycol) [45] are able to be physically crosslinked by freeze-thawing treatments while the other polymers can be crosslinked using chemical methods. For example, poly(acrylic acid) can be cured by photo-crosslinking [46] and gelatin by chemical crosslinking using dextran dialdehyde [47].

2.8 Recent Advances in Tissue Adhesive Systems: Nanocomposite Materials

Nanocomposite polymers are a class of composite materials that are particle-filled polymers for which at least one dimension of the dispersed particles is in the nanometer range [48]. Nanofillers have been added to polymers in order to modify their properties but only limited bioadhesive nanocomposite material research has been published. Nanofillers may be added to bioadhesive matrices to modify hydrophilicity, mechanical properties, and adhesive properties, as well as to impart other properties, e.g., to promote wound healing. The added value brought to a bioadhesive by incorporating nanomaterials

is varied. Not only should one expect property modifications to the polymer (e.g., increased tensile strength) but also new properties such as enhanced wound healing [49], antibacterial [50, 51] and haemostatic properties [49] among many others. These modifications can occur at very low nanofiller loadings and often result in little to no sacrifice of other important properties. By employing nanofillers which impart certain properties to the bioadhesive, one can avoid efforts to synthesize new polymer structures in order to achieve similar functionality. Some notable advances are discussed briefly below.

Lee et al. (2004) prepared a series of nanocomposite hydrogels for bioadhesive applications from acrylic acid, poly (ethylene glycol methyl ether acrylate), and intercalated hydrotalcite (HT) via photopolymerization. They showed that the swelling ratio for these nanocomposite hydrogels increased with HT content, but at the expense of gel strength and adhesive force. The drug-release behavior for these gels was also examined [20].

In orthodontic adhesives, the effect of silica nanofillers and silver nanoparticles on surface characteristics, physical properties and antibacterial activity against cariogenic streptococci was investigated by Ahn et al. (2009). They found that incorporation of silver nanoparticles into the adhesives was indeed possible and they found a measured effect on both physical and antimicrobial properties [52].

Puntuwat et al. (2010) reported on rice starch hydroxyapatite (HA) nanocomposites. They investigated the adhesive properties of the final product and concluded that the nanocomposite bioadhesive had a high water resistance (i.e., the bioadhesive dissolved only after 7 days) which could be useful in the human body.

Moreover, their bioadhesive could provide direct, extended and immediate bonding to a glass surface in water, was biocompatible, bioabsorbable, of low cost, and was eco-friendly [29]. They also prepared gelatin/nanocarbon nanocomposites and showed that with the addition of 0.3 wt% carbon nanopowder, improvement to the maximum bonding strength of this adhesive to porcine muscle tissue was noted [53].

2.9 Bioadhesive Drug Delivery Systems

The concept of a bioadhesive drug delivery system is a relatively straightforward idea: one can simply combine a bioadhesive, which should already be fully biocompatible, with a drug of choice. Specifically, certain water-soluble polymers, which become adhesive on hydration, can be used for targeting a drug to a particular region of the body for an extended period of time. The bioadhesive delivery system includes buccal, oral, rectal, vaginal, ocular and nasal drug delivery systems [54].

The concept of controlled drug delivery began in the mid-1960s [55]. It has been since used to obtain specific drug release rates or localized targeting of active ingredients [7]. The combination of drug delivery with bioadhesives was first introduced by Park and Robinson in 1984 [56]. Typically, these consist of a controlled-release hydrogel matrix surrounded by a second polymer with adhesive properties [87].

An oral or intravenous drug delivery system for drug delivery can only partly satisfy therapeutic and biopharmaceutical needs. A drug delivery system guaranteeing site- and rate-specific delivery often is needed to release locally effective drugs at their target site or to provide a pulsed drug release [58]. The main advantages of bioadhesive delivery systems include extended residence time of the delivery system at the site of

action, local delivery to a selected site (targeting of the drug), fewer drugs required to heal the disease state, minimization of possible side effects, and enhancement of the efficacy of treatment [15, 57].

Drug delivery bioadhesive systems come in the following general forms: gels (or more specifically, hydrogels), micro- and nano-spheres, and membranes. Each of these can consist of a single bioadhesive, a blend of two or more bioadhesives, as well as containing a filler to form a composite material. Gels are crosslinked, three-dimensional, polymeric networks. Hydrogels are a subset of gels and imply materials swollen in water but more specifically, the crosslinked network is comprised of hydrophilic polymers. They maintain their three-dimensional structure while maintaining the capacity to absorb large amounts of water and swell [59, 60].

Hydrogels can be produced from natural or synthetic materials to form neutral or ionic polymers. For example, polyelectrolytes (e.g., proteins, polypeptides, polyamines and poly(acrylic acid)) are ionizable hydrogels able to achieve high degrees of swelling. Hydrogel swelling and/or drug release characteristics can be modified by the polymer microstructure (e.g., degree of crosslinking, polymer molecular weight), the presence of ionic groups and the ability of the hydrogel to respond to external stimuli such as temperature and pH [60].

Microspheres and nanospheres in drug delivery applications often consist of a polymer matrix (e.g., hydrogel) swollen with a drug either as a distinct particle or in a core surrounded by a shell with a second polymer suspended in a liquid medium [61]. The micro/nanospheres can be applied to a backing as a patch or as a coating requiring evaporation of the liquid medium. The incorporation of bioadhesive properties to these

micro/nanospheres provides additional advantages. These advantages include increased drug stability, higher absorption efficiencies, improved contact with the target tissue, and improved targeting of the drug by anchoring it to a specific absorption site [7].

Membrane drug delivery bioadhesives are ideal for use as topical drug delivery patches. Generally, they are used either as a matrix for drug loading to be delivered to the body [62] or as a coating for other drug containing systems like tablets and capsules and to modify the rate of drug release [63]. Membrane bioadhesive drug delivery systems present some advantages compared to other drug delivery systems. For example, high water flux is achievable which facilitates the osmotic delivery of drugs. In addition, the permeability of the membrane, which changes the rate of drug release, can be easily adjusted by changing the membrane morphology, e.g., changing the pore size and overall porosity of the membrane [63].

Bioadhesive strength is defined as the maximum adhesion force between the target substrate (i.e., tissue) and bioadhesive. It is a critical characteristic for bioadhesives used in drug delivery applications because it is important that the drug is maintained at the specific site for the necessary time period. To test bioadhesive strength, tensile testing equipment is employed in a way similar to what was described earlier for simple tissue adhesive systems. In this case, however, the bioadhesive is applied to a substrate or backing which is held in place in the tensile tester. The tissue sample is brought into contact with the adhesive and the force required to separate the tissue from the adhesive is measured. A pre-specified contact time before loading is needed for the formation of the adhesion bonds. Also, it is recommended to perform the entire test under physiological conditions.

In the case of gel and hydrogel drug delivery systems, one can also measure the gel strength. One approach involves placing the gel in a graduated cylinder at physiological conditions. A defined force is applied to a perforated disk which allows the gel to flow through the disk as it descends through the gel. The gel (or hydrogel) strength is measured as a viscosity and is determined by the time for the perforated disk to sink 5 cm through the gel [64].

2.9.1 Market Share

The use of drug delivery systems has increased markedly over the past decade and is predicted to continue. Predictions for $196.4 billion in total sales for drug delivery systems by 2014 equate to a compound annual growth rate (CAGR) of 7.2% over a 5-year period. The largest market segment is targeted drug delivery, which is expected to increase to $80.2 billion in 2014, for a CAGR of 9.5%. Sustained-release products own the second-largest market share, with estimated sales of $45.8 billion in 2014, for a CAGR of 4.9%. Thus, significant expansion of the bioadhesive drug delivery sector is highly likely [65].

2.9.2 Drug Delivery Bioadhesive Synthesis

Bioadhesive drug delivery systems come in three major forms: gels/hydrogels, micro/nanoparticles and membranes. In this section, the methods for preparation of these systems are discussed following a review of the materials which can be used in their preparation.

2.9.3 Materials Used in Bioadhesive Drug Delivery Systems

As noted earlier in Table 2.2, a broad range of materials have been used in bioadhesive applications tailored to drug delivery. Materials used in drug delivery applications must meet several compatibility requirements: the adhesive (and materials used in their synthesis) must be biocompatible, blood compatible, biodegradable, and the degradation products must be biocompatible. Additional requirements include adequate cellular adhesion, ease of synthesis, controlled drug delivery and maintenance of drug stability. A number of the materials shown in Table 2.2 have been developed further into drug delivery systems. A number of key examples are shown in Table 2.3.

Among the aforementioned polymers, the natural polymers and their degradation products are usually biocompatible but they often require chemical modification to alter the degradation rate, drug release rate and mechanical properties of the drug carrier [68]. These chemical modifications may include the formation of crosslinks, the addition of fillers, or surface modifications such as polymer grafting. Agents to enable these modifications may present biocompatibility issues. On the other hand, synthetic polymers usually prevent one from in situ (i.e., in or near the tissue) polymerization approaches but post-polymerization modification, such as crosslinking can be accomplished with biocompatible compounds, e.g., using sucrose [78]. In some cases, such as with PEG, further chemical modification may be unnecessary because the polymer may show the appropriate integrity without chemical crosslinks.

The large number of polymer based drug delivery systems either approved for clinical use or currently in clinical trials supports the notion that these are no longer just an academic curiosity.

Table 2.3 Bioadhesives used in drug delivery and associated drugs.

Bioadhesive Polymer Type	Material	Drug delivered
Natural	Alginate	Bromothymol blue (model drug) [66] Doxorubicin [67] Insulin [68]
	Cellulose	Beta-blocker drug [69]
	Chitosan	Adriamycin [70] Clotrimazole [71] Insulin [72] Bovine serum albumin [73]
	Collagen	Antibiotic agents, such as gentamicin and tetracycline anticancer agent Medroxyprogesterone acetate Nifedipine [74]
	Pectin	Diltiazem [75]
	Gelatin	Antitumor drug TAPP-Br [76]
	Starch	Theophylline [77]
Synthetic	Polyacrylic acid	Metoclopramide [78]
	Polyethylene glycol (PEG)	Anticancer Agents [79]
	(N-vinyl 2 pyrrolidone /methacrylamide /itaconic acid) terpolymer	Insulin [80]

Some first-to-market products, with their brand name and year of approval in parentheses, include PEG-l-asparaginase (Oncaspar, 1994) for leukemia, styrene maleic anhydride-neocarzinostatin (Zinostatin Stimalmer, 1993) for hepatocellular carcinoma, PEG-granulocyte colony-stimulating factor (Neulasta, 2002) for neutropenia prevention, PEG-interferon-α (PEGasys, 2002) for hepatitis C, and PEG-adenosine deaminase (Adagen, 1990) for severe combined immunodeficiency disease [81].

2.9.4 Hydrogel Drug Delivery System Synthesis

Gel or hydrogel drug delivery systems involve either post-polymerization crosslinking of linear polymers or the in situ formation of a polymer network using added crosslinkers or multifunctional monomers. As noted in Table 2.3, synthetic or natural polymers can be employed. The presence of functional groups on the polymer chains is desired to encourage adhesion to the tissue; these include hydroxyl, amine, amide, ether, carboxylate and sulfonate moieties. A stepwise methodology is used to prepare the drug delivery system as shown schematically in Figure 2.2 [59]. Afterwards, the hydrogel is dispersed in demineralized water and is mixed until a transparent gel appears. Temperature, and time and rate of mixing are manipulated to achieve the desired results. Aside from the methodology shown in Figure 2.2, drug addition can occur prior to gel formation (i.e., in situ during polymerization) but this may lead to mixing difficulties and would restrict the polymerization temperature to a range suitable to preserve the drug's activity [80, 82]. Hydrogel-based bioadhesives have been reportedly used in ear, nasal and oral cavities, lungs, stomach, skin, colon, small intestine, etc. [83].

2.9.5 Micro- and Nano-Sphere Drug Delivery System Preparation

Several methods for polymeric micro- and nano-particle production have been developed. The idea is to prepare a suspension of drug-infused particles. Differences in the methods largely depend on how and when the drug is added to the biopolymer matrix, and how and when the polymer and the suspension are formed [84].

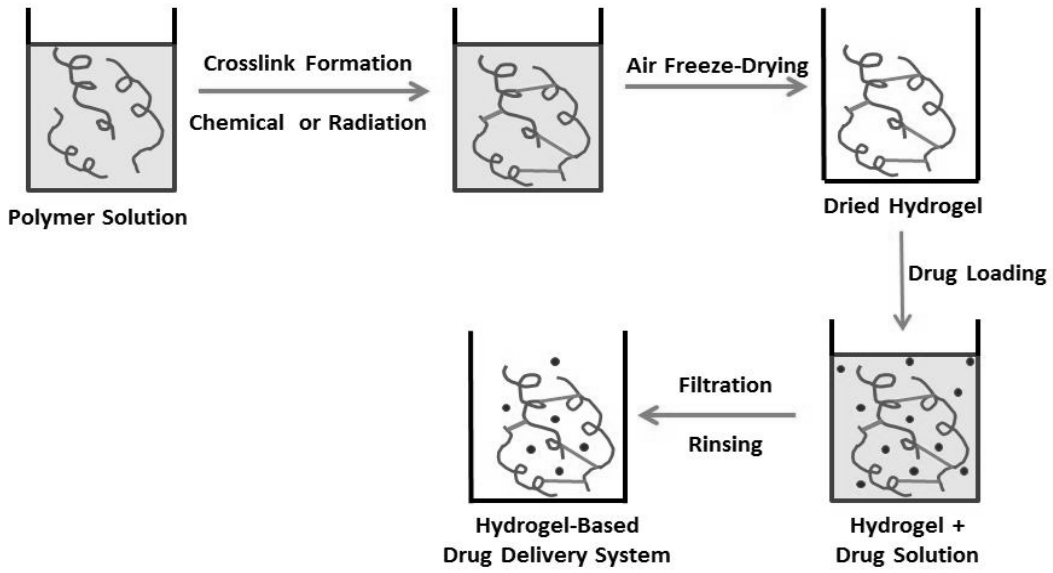

Figure 2.2 Schematic representation of the steps involved in the preparation of a hydrogel-based drug delivery system (Long curly lines represent polymer; short straight lines represent crosslinks; and circles represent drug particles) [59].

***a) Solvent Evaporation*:** In this method, a pre-formed biopolymer is dissolved in an organic solvent. The drug is dissolved or dispersed into the polymer solution, and then this mixture is emulsified under high speed agitation and/or sonication into an aqueous solution to generate an oil-in-water emulsion. After the formation of a stable emulsion mixture including stable spherical drug containing particles, the organic solvent is evaporated either by increasing the temperature/under reduced pressure or by continuous stirring at constant temperature. These procedures are appropriate for laboratory-scale operation, but for large-scale production, alternative methods using low-energy emulsification are required. By means of this method, particle sizes from 1 to 100 μm have been reported [7].

***b) Spontaneous Emulsification/Solvent Diffusion*:** This method could be considered as a modification to the solvent evaporation method. In this method a water-soluble solvent along with a water insoluble organic solvent are used to disperse the polymer solution. One of acetone or methanol, along with either dichloromethane or chloroform, form commonly used solvent pairs. After pouring the resulting polymer solution into the emulsified aqueous solution under agitation, nanoparticles are formed via the following steps: when the polymer solution is added to the emulsified aqueous solution, emulsion droplets are formed in the aqueous phase; the water-insoluble solvent diffuses out from the emulsion droplets, which causes the droplets to shrink even to the nano-scale. After the solvent-evaporation step, in which the remaining solvent is removed, the droplets solidify to form polymeric nanoparticles [85]. One can conclude that in this method, the higher concentration of water-soluble solvent results in a greater reduction in particle size.

***c) Emulsification Reverse Salting Out*:** The emulsification reverse salting-out technique involves the addition of a solution containing the polymer, the drug and a water-miscible solvent, such as acetone, to an aqueous solution containing the salting-out agent (e.g., magnesium chloride, calcium chloride) and a colloidal stabilizer (e.g., polyvinyl pyrrolidone) under vigorous mechanical stirring. When this oil-in-water emulsion is diluted with a sufficient volume of water, it induces the formation of nanoparticles by enhancing the diffusion of acetone into the aqueous phase. The dilution produces a sudden decrease in salt concentration in the

continuous phase of the emulsion, forcing the polymer solvent to migrate out of the emulsion droplets. The remaining solvent and salting-out agent can be removed by filtration. Although the emulsification-diffusion method is a modification of the salting-out procedure, it has the advantage of avoiding the use of salts and thus, eliminates the need for intensive purification steps [84].

***d) Precipitation*:** The precipitation method is a one-step procedure, also known as the solvent displacement method. It is usually employed to incorporate lipophilic drugs into the carriers based on the interfacial deposition of a polymer. In general, nanoprecipitation is performed using systems containing three basic ingredients: polymer, a solvent, and a non-solvent of the polymer. The solvent should be organic, miscible in water, and easily removed by evaporation. In some cases, this could be a binary blend of solvents (e.g., acetone with a small amount of water, or ethanol and acetone). Of course, this depends on the nature of the polymer (i.e., water-soluble or not). Thus, the polymer, the drug, and a lipophilic surfactant are first dissolved in the semi-polar water-miscible solvent. The resulting solution is then poured or injected into an aqueous solution containing stabilizer while mixing. Nanoparticles are formed immediately by rapid solvent diffusion. Finally, the solvent is removed from the suspension under reduced pressure [84].

***e) Hot Melt Microencapsulation*:** In this method, the polymer is first melted and then mixed with solid particles of the drug that have been sieved to less than 50 μm. The mixture is suspended in a non-miscible solvent (e.g., silicone oil), continuously

stirred, and heated to 5°C above the melting point of the polymer. Once the emulsion is stabilized, it is cooled until the polymer particles solidify. The resulting microspheres are washed by decantation with petroleum ether. The primary objective of this method is to develop a microencapsulation process suitable for water labile polymers, e.g., polyanhydrides. Microspheres with diameters from 1 to 1000 μm can be obtained and the size distribution can be easily controlled by altering the stirring rate. The only disadvantage of this method is the temperature to which the drug is exposed [7, 86].

f) Inverse Emulsion Polymerization: Inverse emulsion polymerization consists of the addition of a water-soluble monomer/water solution to an organic suspending medium (e.g., paraffin oil) in the presence of an emulsifier. Unlike conventional emulsion polymerization, inverse emulsion polymerization results in the formation of a particle from every single droplet. The drug could be dissolved in the aqueous phase either before the addition of the monomer or at the end of the polymerization reaction. Purification is needed after the polymerization in order to separate the particles from the media e.g., via centrifugation, rinsing, re-suspension of the particles in an isotonic surfactant-free medium and precipitation [61].

Generally, an ideal micro/nano particle drug delivery system has a high drug loading capacity to reduce the quantity of the carrier biomaterial required for hosting the drug. Drug loading into the particles is achieved by two methods: 1- by incorporating the drug at the time of particle production; or 2- by adsorbing the drug after the formation of

particles by incubating them in the drug solution. It is likely that a large amount of drug can be entrapped by the incorporation method when compared to that using adsorption [61].

The compatibility of the drug with a particular solvent/polymer delivery system is always tested. Thus, the selection of which drug-delivery system to use relies heavily on the ability for the drug's efficacy to remain intact. A comparison of the methods presented above is shown in Table 2.4.

Table 2.4 Summary of methods for micro/nano particle drug delivery adhesives preparation [7, 61, 84, 85, 86].

Method	**Product particle size achieved**	**Solvent needed?**	**High temperature needed?**	**Purification needed?**	**Controlling polymer synthesis needed?**
Solvent Evaporation	1 - 100 μm	Yes	No	No	No
Spontaneous Emulsification/Solvent Diffusion	Nano range	Yes	No	No	No
Emulsification Reverse Salting Out	Nano range	Yes	No	Yes	No
Precipitation	Nano range	Yes	No	No	No
Hot Melt Microencapsulation	1 - 1000 μm	No	Yes	No	No
Inverse Emulsion Polymerization	Nano and micro range	Yes	Maybe	Yes	Yes

While keeping other physical and chemical parameters constant, decreasing the particle size increases the rate of drug delivery. Polymers used in nano/microsphere drug

delivery systems are themselves, bioadhesives. However, if one wishes to modify the drug release rate and increase the adhesive strength of the particle-tissue bond, one can coat the surface of the nano/microspheres with another bioadhesive polymer [87].

Emulsification/chemical crosslinking [88], ionic gelation, interfacial deposition, phase inversion, nanoencapsulation and spray drying are other, less-investigated nano/microsphere bioadhesive drug delivery system synthesis methods [7, 89].

2.9.6 Membrane Drug Delivery Bioadhesives

For membrane drug delivery bioadhesive synthesis, a solvent casting method is used in which the polymer or a mixture of polymers along with the drug are dissolved in a solvent and the solution is cast into a mold. After allowing the solvent to evaporate, vacuum drying is applied to remove any remaining solvent [62]. It should be noted that the only difference compared to conventional membrane drug delivery is the fact that a bioadhesive function is imparted to the membrane.

2.9.7 Recent Advances in Drug Delivery Bioadhesion

a) Smart Drug Delivery Bioadhesives

So-called “smart” polymeric systems show changes in properties in response to various physical or chemical stimuli [90]. These stimuli include temperature, photo-radiation (UV, visible light), solvents, electric and magnetic fields, mechanical stress, pressure, sonic radiation, pH, specific ions, chemical agents and enzymes [91]. From a drug delivery perspective, one or more of these stimuli can be utilized to regulate the release of

drugs [92]. Temperature-sensitive and pH-sensitive drug delivery systems are common. The human body presents variations in pH along the gastro-intestinal tract, and also in specific areas such as in certain tissues (e.g., tumors) or sub-cellular compartments. Such "smart" polymer systems are important for the release of the drug via a "switch", such as pH, permitting transport and action of the drug at the desired target [90].

Polymers are typically thermally sensitive as they have temperature dependent mechanical properties, but those with glass to rubber transition temperatures (T_g) close to the physiological temperature offer many possibilities as drug delivery bioadhesives [90]. Having a T_g at or below the physiological temperature allows the polymer to exist in a rubbery state and thus facilitate drug delivery once in the host. The use of pH-sensitive polymers to deliver drugs to tumor tissues, which are acidic, was proposed by Hoffman [91]. Choi et al. produced a pH- and temperature-sensitive gel with a sol-gel transition temperature at that of the human body, which permitted the dissociation of the gel at the more acidic tumor location [92]. The mechanism of action of all stimuli-responsive drug delivery hydrogels are based on the release of the drug due to swelling of the hydrogel [93]. This is shown schematically in Figure 2.3. A variety of stimuli-sensitive drug delivery bioadhesive systems have been investigated. Some examples of temperature- and pH-sensitive systems are presented in Table 2.5. Other noteworthy examples are discussed below.

In a review of temperature-sensitive in situ hydrogel formation, drug delivery systems were discussed therein, thermo-sensitive bioadhesive systems from poly(NIPAAm) and its derivatives, poly(lactic-co-glycolic acid) or PLGA, PEG, and others were presented [92].

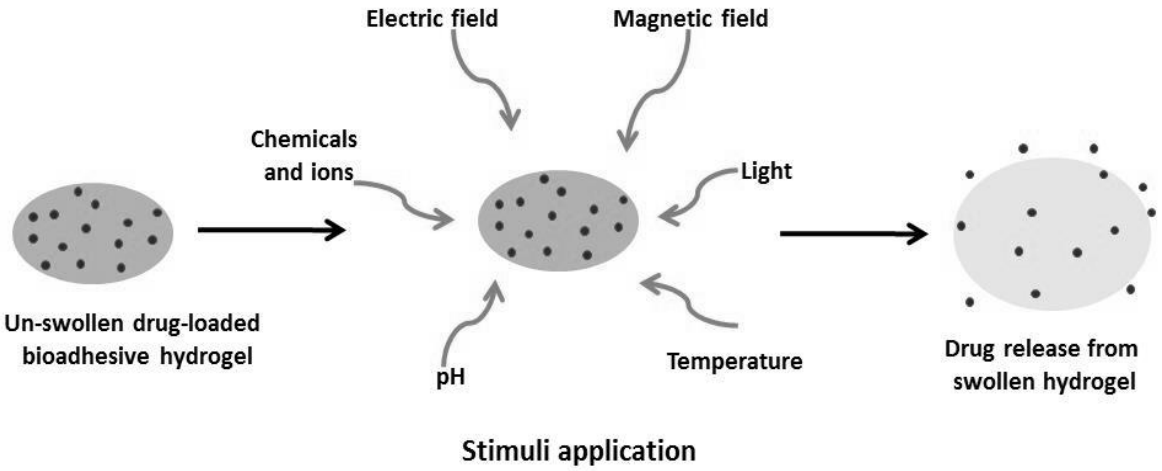

Figure 2.3 Stimuli responsive swelling of drug delivery hydrogels [59].

A less studied "smart" drug delivery system uses a mild electrical current as the principal stimulus. Electro-responsive drug delivery hydrogels undergo shrinkage or swelling in an applied electric field. The principle involves dynamic swelling of the hydrogels, i.e., swelling on one side and shrinkage on the other side, which results in bending of the hydrogels and subsequent release of the drug [99]. Bioactive materials, such as pilocarpine hydrochloride, glucose and insulin, were successfully released from a

gel using an alternating electrical field [100]. Similarly, a pulsating release of hydrocortisone was controlled using a PAA-sodium alginate composite device. The applied electric current was achieved by placing the composite device between two electrodes. Both the current and voltage were within tolerable ranges [101].

Table 2.5 Stimuli-responsive bioadhesive drug delivery systems, since 2000.

Stimulus	Polymers	Summary
pH	Thiolated chitosan and HPMCAM (hydroxypropyl methylcellulose acetate maleate) [88]	Thiolated chitosan muco-adhesive microspheres synthesized and coated with HPMCAM for duodenal ulcer application; insoluble below pH 3.0.
	Poly(β-amino ester)-poly(ethylene glycol)- poly(β-amino ester) triblock copolymer (PAE-PEG-PAE) [94]	PAE-PEG-PAE synthesized for in vitro controlled release of lidocaine. Concentrated polymer solutions (30 wt%) exhibited gel-to-sol transition in pH range 6.4-7.8.
	Chitosan and polyvinyl pyrrolidone (PVP) [95]	Semi-interpenetrating polymer network of chitosan/PVP for antibiotic delivery synthesized; resulted in high drug delivery at pH 1.0.
Temperature	Ethyl acrylate/methyl methacrylate/methacrylic acid (EA/MMA/MAA) copolymer and polyethylene glycol (PEG) [62]	Blended EA/MMA/MAA-PEG membranes with T_g near body temperature (32–42°C). Study of drug permeation through EPG membranes using acetaminophen (AAP) and aminopyrine (AMP). The permeability of AAP and AMP through the membranes increased steeply above T_g of the membranes.
	Elastin-like polypeptide (ELP) and N-isopropylacrylamide (NIPAAm)/acrylamide (AAm) copolymer [96]	Thermally responsive polymeric carriers in combination with hyperthermia to achieve a late significant increase in drug delivery to solid tumors.
	N-isopropylacrylamide (NIPAAm)/butyl methacrylate (BMA) copolymer and NIPAAm/acrylic acid (AA) copolymer [97]	Heparin release from NIPAAm/BMA copolymer gel showed temperature-dependent properties of the skin-type diffusional barrier formed on the gel surface.
	Hyaluronic acid (HA) [98]	Addition of hyaluronic acid HA to polyoxamer blends shown to be a useful tool to modify thermos-sensitive properties of polymeric platforms for drug delivery by engineering the gelation behaviour.

a) Nanotechnology in Drug Delivery Bioadhesives

Another exciting area of development in drug delivery bioadhesive systems employs nanotechnology in two different ways. One involves the use of bioadhesives in the form of nano-sized particles infused with a drug [7, 61]. The other consists of bioadhesive polymer matrices combined with a nanoparticle as a nanocomposite drug delivery system [3, 60, 102].

b) Nanoparticle Drug Delivery Systems

Advances in polymer science have led to the development of bioadhesive drug delivery nanospheres that have placed great emphasis on the bioadhesive properties in drug delivery. By combining the drug delivery function to a nano-sized drug carrier particle, the drug release and absorption characteristics can be modified by decreasing the particle size to the nano-scale. As a result, the active surface area for drug release increases dramatically [7, 61].

c) Nanocomposite Drug Delivery Systems

There are several reasons for combining nanoparticles with polymeric materials as composite drug delivery systems. For example, to be used in drug delivery, polymeric matrices must maintain suitable mechanical integrity during the drug dosage operation and during the administration of the drug to the host. Nanocomposite materials have been shown to provide the necessary strength and rheological properties, but the resulting

decreased water absorption capacity leads to reduced drug delivery rates [60]. Nano-clays, for example, are appropriate and safe fillers for drug delivery systems. The presence of clay nanoparticles can dramatically change the properties of the system, compared to common drug delivery polymer systems. The changes include enhanced mechanical properties as well as controlled release characteristics. It also alters erosion, swelling and dissolution behaviour of the polymer matrices and consequently influences drug delivery patterns. Moreover, the presence of clay in the polymer matrix changes the ionic strength of the composite material, which affects the release of the ionic drugs [3, 102].

2.10 Conclusion

In this review, we have not exhaustively reported on every instance of bioadhesive applications for tissue adhesion or drug delivery. Not surprisingly, many of the publications in the open literature report on the substitution of different bioadhesive polymers using similar methods, evaluation techniques and applications as were discussed here. As noted, there have been many advances in the design and synthesis of controlled drug release materials. At the same time, progress and significant interest in nanotechnology has led to the development of a broad range of polymer composite materials. These advances provide fertile ground for the development of new bioadhesives. Specific to tissue adhesives, there is a need for materials which can be applied to a broader range of tissue types and tissue environments (i.e., both wet and dry tissues). Another important research direction would see the combination of tissue

adhesives and drug delivery technology as a means to promote healing rates in pathologic surgeries.

2.11 Acknowledgments

The authors acknowledge the financial support of the Natural Sciences and Engineering Research Council of Canada.

2.12 References

[1] S. K. Roy, and B. Prabhakar, *Bioadhesive Polymeric Platforms for Transmucosal Drug Delivery Systems – a Review*, Tropical Journal of Pharmaceutical Research, **2010**, *9*: 91-104.

[2] J. D. Smart, *The Basics and Underlying Mechanisms of Mucoadhesion,* Advanced Drug Delivery Reviews, **2005**, *57*: 1556-1568.

[3] W. F. Lee, and Y. C. Chen, *Effect of Bentonite on the Physical Properties and Drug-Release Behavior of Poly (AA-co-PEGMEA)/Bentonite Nanocomposite Hydrogels for Mucoadhesive,* Journal of Applied Polymer Science, **2004**, *91*: 2934-2941.

[4] M. Matsuda, M. Inoue, and T. Taguchi, *Adhesive Properties and Biocompatibility of Tissue Adhesives Composed of Various Hydrophobically Modified Gelatins and Disuccinimidyl Tartrate*, Journal of Bioactive and Compatible Polymers, **2012**, *27*: 481-498.

[5] P. Ferreira, and M. H. Gil, *Development of a New Photocrosslinkable Biodegradable Bioadhesive,* Internationa Journal of Pharmaceutic, **2008**, *352*: 172-181.

[6] P. G. Mizina, V. A. Kurkin,1 M. A. Byakov, and P. P. Purygin, *A Device For Determining the Adhesion of Medicinal Films In Vitro,* Pharmaceutical Chemistry Journal, **2001**, *35*: 44-46.

[7] J. K. Vasir, K. Tambwekar, and S. Garg, *Bioadhesive Microspheres as a Controlled Drug Delivery System*, International Journal of Pharmaceutic, **2003,** *255*: 13-32.

[8] D. E. Packham, *Handbook of Adhesion*, 2nd Edition, John Wiley and Sons, Ltd., Bath UK, **2005.**

[9] L. Qie, and M. A. Dubé, *Manipulating Latex Polymer Microstructure using Chain Transfer Agent and Cross-linker to Modify PSA Performance and Viscoelasticity*, Macromolecular Reaction Engineering, **2011**, *5*: 117-128.

[10] G. E. Fonseca, T. F. M. McKenna, and M. A. Dubé, *Effect of Bimodality on the Adhesive Properties of PSA: Role of Bimodal Particle Size and Molecular Weight Distributions*, Industrial and Engineering Chemistry Research, **2010**, *49*: 7303-7312.

[11] W. F. Lee, and K. T. Tsao, *Effect of Silver Nanoparticles Content on the Various Properties of Nanocomposite Hydrogels by in Situ Polymerization*, *Journal of Material Science,* **2010**, *45*: 89-97.

[12] G. Tripathi, P. Choudhury and B. Basu, *Development of Polymer Based Biocomposites: a Review*, *Materials Technology*, **2010**, 25: 158-176.

[13] M. H. Casimiroa, M. H. Gil, and J. P. Leal, *Suitability of Gamma Irradiated Chitosan Based Membranes as Matrix in Drug Release System*, International Journal of Pharmaceutic, **2010**, 395: 142-146.

[14] D. S. Hwang, Y. Gim, H. J. Yoo, and H. J. Cha, *Practical Recombinant Hybrid Mussel Bioadhesive fp-151*, Biomaterial, **2007**. 28: 3560-3568.

[15] A. K. Dash, and G. C. Cudworth, *Therapeutic Applications of Implantable Drug Delivery Systems,* Journal of Pharmacological and Toxicological Methods, **1998**, 40: 1-12.

[16] T. Wang, X. Mu, H. Li, W. Wu, J. Nie, and D. Yang, *The Photocrosslinkable Tissue Adhesive Based on Copolymeric Dextran/HEMA*, Carbohydrate Polymers, **2013**, *92*: 1423-1431.

[17] P. Coulthard, H. Worthington, M. Esposito, M. Elst, O. Waes, and J. Cochrane, *Tissue Adhesives for Closure of Surgical Incisions*, Cochrane Database System Review. **2004**, *2*: 4287-4287.

[18] C. D. Hoemann, J. Sun, A. Légare, M. D. McKee, and M. D. Buschmann, *Tissue Engineering of Cartilage Using an Injectable and Adhesive Chitosan-Based Cell-Delivery Vehicle*, Osteoarthritis and Cartilage, **2005**, *13*: 318-329.

[19] D. F. Aukerman, and W. J. Sebastianelli, Clinical inquiries. *How Does Tissue Adhesive Compare with Suturing for Superficial lacerations*? Journal of Family Practice, **2005**, *54*: 378-378.

[20] W. F. Lee, and Y. C. Chen, *Effect of Hydrotalcite on the Physical Properties and Drug-Release Behavior of Nanocomposite Hydrogels Based on Poly[Acrylic Acid-co-Poly(Ethylene Glycol) Methyl Ether Acrylate] Gels*, Journal of Applied Polymer Science, **2004**, *94*: 692-699.

[21] Y. Onuki, M. Nishikawa, M. Morishita, and K. Takayama, *Development of Photocrosslinked Polyacrylic Acid Hydrogel as an Adhesive for Dermatological Patches:*

Involvement of Formulation Factors in Physical Properties and Pharmacological Effects, International Journal of Pharmaceutics, **2008**, *349*: 47-52.

[22] L. P. Bré, Y. Zheng, A. P. Pêgo, and W. Wang, *Taking Tissue Adhesives to the Future: from Traditional Synthetic to New Biomimetic Approaches*. Biomaterials Science, **2013**, *1*: 239-253.

[23] http://blog.mediligence.com/2013/02/06/the-changing-landscape-for-surgical-sealants-glues-hemostats-other-wound-closure-and-anti-adhesion/ accessed February 4th 2015.

[24] D. H. Sierra, *Fibrin Sealant Adhesive Systems: A Review of their Chemistry, Material Properties and Clinical Applications*, Journal of Biomaterials Applications, **1993**, *7*: 309-352.

[25] P. A. Leggat, U. Kedjarune, and D. R. Smith, *Toxicity of Cyanoacrylate Adhesives and their Occupational Impacts for Dental Staff*, Industrial Health, **2004**, *42*: 207-211.

[26] M. Mehdizadeh, H. Weng, D. Gyawali, L. Tang, and J. Yang, *Injectable Citrate-based Mussel-Inspired Tissue Bioadhesives with High Wet Strength for Sutureless Wound Closure*, Biomaterials, **2012**, *33*: 7972-7983.

[27] S. R. Mobley, J. Hilinski, and D. M. Toriumi, *Surgical Tissue Adhesives, Facial Plastic Surgery Clinics of North America*, **2002**, 10: 147-154.

[28] S. Salehpour, C. J. Zuliani, and M. A. Dubé, *Synthesis of Novel Stimuli-Responsive Polyglycerol-Based Hydrogels*, European Journal of Lipid Science and Technology, **2012**, *114*: 92-99.

[29] W. Puntuwat, S. Wongsa, J. Poonyawatpornkul, S. Punyanitya, and A. Raksujarit, *Processing and Characterization of Tissue Adhesive from Rice Starch Nanocomposites,* Advanced Materials Research, **2010**, *123-125*: 363-366.

[30] M. Ryou, and C.C. Thompson, *Tissue Adhesives: A Review*, Technics in Gastrointestinal Endoscopy, **2005**, *8*: 33-37.

[31] H. W. Sung, D. M. Huang, W. H. Chang, R. N. Huang, and J. C. Hsu, *Evaluation of Gelatin Hydrogel Crosslinked with Various Crosslinking Agents as Bioadhesives:* In *Vitro Study*, Journal of Biomedical Materials Research, **1999**, *46*: 520-530.

[32] B. Hoffmann, E. Volkmer, A. Kokott, P. Augat, M. Ohnmacht, N. Sedlmayr, M. Schieker, L. Claes, W. Mutschler, and G. Ziegler, *Characterisation of a New Bioadhesive System Based on Polysaccharides with the Potential to be Used as Bone Glue*, Journal of Materials Science Materials in Medicine, **2009**, *20:* 2001-2009.

[33] R. Anitha, S. Dudhania, and L. Kosaraju, *Bioadhesive Chitosan Nanoparticles: Preparation and Characterization*, Carbohydrate Polymers, **2010**, *81*: 243-251.

[34] N. Wattanakorn, P. Asavapichayont, J. Nunthanid, S. Limmatvapirat, S. Sungthongjeen, D. Chantasart, and P. Sriamornsak, *Pectin-based Bioadhesive Delivery of Carbenoxolone Sodium for Aphthous Ulcers in Oral Cavity*, AAPS Pharmaceutics Science and Technology, **2010**, *11*: 734-751.

[35] A. S. John, B. P. Sathesh, G. Divakar, M. K. Jangid, and K. K. Purohit, *Development and Evaluation of Buccoadhesive Drug Delivery System for Atorvastatin Calcium*, Journal of Current Pharmaceutical Research, **2010**, *1*: 31-38.

[36] N. A. El-Gendy, G. A. Abdelbary, M. H. EL-Komy, and A. E. Saafan, *Design and Evaluation of a Bioadhesive Patch for Topical Delivery of Gentamicin Sulphate,* Current Drug Delivery, **2009**, *6*: 50-57.

[37] B. Kriwet, E. Walter, and T. Kissel, *Synthesis of Bioadhesive Poly(acrylic acid) Nano- and Microparticles Using an Inverse Emulsion Polymerization Method for the Entrapment of Hydrophilic Drug Candidates*, Journal of Controlled Release, **1998**, *56*: 149-158.

[38] N. A. Nafee, N. A. Boraie, F. A. Ismail, and L. M. Mortada, *Design and Characterization of Mucoadhesive Buccal Patches Containing Cetylpyridinium Chloride*, Acta Pharmaceutica, **2003**, *53*: 199-212.

[39] T. F. T. Yvonne, K. K. Peh, and O. Al-Hanbali, *Effect of Carbopol and Polyvinylpyrrolidone on the Mechanical, Rheological, and Release Properties of Bioadhesive Polyethylene Glycol Gels*, AAPS Pharmaceutical Science and Technology, **2000**, *1*: 69-78.

[40] M. K. Nguyen, and D. S. Lee, Bioadhesive PAA-PEG-PAA Triblock Copolymer Hydrogels for Drug Delivery in Oral Cavity, *Macromolecular Research*, **2010**, *18*: 284-288.

[41] N. A. Peppas, and S. R. Stauffer, *Reinforced Uncrosslinked Poly(vinyl alcohol) Gels Produced by Cyclic Freezing–Thawing Processes: A Short Review*, Journal of Controlled Release, **1991**, *16*: 305-310.

[42] P. Deetae, S. Shobsngob, W. Varanyanond, P. Chinachoti, O. Naivikul, and S. Varavinit, *Preparation, Pasting Properties and Freeze–Thaw Stability of Dual Modified Crosslink-Phosphorylated Rice Starch*, Carbohydrate Polymers, **2008**, *73*: 351-358.

[43] C. S. N. Choong, D. W. Hutmacher, and J. T. Triffitt, *Co-culture of Bone Marrow Fibroblasts and Endothelial Cells on Modified Polycaprolactone Substrates for Enhanced Potentials in Bone Tissue Engineering*, Tissue Engineering, **2006**, *12*: 2521-2531.

[44] A. S. Hickey, and N. A. Peppas, *Solute Diffusion in Poly(Vinyl Alcohol)/Poly(Acrylic Acid) Composite Membranes Prepared by Freezing/Thawing Techniques*, Polymer, **1997**, *38*: 5931-5936.

[45] M. Ogris, G. Walker, T. Blessing, R. Kircheis, M. Wolschek, and E. Wagner, *Tumor-Targeted Gene Therapy: Strategies for the Preparation of Ligand-Polyethylene Glycol-Polyethylenimine/DNA Complexes*, Journal of Controlled Release, **2003**, *91*: 173-181.

[46] Y. Onuki, M. Hoshi, H. Okabe, M. Fujikawa, M. Morishita, and K. Takayama, *Formulation Optimization of Photocrosslinked Polyacrylic Acid Modified with 2-Hydroxyethyl Methacrylate Hydrogel as an Adhesive for a Dermatological Patch*, Journal of Controlled Release, **2005**, *108*: 331-340.

[47] J. P. Draye, B. Delaey, A. Van de Voorde, A. Van Den Bulcke, B. De Reu, and E. Schacht, *In Vitro and in Vivo Biocompatibility of Dextran Dialdehyde Cross-linked Gelatin Hydrogel Films*, Biomaterials, **1998**, *19*: 1677-1687.

[48] M. Alexandre, and P. Dubois, *Polymer-Layered Silicate Nanocomposites: Preparation, Properties and Uses of a New Class of Materials*, Materials Science and Engineering: R: Reports, **2000**, *28*: 1-63.

[49] S. P. Akhlaghi, R. C. Berry, and K. C. Tam, *Surface Modification of Cellulose Nanocrystal with Chitosan Oligosaccharide for Drug Delivery Applications*, Cellulose, **2013**, 20: 1747-1764.

[50] W. F. Lee, and K. T. Tsao, *Preparation and Properties of Nanocomposite Hydrogels Containing Silver Nanoparticles by ex Situ Polymerization,* Journal of Applied Polymer Science, **2006**, *100*: 3653-3661.

[51] M. Chamundeeswari, S. S. L. Sobhana, J. P. Jacob, M. G. Kumar, M. P. Devi, T. P. Sastry, and A. B. Mandal, *Preparation, Characterization and Evaluation of a Biopolymeric Gold Nanocomposite with Antimicrobial Activity,* Biotechnology and Applied Biochemistry, **2010**, *55*: 29-35.

[52] S. J. Ahn, S. J. Lee, J. K. Kook, and B. S. Lim, E*xperimental Antimicrobial Orthodontic Adhesives Using Nanofillers and Silver Nanoparticles*, Dental Materials, **2009**, *25*: 206-213.

[53] R. Koonawoot, S. Punyanitya, C. Tirapong, K. Boonchom, and A. Raksujarit, *Fabrication of Gelatin/Carbon Nanocomposite for Human Tissue Adhesive*, Advanced Materials Research, **2010**, *123-125*: 327-330.

[54] A. Harsulkar, and S. A. Sreenivas, *Design and Development of Bioadhesive Bucal Drug Delivery System of Carvedilol,* International Journal of Science Innovations and Discoveries, **2012**, *2*: 580-597.

[55] A. S. Hoffman, *The Origins and Evolution of "Controlled" Drug Delivery Systems*, Journal of Controlled Release, **2008**, *132*: 153-163.

[56] K. Park, and J. R. Robinson, *Bioadhesive Polymers as Platforms for Oral Controlled Drug Delivery: Method to Study Bioadhesion*, International Journal of Pharmaceutics, **1984**, *198*: 107-127.

[57] F. Gabor, M. P. Szostak, and W. Lubitz, *An Adhesive Drug Delivery System Based on K99-fimbriae*, European Journal of Pharmaceutical Sciences, **1995**, *3*: 293-299.

[58] K. Klokkers-Bethke, and W. Fischer, *Development of a Multiple Unit Drug Delivery System for Positioned Release in the Gastrointestinal Tract*, Journal of Controlled Release, **1991**, *15*: 105-112.

[59] P. Gupta, K. Vermani, and S. Garg, *Hydrogels: from Controlled Release to pH-Responsive Drug Delivery*, Drug Discovery Today, **2002**, *7:* 569-579.

[60] C. Viseras, C. Aguzzi, P. Cerezo and M. C. Bedmar, *Biopolymer–Clay Nanocomposites for Controlled Drug Delivery*, Materials Science and Technology, **2008**, *24*: 1020-1026.

[61] K. S. Soppimath, T. M. Aminabhavi, A. R. Kulkarni, and W. E. Rudzinski, *Biodegradable Polymeric Nanoparticles as Drug Delivery Devices*, Journal of Controlled Release, **2001**, *70*: 1-20.

[62] J. Fujimori, Y. Yoshihashi, E. Yonemochi, and K. Terada, *Application of Eudragit RS to Thermo-Sensitive Drug Delivery Systems II. Effect of Temperature on Drug*

Permeability Through Membrane Consisting of Eudragit RS/PEG 400 Blend Polymers, Journal of Controlled Release, **2005**, *102*: 49-57.

[63] S. M. Herbig, J. R. Cardinal, R. W. Korsmeyer, and K. L. Smith, *Asymmetric-Membrane Tablet Coating for Osmotic Drug Delivery*, Journal of Controlled Release, **1995**, *35*: 127-136.

[64] C. S. Yong, J. S. Choi, Q. Z. Quan, J. D. Rhee, C. K. Kim, S. J. Lim, K. M. Kim, P. S. Oh, and H. G. Choi, *Effect of Sodium Chloride on the Gelation Temperature, Gel Strength and Bioadhesive Force of Poloxamer Gels Containing Diclofenac Sodium*, International Journal of Pharmaceutics, **2001**, *226*: 195-205.

[65] http://www.dolcera.com/wiki/index.php?title=Smart_Drug_Delivery_Systems accessed April 2013.

[66] M. Ramdas, K. Dileep, Y. Anitha, W. Paul, and C. Sharma, *Alginate Encapsulated Bioadhesive Chitosan Microspheres for Intestinal Drug Delivery*, Journal of Biomaterials Applications, **1999**, *13*: 290-296.

[67] Z. Ahmad, and G. K. Khuller, *Alginate-Based Sustained Release Drug Delivery Systems for Tuberculosis, Expert Opinion on Drug Delivery,* **2008**, *5*, 1323-1334.

[68] M. Mahkam, *Bioadhesive Alginate Copolymers as Platforms for Oral Delivery of Insulin*, Nature and Science, **2009**, *7*: 61-69.

[69] M. R. JimCnez-Castellanos, H. Zia, C. T. Rhodes, *Design and Testing in Vitro of a Bioadhesive and Floating Drug Delivery System for Oral Application,* International Journal of Pharmaceutics, **1994**, *105*: 65-70.

[70] J. H. Park, G. Saravanakumar, K. Kim, I. C. Kwon, *Targeted Delivery of Low Molecular Drugs Using Chitosan and its Derivatives*, Advanced Drug Delivery Review. **2010**, *62*: 28-41.

[71] C. E. Kast, C. Valenta, M. Leopold, and A. Bernkop-Schnurch, *Design and in Vitro Evaluation of a Novel Bioadhesive Vaginal Drug Delivery System for Clotrimazole*, Journal of Controlled Release, **2002**, *81*: 347-354.

[72] O. Felt, P. Buri, and R. Gurny, *Chitosan: A Unique Polysaccharide for Drug Delivery*, Drug Development and Industrial Pharmacy, **1998**, *24*: 979-993.

[73] X. Wang, Y. Du, J. Luo, B. Lin, and J. F. Kennedy, *Chitosan/Organic Rectorite Nanocomposite Films: Structure, Characteristic and Drug Delivery Behaviour*, Carbohydrate Polymers, **2007**, *69*: 41-49.

[74] C. H. Lee, A. Singla, and Y. Lee, *Biomedical Applications of Collagen*, International Journal of Pharmaceutics, **2001**, *221*: 1-22.

[75] S. Miyazaki, N. Kawasaki, T. Nakamura, M. Iwatsu, T. Hayashi, W. M. Hou, and D. Attwood, *Oral Mucosal Bioadhesive Tablets of Pectin and HPMC: in Vitro and in Vivo Evaluation*, International Journal of Pharmaceutics, **2000**, *204*: 127-132.

[76] R. Cortesi, E. Esposito, M. Osti, G. Squarzoni, E. Menegatti, S. S. Davis, and C. Nastruzzi, *Dextran Cross-linked Gelatin Microspheres as a Drug Delivery System*, European Journal of Pharmaceutics and Biopharmaceutics, **1999**, *47*: 153-160.

[77] S. Geresh, G. Y. Gdalevsky, I. Gilboa, J. Voorspoels, J. P. Remon, and J. Kost, *Bioadhesive Grafted Starch Copolymers as Platforms for Peroral Drug Delivery: a Study of Theophylline Release,* Journal of Controlled Release, **2004**, *94*: 391-399.

[78] N. Garcia-Gonziilez, I. W. Kellaway, H. Blanco-Fuente, S. Anguiano-Igea, B. Delgado-Charro, F. J. Otero-Espinar and J. Blanco-Mendez, *Design and Evaluation of Buccoadhesive Metoclopramide Hydrogels Composed of Poly(acrylic acid) Crosslinked with Sucrose,* International Journal of Pharmaceutics, **1993**, *100*: 65.-70.

[79] A. N. Lukyanov, Z. Gao, and V. P. Torchilin, *Micelles from Polyethylene Glycol /Phosphatidylethanolamine Conjugates for Tumor Drug Delivery,* Journal of Controlled Release, **2003**, *91*: 97-102.

[80] S. K. Bajpai, and S. S. Saggu, *Insulin Release Behavior of Poly (Methacrylamide-co-N-vinyl-2-Pyrrolidone-co-Itaconic Acid) Hydrogel: An Interesting Probe. Part II,* Journal of Macromolecular Science Part A: Pure and Applied Chemistry, **2007**, *44*: 153-158.

[81] W. B. Liechty, D. R. Kryscio, B. V. Slaughter, and N. A. Peppas, *Polymers for Drug Delivery Systems,* Annual Review of Chemical and Biomolecular Engineering, 2010, *1*: 149-173.

[82] Z. Pavelic, N. Skalko-Basnet, and I. Jalsenjak, *Characterisation and in Vitro Evaluation of Bioadhesive Liposome Gels for Local Therapy of Vaginitis,* International Journal of Pharmaceutics, **2005**, *301*: 140-148.

[83] K. Pal, A. K. Banthia, and D. K. Majumdar, *Polymeric Hydrogels: Characterization and Biomedical Applications –A Mini Review,* Designed Monomers and Polymers, **2009**, *2*: 197-220.

[84] R. Dinarvand, N. Sepehri, S. Manoochehri, H. Rouhani, and F. Atyabi, *Polylactide-co-Glycolide Nanoparticles for Controlled Delivery of Anticancer Agents*, International Journal of Nanomedicine, **2011**, *6*: 877-895.

[85] H. Murakami, M. Kobayashi, H. Takeuchi, and Y. Kawashima, *Preparation of poly(DL-lactide-co-glycolide) Nanoparticles by Modified Spontaneous Emulsification Solvent Diffusion Method,* International Journal of Pharmaceutics, **1999**, *187*: 143-152.

[86] H. Parmar, S. Bakliwal, N. Gujarathi, B. Rane, and S. Pawar, *Different Methods of Formulation and Evaluation of Mucoadhesive Microsphere,* International Journal of Applied Biology and Pharmaceutical Technology, **2010**, *1*: 1157-1167.

[87] H. Takeuchi, H. Yamamoto, and Y. Kawashima, *Mucoadhesive Nanoparticulate Systems for Peptide Drug Delivery,* Advanced Drug Delivery Reviews, **2001**, *47*: 39-54.

[88] Y. H. Liu, X. Zhu, D. Zhou, Y. Jin, C. Y. Zhao, Z. R. Zhang, and Y. Huang, *pH-Sensitive and Mucoadhesive Microspheres for Duodenum-Specific Drug Delivery System,* Drug Development and Industrial Pharmacy, **2011**, *37*: 868-874.

[89] M. L. Hans, and A. M. Lowman, *Biodegradable Nanoparticles for Drug Delivery and Targeting,* Current Opinion in Solid State Materials Science, **2002**, *6*: 319-327.

[90] M. R. Aguilar, C. Elvira, A. Gallardo, B. Vázquez, and J. S. Román, *Smart Polymers and Their Applications as Biomaterials,* Topics in Tissue Engineering, **2007**, *3*: 1-27.

[91] A. S. Hoffman, *Stimuli-Responsive Polymers: Biomedical Applications and Challenges for Clinical Translation,* Advanced Drug Delivery Reviews, **2013**, *65*: 10-16.

[92] S. W. Choi, Y. Zhang, and Y. Xia, *A Temperature-Sensitive Drug Release System Based on Phase-Change Materials,* Angewandte Chemie, International Eddition, **2010**, *49*: 7904-7908.

[93] O. Pillai, and R. Panchagnula, *Polymers in Drug Delivery*, Current Opinion in Chemical Biology, **2001**, *5*: 447-451.

[94] M. K. Nguyen, C. T. Huynh, and D. S. Lee, *pH-Sensitive and Bioadhesive Poly(β-amino ester)-Poly(ethylene glycol)-Poly(β-amino ester) Triblock Copolymer Hydrogels with Potential for Drug Delivery in Oral Mucosal Surfaces*, Polymer, **2009**, *50*: 5205-5210.

[95] M. V. Risbud, A. A. Hardikar, S. V. Bhat , and R. R. Bhonde, *pH-Sensitive Freeze-Dried Chitosan–Polyvinyl Pyrrolidone Hydrogels as Controlled Release System for Antibiotic Delivery*, Journal of Controlled Release, **2000**, *68*: 23-30.

[96] D. E. Meyer, B. C. Shin, G. A. Kong, M. W. Dewhirst, and A. Chilkoti, *Drug Targeting Using Thermally Responsive Polymers and Local Hyperthermia*, Journal of Controlled Release, **2001**, *74*: 213-224.

[97] Y. H. Bae, J. Feijen, and S. W. Kim, *Heparin Release from Thermosensitive Hydrogels*, Journal of Controlled Release, **1992**, *22*: 95-104.

[98] L. Mayol, F. Quaglia, A. Borzacchiello, L. Ambrosio, and M. I. La Rotonda, A Novel Poloxamers/Hyaluronic Acid In Situ Forming Hydrogel for Drug Delivery:

Rheological, Mucoadhesive and In Vitro Release Properties, *European Journal of Pharmaceutics and Biopharmaceutics,* **2008**, 70: 199-206.

[99] Y. Qiu, and K. Park, *Environment-Sensitive Hydrogels for Drug Delivery*, Advanced Drug Delivery Reviews, **2012**, *64*: 49-60.

[100] K. Sawahata, M. Hara, H. Yasunaga, and Y. Osada, *Electrically Controlled Drug Delivery System Using Polyelectrolyte Gels*, Journal of Controlled Release, **1990**, *14*: 253-262.

[101] S. H. Yuk, S. H. Cho, and H. B. Lee, *Electric Current-Sensitive Drug Delivery Systems Using Sodium Alginate/Polyacrylic Acid Composite*, Pharmaceutical Research, **1992**, *9*: 955-957.

[102] Y. Dong, and S. Feng, *Poly(D,L-lactide-co-glycolide)/Montmorillonite Nanoparticles for Oral Delivery of Anticancer Drugs*, Biomaterials, **2005**, *26*: 6068-6076.

Chapter 3: Effect of pH on Poly(acrylic acid) Solution Polymerization

S. Khanlari and M. A. Dubé, *Journal of Macromolecular Science, Part A: Pure and Applied Chemistry* (2015), Volume 52, pages 587–592.

Abstract: The free-radical redox-initiated aqueous solution polymerization of fully and partially neutralized acrylic acid was carried out at room temperature under full exposure to air. The effect of neutralization degree on the polymerization rate and product properties was studied. Increasing neutralization of the reaction mixture with sodium hydroxide resulted in greater conversion of acrylic acid to sodium acrylate. The rate of polymerization, determined from a gravimetric off-line water removal technique, was shown to decrease significantly with decreasing degree of neutralization. Molecular weight also decreased with decreasing degree of neutralization. The glass transition temperature and hydrophilicity of the polymer product decreased with increasing degree of neutralization. In-line infrared monitoring was also used to monitor the reaction progress and was shown to be an effective tool for this purpose.

3.1 Introduction

Poly(acrylic acid), also known as carbomer, has found widespread use as a superabsorbent polymer, a dispersant, and in many other applications [1, 2]. Poly(acrylic acid) is of particular interest because it is biocompatible and biodegradable [3]. Its

carboxylic acid functionality also imparts very high adhesive strength when it is in contact with animal tissues [4]. Moreover, it has been used in drug delivery systems [5].

Poly(acrylic acid) responds to changes in pH and ionic strength with changes in its properties; e.g., at pH < 4 precipitation occurs in aqueous solutions due to protonation of the carboxylate groups, which renders the polymer sparsely soluble in water [6]. Gao and Penlidis provide an exceptionally complete review of acrylic acid polymerization kinetics and modeling [7].

a)

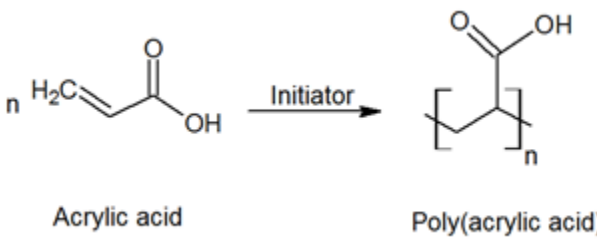

b)

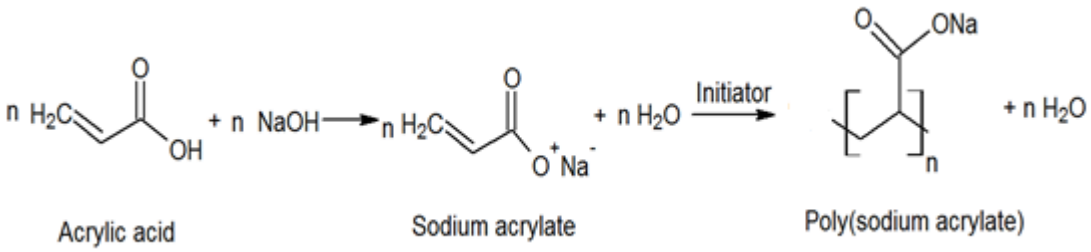

Figure 3.1 Schematic representation of a) Poly(acrylic acid) synthesis and b) Poly(sodium acrylate) synthesis.

The polymerization of acrylic acid is highly affected by the pH level of the reaction mixture (see Figure 3.1). For example, in the presence of dissolved sodium

hydroxide, neutralization converts the acrylic acid monomer to sodium acrylate monomer (see Figure 3.1b).

Poly(acrylic acid) has been synthesized via different radical polymerization methods e.g., inverse emulsion polymerization [8] and bulk polymerization [9, 10]. In bulk polymerization, the growing polymer chains are not soluble in the monomer resulting in a precipitation polymerization; this may pose practical challenges in terms of mixing and heat transfer. Solution polymerization provides a simple and effective means around these issues.

Redox initiation is a very effective method of generating free radicals under mild conditions to initiate polymerization. This method has found wide application in low-temperature emulsion polymerizations [11]. We recently investigated the aqueous solution polymerization of poly(sodium acrylate) using a redox initiation system for the purpose of nanocomposite production [12]. In that work, the reaction medium was fully neutralized. Given that poly(acrylic acid) is a pH responsive polymer [5], it is desired to further investigate the effect of pH on the polymerization mechanism and product properties.

3.2 Experimental

3.2.1 Materials

Stabilized acrylic acid 99.5%+ (Acros Organics), NaOH pellets (Sigma Aldrich), ammonium persulfate 98%+ ($(NH_4)_2S_2O_8$) (APS) (Sigma Aldrich) and potassium disulfite ($K_2S_2O_5$) (PDS) (Sigma Aldrich) were used directly without further purification.

The solvent was distilled deionized water (DDW) and hydroquinone (JT Baker Chemicals) was used to short-stop the reaction.

3.2.2 Synthesis

The pH of the reaction mixture in this study was varied from 7 to 4 for different runs. Pre-determined amounts of NaOH based on the formulation (see Table 3.1) dissolved in 26 mL of DDW were added to 14.9 g acrylic acid and stirred by magnetic stirrer in a 200 mL beaker at room temperature and under full exposure to the atmosphere. 0.35 g of APS and 0.34 g of PDS, each dissolved in 3 mL of DDW separately, were added to the monomer mixture. Almost immediately, the reaction mixture viscosity increased significantly and polymer formation was observed. A temperature increase of ~60 ^{o}C was noted in each experiment. More details about the synthesis are mentioned elsewhere [12]. Table 3.1 shows the amounts of NaOH added to the monomer mixture.

Table 3.1 Reaction formulation.

Run #	**Sample name**	**NaOH (g)**	**pH of the reaction mixture**
1	NaA7	8.3	7
2	NaA6	7	6
3	NaA5	5.5	5
4	NaA4	2.8	4

3.2.3 Characterizations

Monomer conversion (x in wt. %) was measured using a standard gravimetric method based on total dried polymer weight based on water removal method.

$$x(wt.\%) = \frac{\%\,Solids - Any\ Solids\ (neutralizer,\ \ initiator,\ldots)wt.\%}{Initial\ wt.\%\ of\ monomer} \times 100 \qquad (3.1)$$

where

$$\%\,Solids = \frac{Dry\ polymer}{Initial\ sample} \times 100 \qquad (3.2)$$

The polymer was dried in a vacuum oven at room temperature for a minimum of 24 h until a constant dry weight was achieved. Because the material is a homopolymer, the conversion in equation (3.1) is theoretically equivalent to:

$$x\ (mol\%) = \frac{[M]_0 - [M]_t}{[M]_0} \times 100 \qquad (3.3)$$

where $[M]_0$ is the initial concentration of the monomer and $[M]_t$ is the concentration of the monomer at time *t*.

The chemical structure of the products was studied via ATR-FTIR spectroscopy using a ReactIR45™ (Mettler Toledo) in-line fibre optic probe immersed in the reaction mixture. The ReactIR45™ permits one to track polymer formation and/or monomer disappearance. Spectra were obtained within the range of 3000–650 cm^{-1}. The reaction temperature was also recorded by the probe. A multivariate calibration model was developed using the QUANTIR ("iC IR 4.3") software provided with the ReactIR45™.

Measurement of the polymer molecular weight and distribution was accomplished using a Waters gel permeation chromatograph (GPC). The GPC system consisted of a Waters 610 Fluid Unit pump, a Waters 410 differential refractometer, and a PL aquagel-OH 30 8µm column. The sample injection volume was 50 µL and the mobile phase,

water, was run at 1 mL min^{-1}. All samples were dissolved in water to a concentration of 5 mg/mL and filtered through a 0.45 μm disposable poly(vinylidene fluoride) membrane filter (Whatman) prior to injection. Poly(ethylene oxide) (PEO) standards (Agilent) were used to construct a calibration curve for analysis using a universal calibration technique. The following Mark-Houwink parameters were used as part of the universal calibration to calculate the molecular weight of the synthesized polymers: for PEO, α = 0.7800 and K= 0.0001250 $cm^3\,g^{-1}\,mol^{-1}$; and for poly(acrylic acid), α = 0.50 and K = 0.001740 $cm^3\,g^{-1}\,mol^{-1}$ for M_w <20,000, and α = 0.86 and K = 0.000040 $cm^3\,g^{-1}\,mol^{-1}$ for M_w >20,000.

Differential scanning calorimetry (DSC) was performed using a TA instruments (DSC Q1000) using aluminium crimped pans at a heating rate of 10 ^oC/min under nitrogen atmosphere (flow rate = 20 mL/min) in the range of 0 to 300 ^oC. The sample size was between 4 and 10 mg.

For determination of the wettability (or hydrophilicity) of the synthesized polymers at different pH, the contact angles of a films produced from the synthesized polymers were measured using the Sessile drop method in a video contact angle VCA-Optima system at room temperature. The droplet size was set at 2 μL and five samples were used for each test. Prior to performing the water contact angle measurements, the films were dried and stored in a vacuum oven at 40 °C overnight.

3.3 Results and Discussion

As noted earlier and shown in Table 3.1, four reaction formulations were tested. An additional run was conducted using acrylic acid with no added NaOH at a pH = 2. In that

case, no polymerization occurred. For the case of a fully neutralized sample (run 1 in Table 3.1), pure poly(sodium acrylate) was produced (see Figure 3.1b). For the cases where neutralization was not complete, i.e., at pH <7, poly(acrylic acid-*co*-sodium acrylate) copolymers were synthesized, as shown in Figure 3.2.

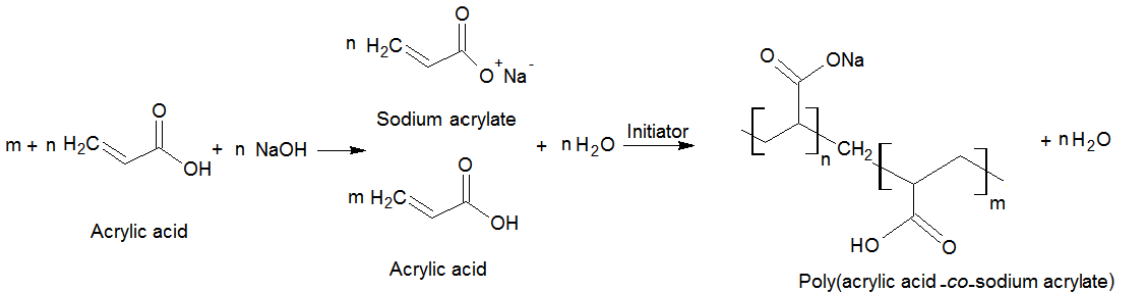

Figure 3.2 Schematic representation of poly(acrylic acid-*co*-sodium acrylate) synthesis.

In Figure 3.3, the ATR-FTIR spectra of the polymers synthesized at different pH, are shown. Peak assignments for the polymerization of pure poly(acrylic acid) and pure poly(sodium acrylate) were reported previously [12]. For the present study, we focus on only the more relevant peaks. For run NaA7 (pH = 7), there are absorbance peaks at 1555 cm^{-1} and 1660 cm^{-1}. The peak appearing at 1555 cm^{-1} is assigned to COO^- while the peak present at 1660 cm^{-1} is assigned to -ONa in poly(sodium acrylate). With decreasing pH (i.e., from run NaA7 to NaA4), a shoulder appears at 1704 cm^{-1}; this peak is assigned to C-OH of poly(acrylic acid). The intensity of the shoulder increases with decreasing pH. One can conclude that the polymer synthesized under fully neutralized conditions (i.e., NaA7) contains only poly(sodium acrylate) and no poly(acrylic acid). With decreasing amounts of NaOH in the reaction mixture (i.e., lower pH) there will be some acrylic acid monomer left unconverted to sodium acrylate. Thus, with decreasing pH, one gets greater

amounts of unconverted acrylic acid and polymers with a range of poly(acrylic acid-*co*-sodium acrylate) compositions.

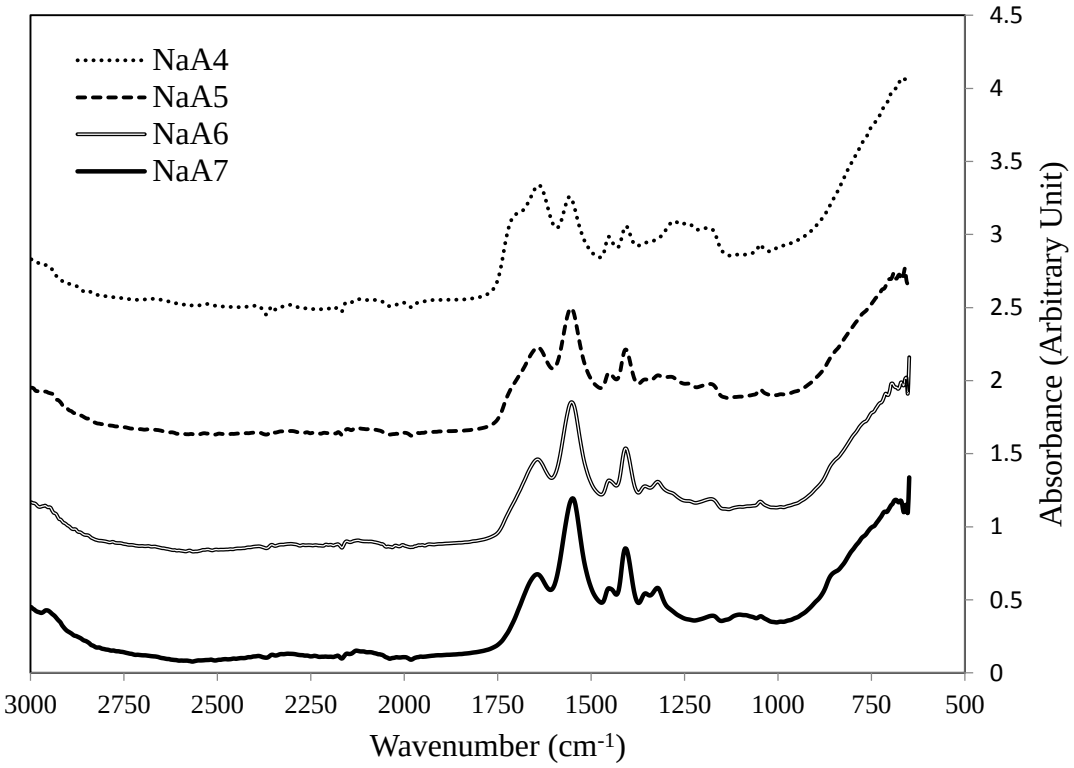

Figure 3.3 ATR-FTIR spectra of the polymers synthesized at different pH (at final conversion).

The reaction kinetics of acrylic acid polymerization at different pH were reviewed by Gao and Penlidis [7]. Herein, we provide a simplified approach as our goals are not to describe all kinetic aspects of the polymerization but rather to focus on the product properties resulting from changes in neutralization.

Figure 3.4 depicts the conversion calculated from off-line gravimetry versus time for different runs. Figure 3.4 shows that polymerization progress reduces noticeably with decreasing degree of neutralization. The rate of polymerization which is proportional to

the slope of the conversion vs. time curves shows that at full neutralization (run NaA7) the highest polymerization rate was achieved. In addition, the fully neutralized reaction mixture reached a higher conversion than the partially neutralized runs. Gao and Penlidis modeled conversion versus time for acrylic acid polymerized at different degrees of neutralization (up to pH =5) and showed similar trends [7].

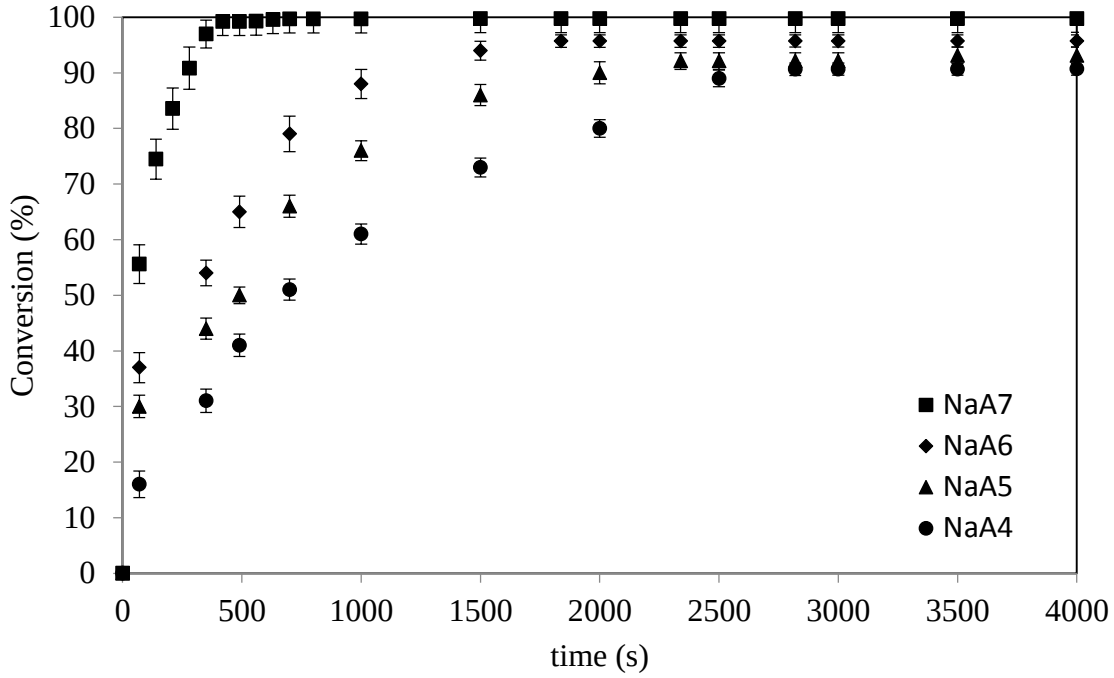

Figure 3.4 Conversion versus time for polymers produced at different degrees of neutralization.

Aside from off-line gravimetric measurements, ATR-FTIR spectroscopy (using the ReactIR45™ in-line fibre optic probe) was used to monitor monomer conversion. The polymerizations studied herein were highly exothermic as evidenced by the reaction temperature profiles for each reaction (see Figure 3.5). The effect of temperature was accounted for when developing a calibration model for ATR-FTIR reaction monitoring.

A procedure similar to that used for the ATR-FTIR monitoring of poly(sodium acrylate) nanocomposites was used herein [13]. A multivariate partial least squares (PLS) calibration with temperature correction was employed.

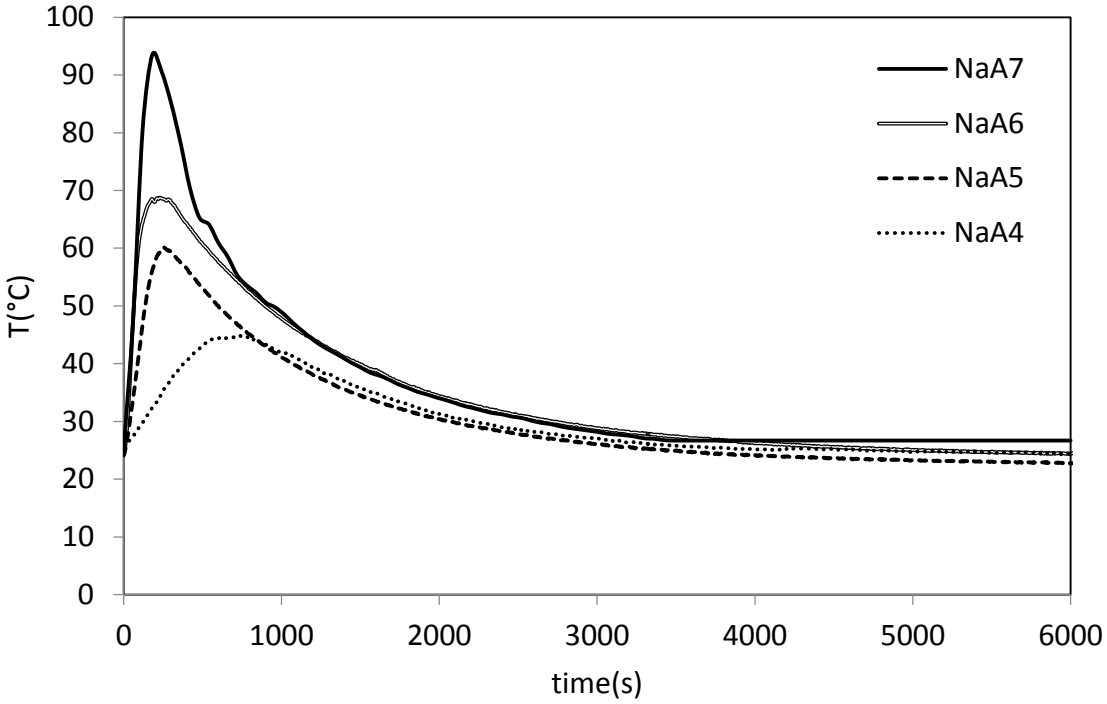

Figure 3.5 Polymerization temperature profiles as a function of different degrees of neutralization.

Figure 3.6 shows how the predicted residual error sum of squares (PRESS) and root mean square error of calibration (RMSEC) values changed with the number of factors used in the multivariate PLS model development. The optimum number of factors for the calibration model was nine. This calibration model was developed using the QUANTIR ("iC IR 4.3") software provided with ReactIR45™. It should be noted that only the data from one run (i.e., PNaA7) were used to generate the calibration model and predict

conversion for the other runs. Figure 3.7 depicts the effectiveness of the calibration model with a coefficient of determination, R^2, of 0.9819. This R^2 value implies that 98.19% of the total variation in predicted conversions can be explained by the linear relationship between the actual conversion and the predicted conversion.

a)

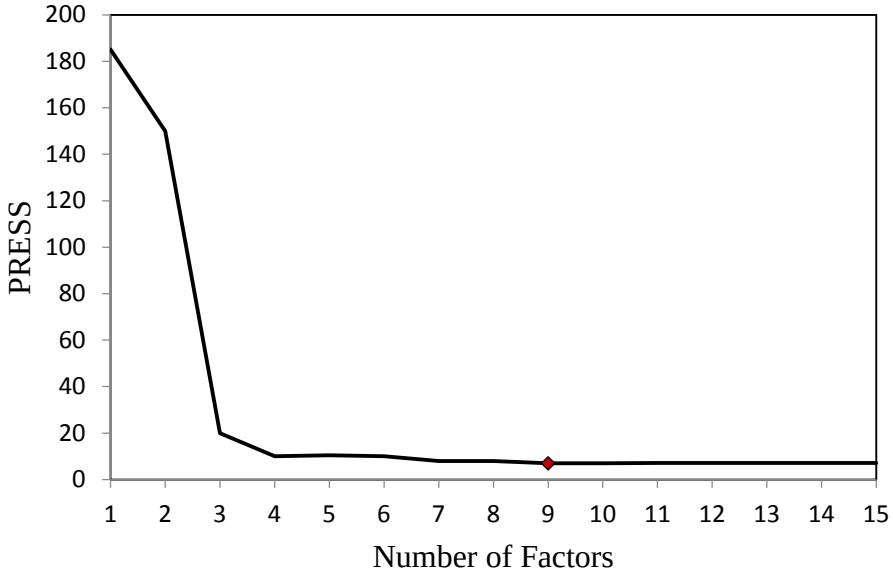

b)

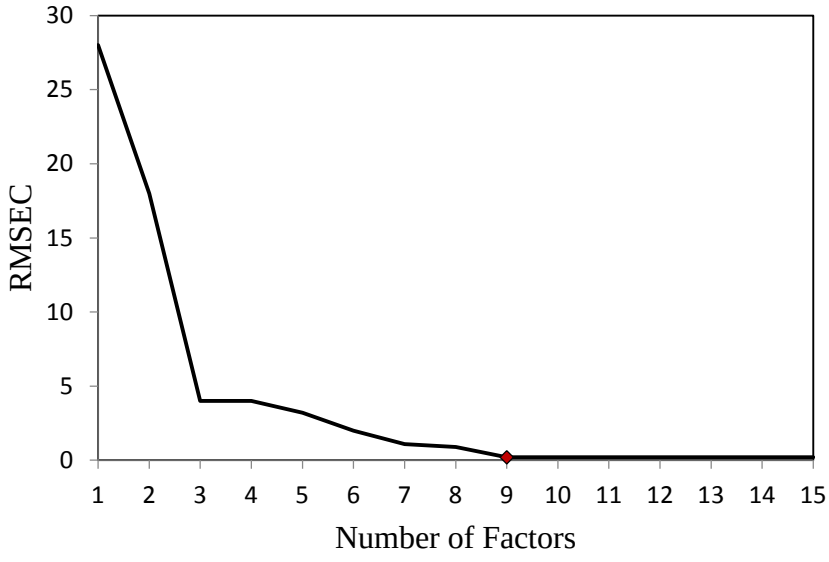

Figure 3.6 a) PRESS analysis and b) RMSEC analysis for the multivariate PLS model.

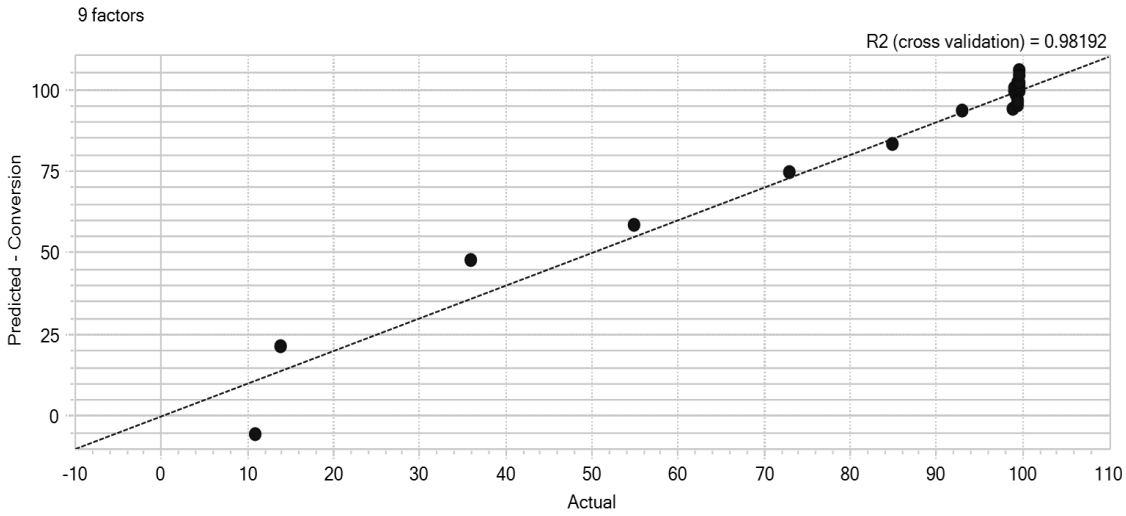

Figure 3.7 Actual versus predicted conversion for calibration model developed using on-line data from run PNaA7.

It should be noted that the peak that appeared at 1660 cm^{-1} was not involved in the model training as the intensity of that peak is not only a function of polymerization progress but also it varies based on the pH of the reaction mixture. If it was not so, the model trained earlier [13] could have been used in this case too.

In order to validate the accuracy and applicability of the PLS multivariate model, data from runs #2, #3 and #4, (not included in the calibration data) were compared to PLS model predictions (see Figure 3.8). According to Hua et al. the error expected from the ReactIR45™ is ±3 wt% [14]. According to Figure 3.8, the prediction of the reaction conversion, validated using the off-line gravimetric data, is excellent over the full conversion range. A paired comparison was carried out between the monomer conversion obtained by off-line data calculated via gravimetry and the PLS multivariate model

predictions. 95% confidence intervals for the paired comparisons were [-1.3405, 0.2782] (mol%) for PNaA6, [-0.8709, 0.4802] (mol%) for PNaA5 and [-0.085, 1.1398] (mol%) for PNaA4. As each of these intervals contains *zero*, no significant difference between the in-line and off-line data exists and the ATR-FTIR method is shown to be effective in predicting a wide range of reaction conditions for this polymer system.

a)

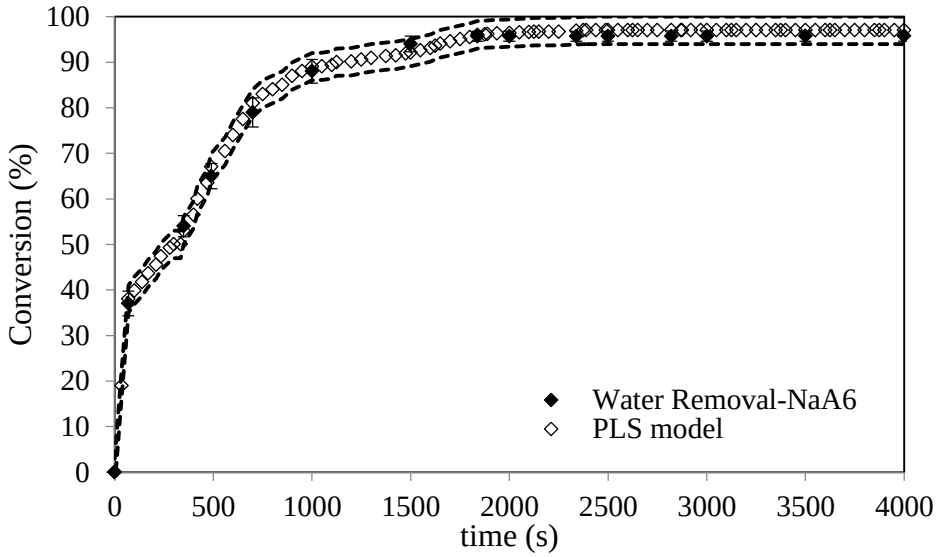

b)

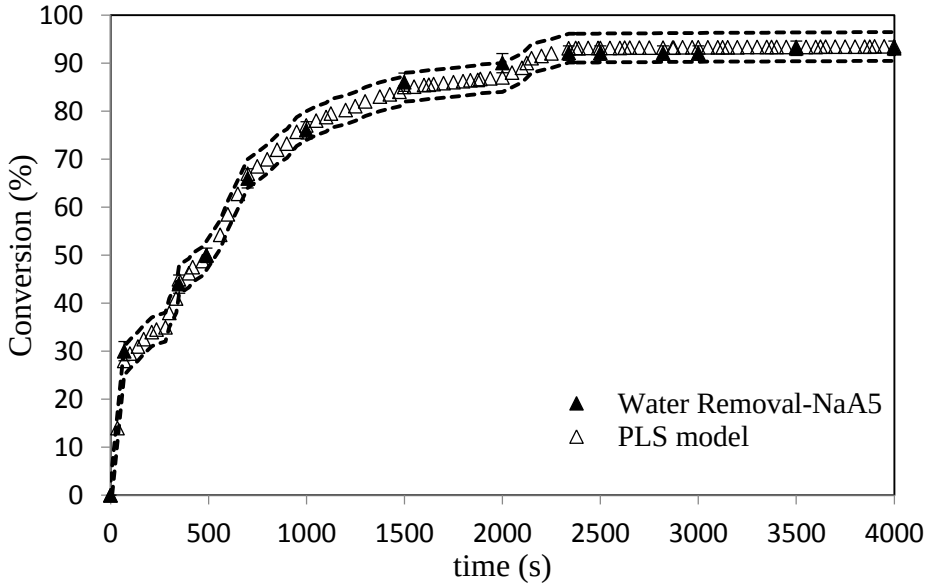

c)

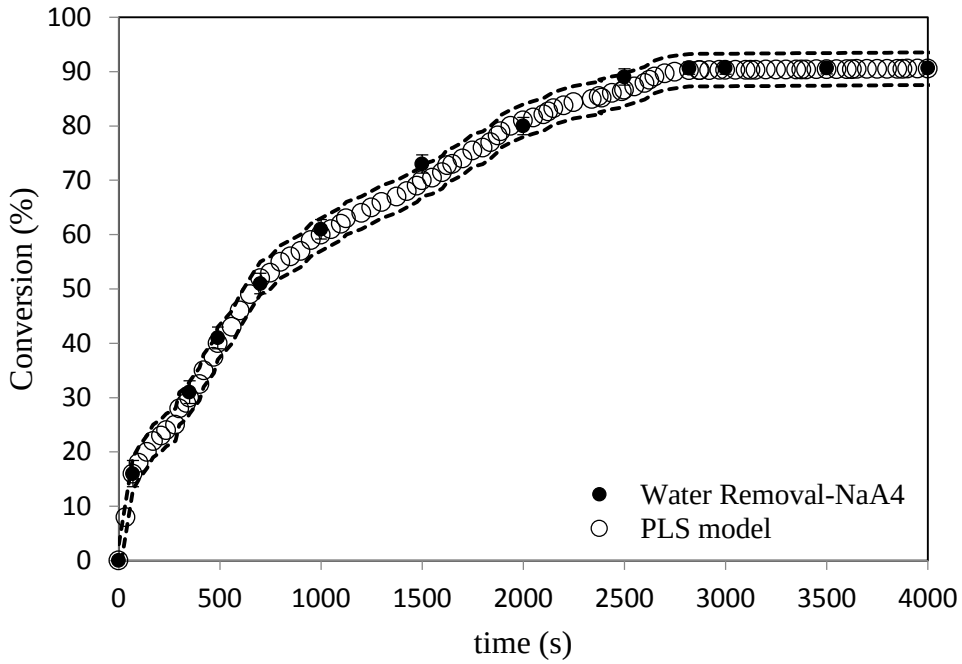

Figure 3.8 ATR-FTIR reaction monitoring for a) PNaA6 b) PNaA5 c) PNaA4.

Figure 3.8 also shows that by decreasing the degree of neutralization, the overall monomer conversion decreased and more residual monomer remained in the polymer product. Residual monomer is obviously not desirable for biomedical applications and thus, higher degrees of neutralization would be desired.

Table 3.2 shows the molecular weight and polydispersity index (PDI) for the polymers synthesized at different pH. As noted earlier, the effect of the decrease in extent of neutralization was to decrease the reaction rate. The molecular weight increase with degree of neutralization is entirely consistent with the reaction rate trends seen earlier in Figure 3.4; that is, the higher rate of polymerization in NaA7 corresponds to a higher

molecular weight. In all of the samples, the PDI remained the same despite changes in molecular weight.

Table 3.2 Molecular weight and distribution of polymers synthesized at different pH.

Sample	**$\bar{M}_n$ (g/mol)**	**$\bar{M}_w$ (g/mol)**	**PDI**
NaA7	76600	79600	1.04
NaA6	70700	73400	1.04
NaA5	67900	70500	1.04
NaA4	64000	66400	1.04

DSC analysis was used to determine the glass to rubber transition temperature (T_g) of the amorphous polymers (see Figure 3.9). For the polymer sample from run NaA7 the T_g was 114.4 °C, while the T_g decreased to 110.3, 72.46 and 44.92 °C for NaA6, NaA5 and NaA4, respectively. The changes in polymer composition or more specifically, the conversion of acrylic acid to sodium acrylate due to increasing neutralization yielded a change in T_g. This trend in T_g is likely due to the limitations in movement of the bulkier -O-Na groups due to sodium acrylate compared to -O-H groups associated with acrylic acid. For all of the polymers synthesized at partially neutralized pH (NaA6, NaA5 and NaA4) only one distinct T_g was observed (see Figure 3.9) which implies that the synthesized polymers are copolymers of acrylic acid and sodium acrylate rather than a mixture of two homopolymers.

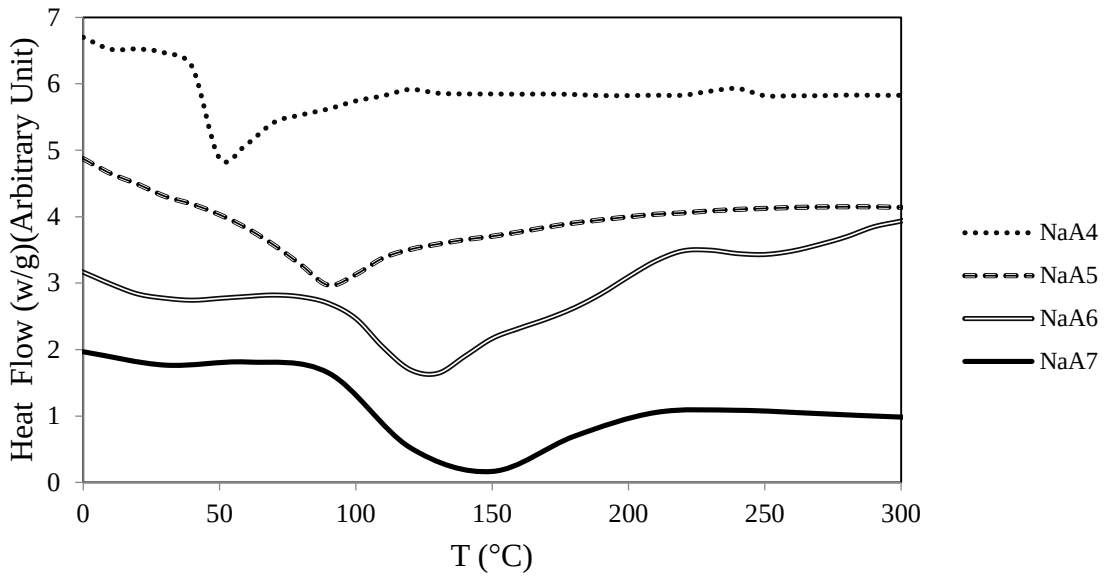

Figure 3.9 DSC thermograms of polymers synthesized at different pH.

Figure 3.10 shows the hydrophilicity of the polymers synthesized at different pH. The lower reaction mixture pH resulted in lower contact angles, i.e., polymers synthesized at lower pH are more hydrophilic. It was shown earlier in the ATR-FTIR spectra that by increasing the amount of NaOH in the reaction mixture more acrylic acid monomers were converted to sodium acrylate and the polymers synthesized contain more -ONa rather than –OH groups, the latter of which are more hydrophilic.

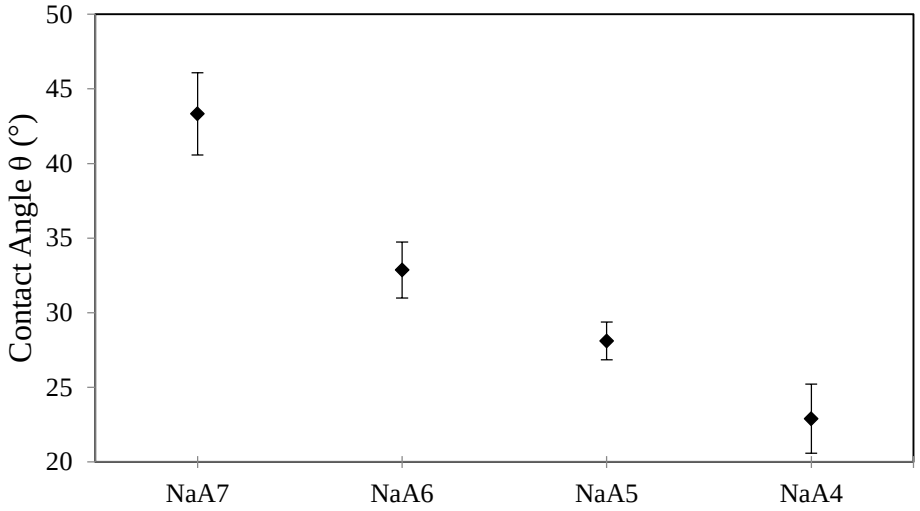

Figure 3.10 Hydrophilicity of polymers synthesized at different pH.

3.4 Conclusion

Acrylic acid polymerization at different degrees of neutralization was successfully done via solution polymerization using a redox initiation system. Remarkably, these polymerizations were able to proceed despite exposure to ambient conditions (i.e., oxygen and room temperature). Results showed that the polymers synthesized at partially neutralized extents are copolymers of poly(acrylic acid) and poly(sodium acrylate). Moreover, by increasing the extent of neutralization of the reaction mixture, the rate of polymerization increases significantly. Nonetheless, high molecular weight polymers were produced and less residual monomers remained in the system at higher degrees of neutralization. It can be concluded that the polymer synthesized at neutral pH is a better candidate for applications in bioadhesives but this will be further dictated by the functionality required of the polymer (or copolymer).

3.5 Acknowledgement

The authors wish to acknowledge the financial support of the Natural Sciences and Engineering Research Council (NSERC) of Canada.

3.6 References

[1] K. Takada, T. Iida, Y. Kawanishi, T. Yasui, and A. Yuchi, *An Electrochemical Actuator Based on Reversible Changes in Volume of Poly(acrylic acid) Gel Induced by Quinone Redox,* Sensors and Actuators B: Chemical, **2011**, *160(1)*: 1586-1592.

[2] N. Hisamatsu, T. Iida, T. Yasui, K. Takada, and A. Yuchi, *Double-Side Coated Electrochemical Actuator Based on Changes in Volume of Poly(acrylic acid) Gel,* Sensors and Actuators B: Chemical, **2014**, *203(0)*: 289-295.

[3] M. Changez, V. Koul, B. Krishna, A. K. Dinda, and V. Choudhary, *Studies on Biodegradation and Release of Gentamicin Sulphate from Interpenetrating Network Hydrogels Based on Poly(acrylic acid) and Gelatin: in Vitro and in Vivo,* Biomaterials, **2004**, *25(1)*: 139-146.

[4] S. Khanlari, and M. A. Dubé, *Bioadhesives: A Review,* Macromolecular Reaction Engineering, **2013**, *7(11)*: 573-587.

[5] Y. Dai, C. Zhang, Z. Cheng, P. Ma, C. Li, X. Kang, D. Yang and J. Lin, *pH-Responsive Drug Delivery System Based on Luminescent CaF_2:Ce_3+/Tb_3+-poly(acrylic acid) Hybrid Microspheres,* Biomaterials, **2012**, *33(8)*: 2583-2592.

[6] M. S. Christine, Z. Mingfu, R. Ezio, H. T. San, Y. K. Chong, E. Katarina, K. Goran and A. H. E. Muller, *A New Double-Responsive Block Copolymer Synthesized via RAFT*

Polymerization: Poly(N-isopropylacrylamide)-block-Poly(acrylic acid), Macromolecules, **2004**, *37*: 7761-7766.

[7] J. Gao and A. Penlidis, *A Comprehensive Simulator/Database Package for Reviewing Free-Radical Homopolymerizations*, Journal of Macromolecular Science-Reviews in Macromolecular Chemistry and Physics, **1996**, *C36(2)*: 199-430.

[8] E.W. Burkhard Kriwet and K. Thomas, *Synthesis of Bioadhesive Poly(acrylic acid) Nano- and Microparticles Using an Inverse Emulsion Polymerization Method for the Entrapment of Hydrophilic Drug Candidates*, Journal of Controlled Release, **1998**, *56*: 149-158.

[9] T. Çaykara and O. Güven, *Kinetic Analysis of the Radiation Induced Polymerization of an Acrylic Acid–Silica System*, European Polymer Journal, **1999**, *35(1)*: 113-119.

[10] F. Yigit and O. Güven, *A Kinetic Investigation of Radiation Induced Bulk Polymerization of Acrylic Acid.* International Journal of Radiation Applications and Instrumentation. Part C. Radiation Physics and Chemistry, **1989**, *33(2)*: 97-101.

[11] F. Yigit and O. Güven, *A Kinetic Investigation of Radiation Induced Bulk Polymerization of Acrylic Acid.* International Journal of Radiation Applications and Instrumentation. Part C. Radiation Physics and Chemistry, **1989**, *33(2)*: 97-101.

[12] S. Khanlari, and M. A. Dubé, *In Situ Poly(sodium acrylate)-based Nanocomposite Formation by Redox-Initiated Solution Polymerization.* Polymer Engineering and Science, **2015**, *55(6)*: 1230-1236.

[13] S. Khanlari and M. A. Dubé, *Reaction Monitoring of In-Situ Formation of Poly(sodium acrylate) Based Nanocomposites Using ATR-FTIR Spectroscopy*, Industrial and Engineering Chemistry Research, **2015**, *54*, 5598-5603.

[14] H. Hua and M. A. Dubé, *In-Line Monitoring of Emulsion Homo- and Copolymerizations Using ATR-FTIR Spectrometry,* Polymer Reaction Engineering, **2002**, *10(1-2)*: 21-39.

Chapter 4: *In situ* Poly(Sodium Acrylate)-Based Nanocomposite Formation by Redox-Initiated Solution Polymerization

S. Khanlari and M. A. Dubé, *Polymer Engineering and Science* (2015), Volume 55, Issue 6, pages 1230–1236.

Abstract: Polymer-based nanocomposites have been widely investigated as a potential method to modify polymer and biopolymer properties. Poly(sodium acrylate) (PNaA)/nanosilver nanocomposites with 0.5, 1, 2 and 3 wt.% nanofiller were prepared by *in situ* polymerization. The free radical, redox-initiated, aqueous solution polymerization of NaOH-neutralized acrylic acid was conducted in the presence of nanosilver. The progress of the polymerization was monitored using gravimetric conversion measurements. The addition of 0.5 wt.% nanosilver to the polymerization resulted in a significant decrease in rate of polymerization. The effect on rate was noticeably reduced when the experiment was repeated with nanoclay, a non-metallic nanofiller, in lieu of nanosilver.

4.1 Introduction

Polymers and copolymers based on acrylic acid (AA) are often used as thickening agents for latexes and adhesives, as well as in pharmaceutical ingredients, cosmetics, coatings, agricultural chemicals [1] and bioadhesives [2]. These AA-based materials are

particularly attractive because of their biocompatibility and adhesive properties [2]. There are several methods to synthesize PAA. For example, Kriwet et al. synthesized PAA in a stabilized water-in-oil emulsion system (called inverse emulsion) to produce PAA micro- and nanoparticles. These particles yielded excellent bioadhesive properties in an in-vitro assay [3]. Other examples of PAA synthesis in conventional free-radical systems have also been reported [4, 5]. In most of these cases, reactions were carried out at temperatures near 60 ^{o}C (with external heating) for 4 h or longer reaction times.

In the preparation of PAA, manipulation of the pH using sodium hydroxide (NaOH) can result in the production of poly(sodium acrylate) (PNaA) [6]. Figure 4.1 shows a schematic representation of sodium acrylate polymerization using acrylic acid as a starting material. Similar to PAA, PNaA hydrogels possess adhesive capabilities [7]. This polymer is also used as a superabsorbent [8].

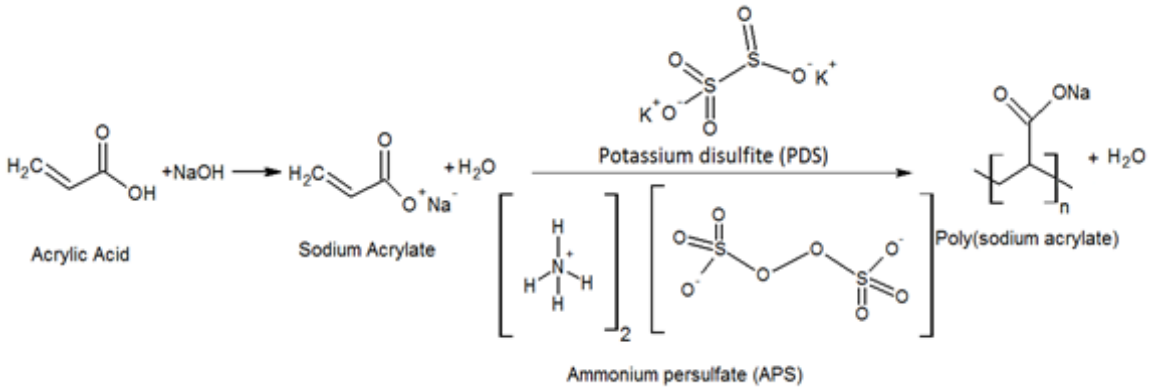

Figure 4.1 Schematic representation of PNaA synthesis.

Free-radical chain reactions require an initiation step in which free radicals are generated to start the polymerization [9]. Free-radical initiation can be subdivided into

two general types: 1) Hemolytic decomposition of covalent bonds by energy absorption, which requires a bond dissociation energy in the range of 125–160 kJ mol^{-1}; and 2) electron transfer from atoms or ions containing unpaired electrons followed by bond dissociation in the acceptor molecule – so-called reduction-oxidation or redox systems. Redox initiation is a very effective method of generating free radicals. It has found wide application for initiating polymerization reactions and can be used at low temperatures (even room temperature) which is very attractive from an energy conservation point of view [9].

Nanofillers may be added to polymer matrices to modify mechanical properties, hydrophilicity, adhesive properties, and many others. The added value brought to a bioadhesive by incorporating nanomaterials is therefore varied. Due to their high surface to volume ratio, nanofillers are typically added to the polymer matrices at very low loadings [2].

Nanosilver is one nanomaterial that is under high scrutiny today and its effects are studied widely. Nanosilver particles are not perfectly spherical and have a characteristic dimension less than 100 nm. These particles generally contain 20-15,000 silver atoms [10]. Products containing nanosilver particles have been commercially available for over 100 years and were used in applications as diverse as pigments, in photography, wound treatment, conductive/antistatic composites, catalysts, and as a biocide [11]. Nanosilver has received particular attention due to its anti-bacterial properties [12, 13]. It should be noted that most research, until very recently, did not use the “nano” nomenclature to describe nanosilver [11].

There are three main, conventional methods to produce polymer-based nanocomposites: solution blending, melt mixing, and *in situ* polymerization. *In situ* polymerization is based on direct nanocomposite preparation, via polymerization in the presence of the nanofiller. In this type of polymerization, the dispersion of the inorganic particles in the polymer matrix is enhanced and compatibility between the inorganic particles and the polymer is improved. *In situ* polymerization is considered the most promising technique to produce polymer nanocomposites [14].

In this work, the free radical aqueous solution polymerization of sodium acrylate using a redox initiation system was performed. The incorporation of nanosilver (NS) to form PNaA-NS nanocomposite materials was accomplished.

4.2 Experimental

4.2.1 Materials

Acrylic acid (>99.5%, Acros Organics), NaOH pellets (Sigma Aldrich), ammonium persulfate (APS, 98%+, Sigma Aldrich) and potassium disulfite (KDS, Sigma Aldrich) were used without further purification. The solvent was distilled deionized water. Nanosilver powder (Sigma-Aldrich) with an average particle size of < 100 nm and nanoclay (SUD-Chemie-Mexico) with an interlayer spacing of d = 1.52454 nm were used as nanofiller. The nanoclay was pre-treated at 60 °C overnight prior to use.

4.2.2 Synthesis

Pre-determined amounts of nanoparticles based on the formulation (see Table 4.1) was added to 14.9 g acrylic acid with NaOH dissolved in distilled, de-ionized water until total

neutralization. The mixture was stirred magnetically at room temperature under full exposure to the atmosphere. 0.35 g of APS and 0.34 g of PDS, each dissolved in 3 mL of distilled, de-ionized water separately, were added to the monomer/nanoparticle mixture. Early during the reaction, the mixture viscosity increased significantly and polymer formation was observed.

Table 4.1 Sample identification and nanoparticle loadings (NS = nanosilver; NC = nanoclay).

Run #	Sample name	NS (g)	Run #	Sample name	NC (g)
1	PNaANS0	0	6	PNaANC0	0
2	PNaANS0.5	0.075	7	PNaANC0.5	0.075
3	PNaANS1	0.15	8	PNaANC1	0.15
4	PNaANS2	0.3	9	PNaANC2	0.3
5	PNaANS3	0.46	10	PNaANC3	0.46

4.2.3 Characterization

Monomer conversion (X in wt.%) was measured using a standard gravimetric method based on total dried polymer weight.

$$X(\%) = \frac{\%\ Solids - Nanoparticle\ wt.\% - Other\ Solids\ wt.\%}{Initial\ wt.fraction\ of\ monomer\ \%} \times 100 \qquad (4.1)$$

where

$$\%\ Solids = \frac{Dry\ polymer}{Initial\ sample} \times 100 \qquad (4.2)$$

The polymer was dried under vacuum at room temperature for a minimum of 24 h until a constant dry weight was achieved. The gravimetric mass-based conversions were converted to molar conversions using the molar mass of acrylic acid (72 g/mol).

The polymerization was also monitored with attenuated total reflectance Fourier transform infrared (ATR-FTIR) spectroscopy using the ReactIR45™ (Mettler Toledo) in-line fibre optic probe. The ReactIR45™ was immersed into the reaction mixture to track polymer formation and/or monomer disappearance. Spectra were obtained within the range of 3000–650 cm^{-1}. The maximum reaction temperature was recorded by the sensor in the probe and this was achieved 2 to 5 min after addition of the redox solution to the reaction mixture. As all of the reactions achieved full conversion within a few minutes, IR data were collected every 5 s.

X-ray diffraction (XRD) pattern measurements were performed on a thin film of the PNaA/NC nanocomposites and on the NC using a Rigaku Ultima IV diffractometer with a Cu X-ray tube run at 40 kV, 40 mA and $\lambda = 1.54\ A^{\circ}$.

Scanning electronic microscopy (SEM) was performed on thin films of the nanocomposites using a JEOL SEM, (JSM-7500F). The samples were mounted onto metal stubs using double-sided adhesive glue made of graphite colloid and, after being vacuum-coated with a thin layer of gold (thickness= 5 nm) by a Gatan, 682 Precision Etching and Coating system, the samples were scanned.

A Waters gel permeation chromatograph (GPC) was utilized for the measurement of the polymer molecular weight and its distribution. The GPC system consisted of a Waters 610 Fluid Unit pump, a Waters 410 differential refractometer, and a PL aquagel-OH column. The sample injection volume was 50 µL and the mobile phase, distilled de-

ionized water, was run at 1 mL min^{-1}. All samples were dissolved in water to a concentration of 5 mg/mL and filtered through a 0.45 μm disposable poly(vinylidene fluoride) membrane filter (Whatman) prior to injection. Poly (ethylene oxide) (PEO) standards (Agilent) were used to construct a calibration curve for analysis using a universal calibration technique. The following Mark-Houwink parameters were used as part of the universal calibration: for polyethylene glycol, α = 0.57 and K = 0.00104 $cm^3\ g^{-1}\ mol^{-1}$; for PEO, α = 0.7800 and K= 0.0001250 $cm^3\ g^{-1}\ mol^{-1}$; and for PNaA, α = 0.50 and K = 0.001740 $cm^3\ g^{-1}\ mol^{-1}$ for M_w <20,000, and α = 0.86 and K = 0.000040 $cm^3\ g^{-1}\ mol^{-1}$ for M_w >20,000.

Differential scanning calorimetry (DSC) was performed using a TA instruments (DSC Q1000) using aluminium crimped pans at a heating rate of 10 ^oC/min under nitrogen atmosphere (flow rate = 20 mL/min) in the range of −5 to 400 ^oC. The sample size was between 4 and 10 mg.

The wettability (or hydrophilicity) of the polymers was determined using a contact angle measurement via the Sessile drop method in a video contact angle (VCA)-Optima system. The droplet size was set at 2 μL and five samples were used for each test. The average value was reported with standard deviation ±SD.

4.3 Results and Discussion

4.3.1 Nanocomposite Formation

Two types of nanofillers were used in this research, nanosilver and nanoclay, and for each of them there are different ways to show evidence of nanocomposite formation. For nanosilver, the morphology of the nanocomposite could be tracked using SEM while in

the case of layered nanofillers such as nanoclay, XRD is the method of choice to track interlayer spacing after nanocomposite formation [15]. The morphology of the nanosilver in the polymer matrix for nanocomposites containing 0.5, 1, 2 and 3 wt. % of nanosilver is shown in Figure 4.2.

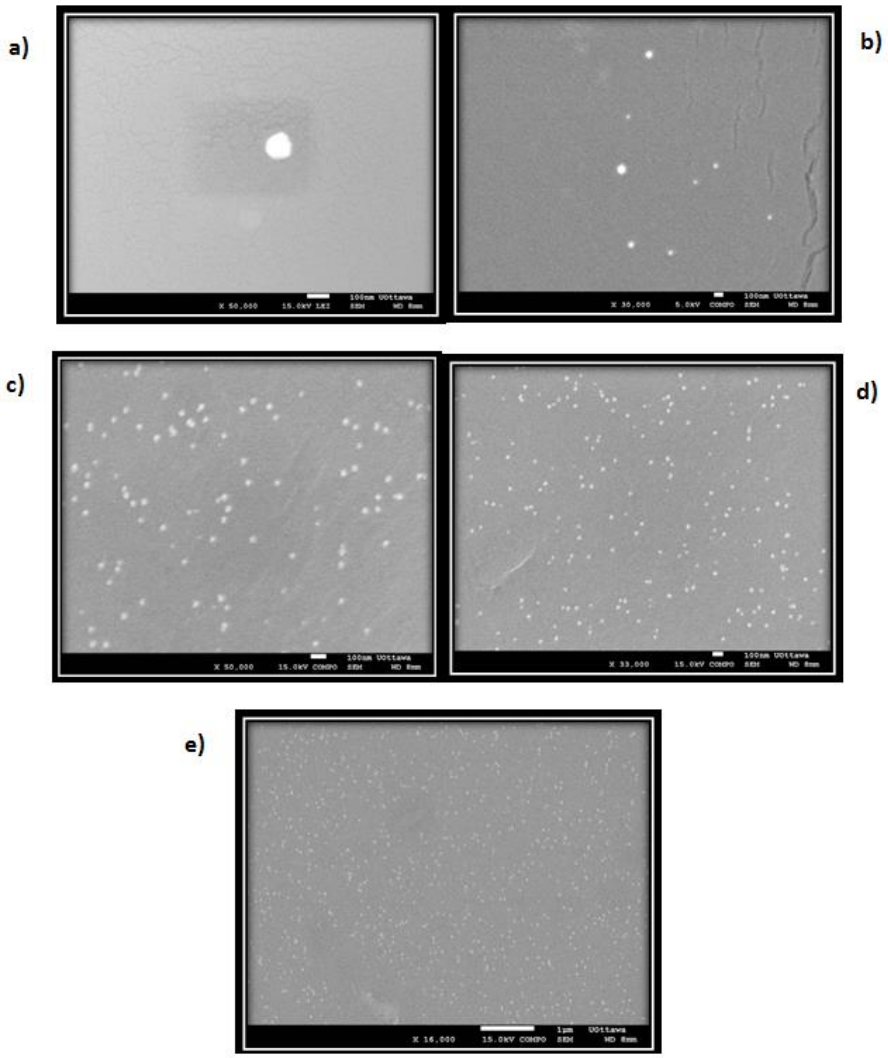

Figure 4.2 SEM images of the PNaA/NS nanocomposites: a) PNaANS0.5, b) PNaANS1, c) PNaANS2, d) PNaANS3, and e) PNaANS3 with lower magnification (scale bar is 100 nm for all samples).

SEM is typically used to scan a sample's surface, but with a higher applied voltage, a greater scanning depth can be achieved. For this reason, we applied the highest possible voltage to all samples analyzed. All samples exhibited a homogeneous dispersion of nanosilver (see Figure 4.2). In other words, no nanosilver agglomeration was detected. Even samples with higher nanosilver loading (i.e., 2 and 3 wt.%) exhibited a fine dispersion of nanosilver on the sample surface. Earlier attempts at these higher nanosilver loadings resulted in some agglomeration. These problems were overcome by increasing the agitation rate and by drying the nanosilver at 60 ^{o}C for 8 h prior to use. At the beginning of the reaction, a high agitation rate permits the even dispersal of the nanosilver in the reaction mixture (the maximum setting on the stirrer was used which is claimed by the manufacturer to reach 1100 rpm). However, the rapid increase in viscosity eventually prevented further agitation (using a magnetic stir bar). Nonetheless, this increased viscosity also prevented gravitational settling of the nanosilver.

In the formation of nanocomposites with a layered structure (e.g., nanoclay), polymer chains grow in the interlayer space of the layered silicates (also known as intercalation) and force the layers apart. XRD is used to quantify this process by determining the spacing between the crystalline layers, which are clay platelets. According to Bragg's equation, $2d \sin\theta = n\lambda$, every peak in the XRD pattern is related to a distance (d), so the first peak observed at 2θ is attributed to the interlayer spacing of the layered silicate[16]. The XRD patterns of PNaA/nanoclay nanocomposites are shown in Figure 4.3. As shown in Figure 4.3, there is a strong peak at the position of $2\theta = 5.8$ for the pure nanoclay, which corresponds to a d-spacing of 1.52 nm. After soaking the nanoclay in the monomer mixture, the polymerization proceeded and the peak was either

eliminated or shifted to 2θ values lower than 0.7. This implies that the nanoclay was completely exfoliated by the polymer formation.

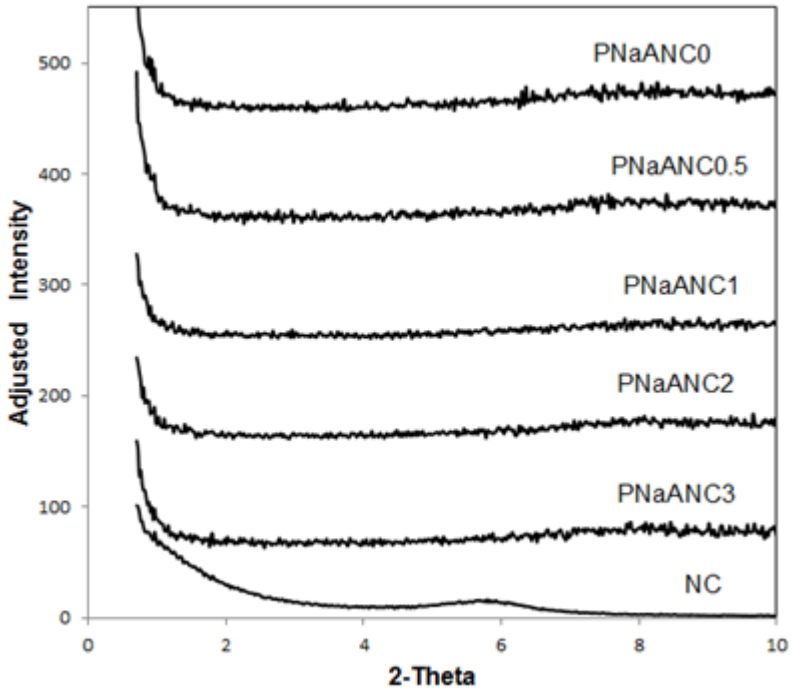

Figure 4.3 X-ray diffraction patterns of unmodified nanoclay, pristine poly(sodium acrylate) and various PNaA/nanoclay nanocomposites (intensities were adjusted to display curves separately).

4.3.2 Monomer Conversion

Figures 4.4 and 4.5 show the off-line (gravimetric) conversion vs. time data for the PNaA/nanosilver and PNaA/nanoclay polymerizations, respectively. Figure 4.4 clearly indicates that the addition of nanosilver had a significant effect on reaction rate (N.B. rate is proportional to the slope of the conversion vs. time curve) but did not vary with nanosilver concentration. It would appear that the metallic nanofiller in the reaction mixture interacted with the redox initiation system. The redox initiation system consists

of ammonium persulfate and potassium disulfite. The reduction-oxidation reaction involves metal ions (K^+), $[NH4]^+$ and $[S_2O_5]^{2-}$ as well as $[S_2O_8]^{2-}$(see figure 4.1) and the presence of silver ions (Ag^+) shed from the nanosilver [17] are likely to combine with the $[S_2O_5]^{2-}$ and $[S_2O_8]^{2-}$ and reduce the initiator's efficiency. Varying the nanosilver content from 0.5 to 3 wt.% would not result in a large enough variation in silver ion concentration to cause further changes to reaction rate. This also contributes to the induction period shown in Figure 4.4. To confirm this effect, experiments were repeated using nanoclay, a non-metallic nanofiller. The impact on rate of polymerization, while still significant, was not as pronounced as that using nanosilver (see Figure 4.5). The lesser effect on polymerization rate due to the nanoclay emanates from the exfoliation process which releases impurities that would consume free-radicals.

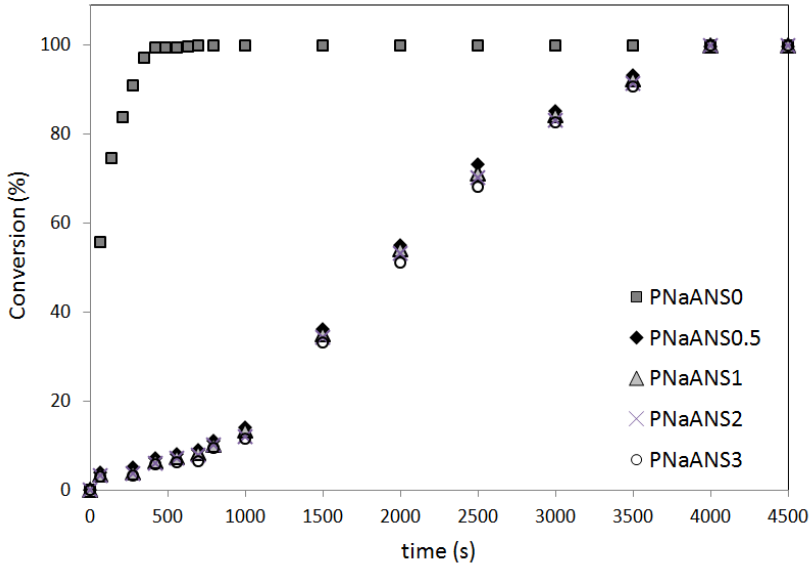

Figure 4.4 Conversion vs. time data at various nanosilver loadings.

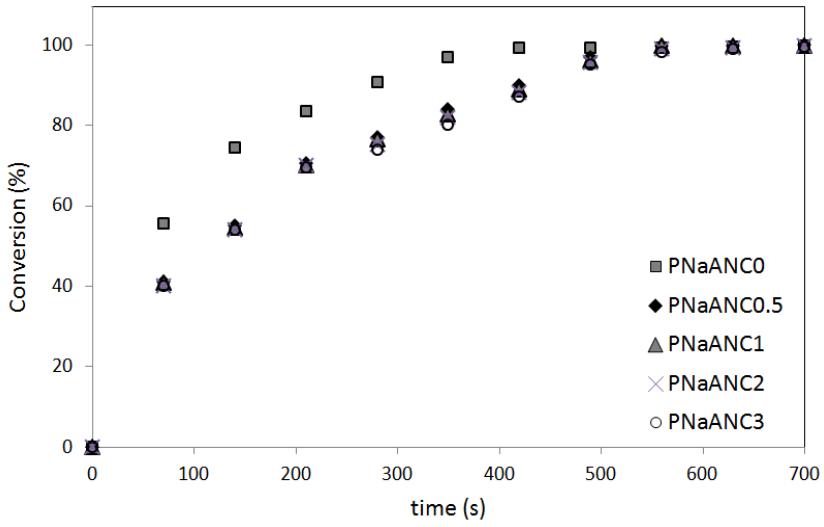

Figure 4.5 Conversion vs. time data at various nanoclay loadings.

4.3.3 IR Studies

ATR-FTIR spectroscopy was used to confirm the chemical structure of the polymer products. At any time during the polymerization reaction, polymer, monomer and water were present in the reaction mixture. Because of the broad signal overlap, subtraction of absorbances due to water was performed. This resulted in less ambiguous spectra, as shown in Figure 4.6. Figure 4.6a shows how the spectra changed during polymerization. One can clearly observe absorbance peaks that decrease with time, which are attributable to the consumption of acrylic acid (i.e., sodium acrylate) monomer. Other peaks increasing with time relate to the production of PNaA. The assignment of the various peaks to the molecular structures found in acrylic acid and PNaA according to various literature sources is shown in Table 4.2. Table 4.3 (and Figure 4.6b), shows our assignment of absorbances to the various reaction components. The spectrum in Figure 4.

6b is taken from the reaction mixture during a time of incomplete conversion; i.e., while there is both polymer and monomer in the system. Peak assignments attributed to the polymer backbone from PAA were used as guidance to assign those of PNaA (compare Tables 4.2 and 4.3).

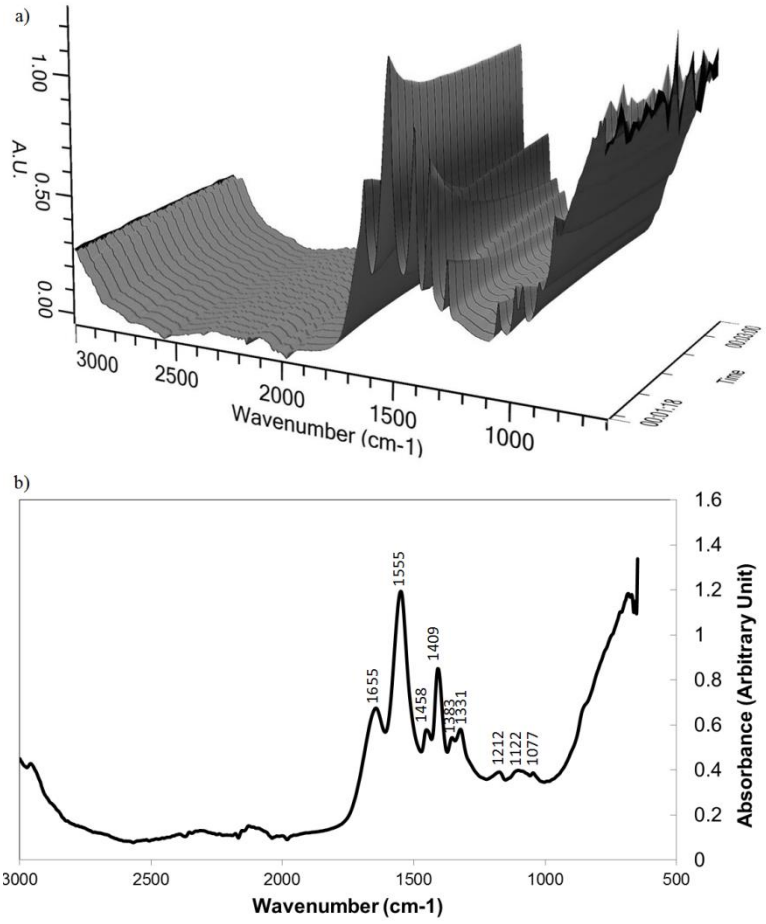

Figure 4.6 a) Typical ATR-FTIR spectra of the polymerization reaction of sodium acrylate redox solution b) single sample reaction spectrum for sodium acrylate polymerization reaction mixture (after solvent subtraction).

Table 4.2 Sodium acrylate and poly(sodium acrylate) infrared peak assignments from literature.

Spectral region (cm^{-1})	**Peak Assignment**
Sodium Acrylate [18]	
1640 m	C=C stretch
1540-1570 s, b	CO_2 asymmetric stretch
1450 s	CO_2 symmetric stretch
1430 m, sh	CH_2 scissors
1368 s	CH bend
1285 s	C-C stretch
1055 m	CH_2 rock
991 s	CH_2 twist
952 s	CH_2 wag
902 m-s	CO_2 deformation
837 s	CH bend
663 m-s	CO_2 rock
Poly(Sodium Acrylate) [19, 20]	
1653	C=O stretch
1651	CONa
1557	COO^-

s=strong, m=medium, sh=shoulder

Table 4.3 Actual peak absorbance values and resulting peak assignments.

Peak absorbance (cm^{-1})	**Assignment**	**Reaction Component**
1655	C=C stretching	Monomer
1555	O=C-O	Monomer and polymer
1458	CO_2 (s)	Monomer
1409	CH_2 bending	Polymer and monomer
1383	CH bending	Monomer
1331	C-O stretching	Polymer
1212	C-O stretching	Polymer
1122	C-CH_2 stretching	Polymer
1077	O-Na out of plane bending	Polymer

Figure 4.7 provides the changes in peak heights over the course of the pure PNaA reaction (i.e., run NaANS0) and allows one to clearly distinguish between the monomer- and polymer-related peaks. For this experiment, the redox initiation system was injected at a time of 80 s, which coincides exactly with the change in slope of the various peaks. Thus, no induction period is evident and the reaction essentially began at the moment the redox initiation system was added. The decreasing peaks in Figure 4.7 relate to the consumption of sodium acrylate monomer and appear at 1383, 1458, 1555 and 1655 cm^{-1}. Conversely, the increasing absorbance peaks at 1077, 1122, 1212, 1331 and 1409 cm^{-1} are assigned to the production of PNaA polymer.

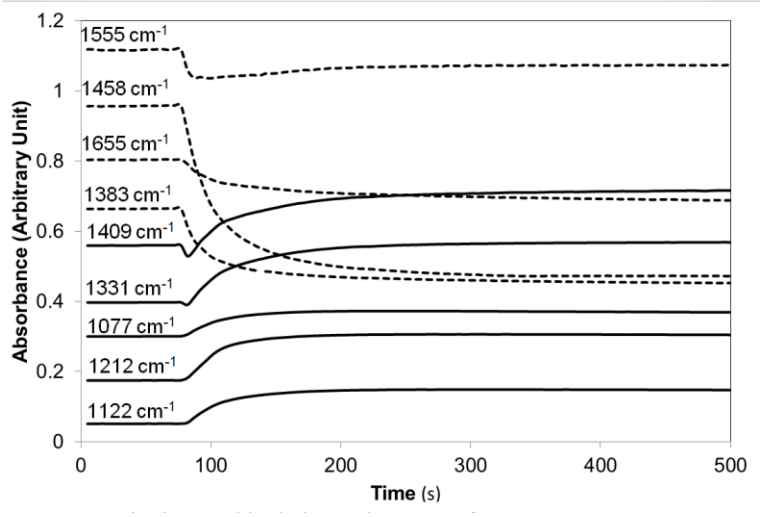

Figure 4.7 ATR-FTIR absorbance peak height during polymerization of reaction NaANS0.

4.3.4 Molecular Weight

Figure 4.8 shows the effect of nanosilver and nanoclay concentration on the weight-average molecular weight of the synthesized polymer. As noted earlier, the effect of the nanofillers was to decrease the reaction rate. The molecular weight increase with nanofiller content is entirely consistent with the trends in polymerization rate; that is, the decrease in polymerization rate, attributed above to the reduction in effective initiator concentration, resulted in higher molecular weight polymers.

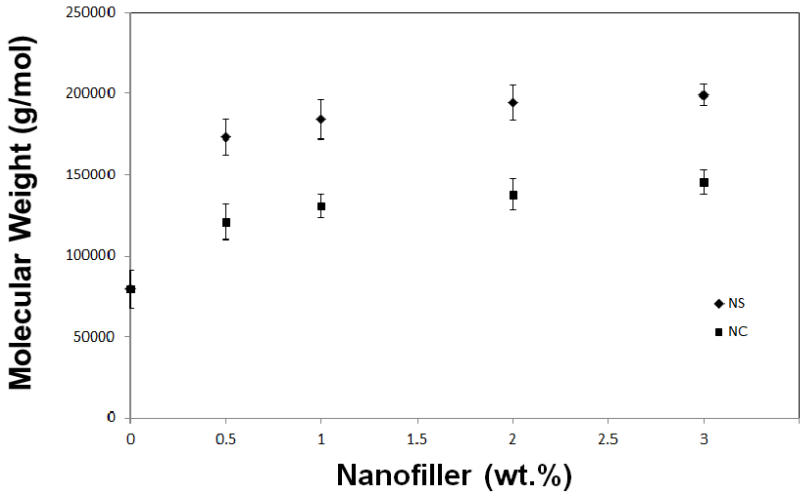

Figure 4.8 Weight-average molecular weight of PNaA synthesised in an *in situ* nanocomposite system of PNaA/NS and PNaA/NC.

4.3.5 Thermal Analysis

Differential scanning calorimetry thermograms of all the PNaA based nanocomposites are depicted in Figure 4.9. Results show an increase in glass transition temperature (T_g) with nanosilver content (T_g = 114.4 ^oC at 0 nanosilver content up to T_g = 155 ^oC at 3 wt.% nanosilver content). The effect of nanofiller on T_g depends strongly on polymer-filler interactions. This is likely why the presence of nanofillers have diverging effects depending on the nanofiller type. In a study of latex-based nanocomposite formation with nanosilver, the T_g of nanocomposites formed using *in situ* polymerization vs. simple blending were compared to the neat polymer[21]. In that study, the addition of 1 wt.% nanosilver via *in situ* polymerization caused a notable increase in T_g (~22 ^oC increase) while adding 2 wt.% nanosilver via blending resulted in a slight decrease in T_g. The

decreasing T_g in the blended nanocomposites was attributed to easier segmental motion of the polymer chains due to the free volume added to the polymer matrix by the addition of nanosilver. For the *in situ* case, the increasing T_g was attributed to polymer-filler interactions which suppressed the polymer segmental motion. As noted earlier, these interactions were expected as they have been shown to be higher in nanocomposites formed by *in situ* polymerization[14].

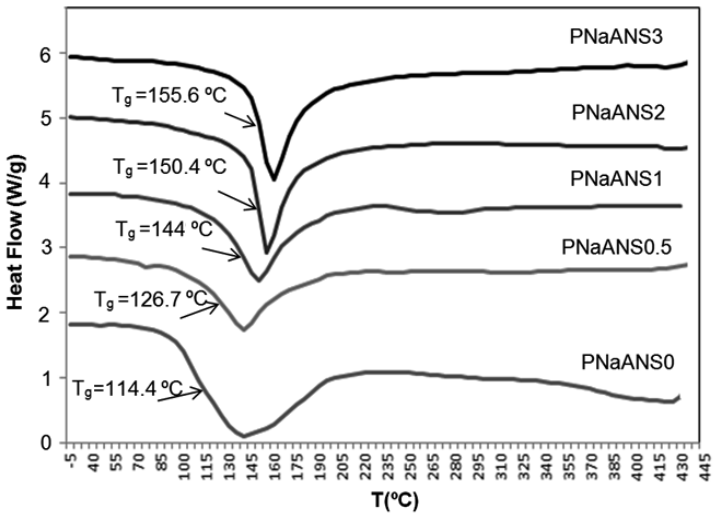

Figure 4.9 DSC thermograms of PNaA nanocomposites.

4.3.6 Contact Angle Measurements

Figure 4.10 depicts the effect of nanosilver and nanoclay on the hydrophilicity of the nanocomposite polymers. The addition of nanosilver to the poly(sodium acrylate) had little if any effect on the polymer's hydrophilicity as noted by an unchanging contact angle. On the other hand, the addition of nanoclay showed a significant increase in hydrophilicity due to the hydrophilic nature of the nanoclay [22].

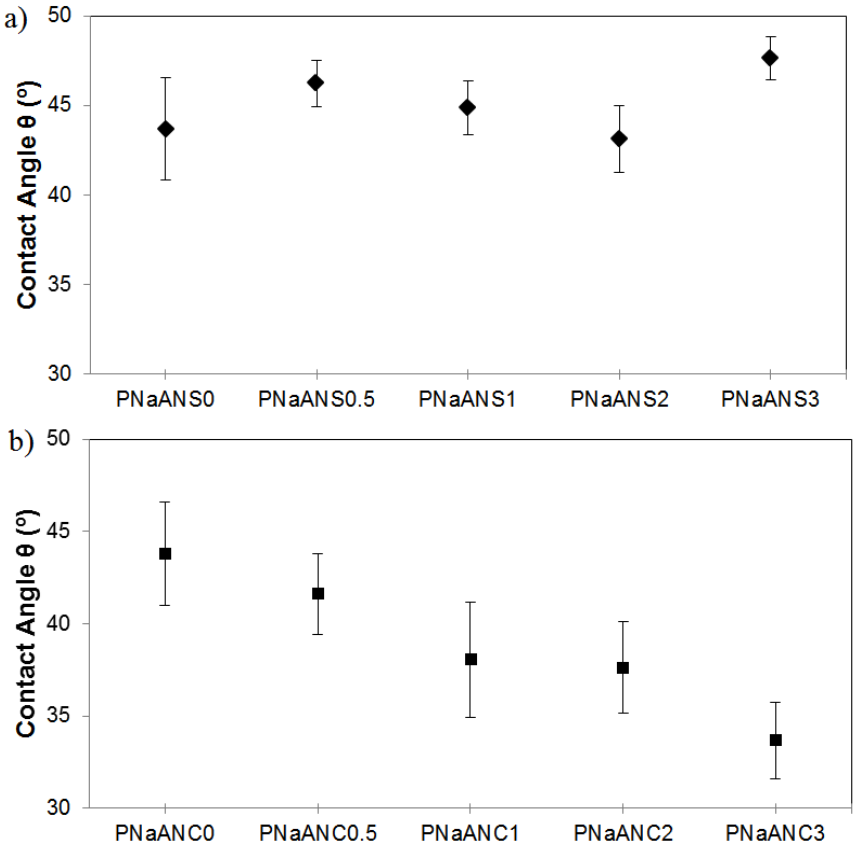

Figure 4.10 Contact angle of nanocomposite polymers containing a) NS and b) NC.

4.4 Conclusion

PNaA/nanosilver nanocomposites were successfully prepared by *in situ* polymerization at room temperature using a redox initiation system. Results showed that by adding 0.5 wt.% of nanosilver to the reaction mixture, the rate of polymerization decreased significantly while the addition of similar amounts of nanoclay had a lesser effect. This decreased polymerization rate pointed to an interaction between the metallic nanosilver with the initiation system. Nonetheless, high molecular weight polymers were produced. The nanosilver did not affect the hydrophilicity of the polymer. The anti-bacterial nature

of the nanosilver and the robust yet straightforward polymerization procedure presented herein, provide an opportunity for many practical applications of these polymers. One example to be pursued includes antibacterial adhesives.

4.5 Acknowledgement

The authors wish to gratefully acknowledge the financial support of the Natural Sciences and Engineering Research Council (NSERC) of Canada.

4.6 References

[1] J. Dong, and Y. Ozaki *Infrared, Raman, and Near-Infrared Spectroscopic Evidence for the Coexistence of Various Hydrogen-Bond Forms in Poly(acrylic acid),* Macromolecules, **1997**, *30*: 1111-1117.

[2] S. Khanlari, and M. A. Dubé *Bioadhesives: A Review,* Macromolecular Reaction Engineering, **2013**, *7*: 573-587.

[3] B. Kriwet, E. Walter, and T. Kissel *Synthesis of Bioadhesive Poly(acrylic acid) Nano and Microparticles Using an Inverse Emulsion Polymerization Method for the Entrapment of Hydrophilic Drug Candidates*, Journal of Controlled Release, **1998**, *56*: 149-158.

[4] J. Lin, J. Wu, Z. Yang, and M. Pu, *Synthesis and Properties of Poly(acrylic acid)/Mica Superabsorbent Nanocomposite,* Macromolecular Rapid Communication, **2001**, *22*: 422-424.

[5] J. Loiseau, N. Doerr, J. M. Suau, J. B. Egraz, M. F. Llauro, and C. Ladavière, *Synthesis and Characterization of Poly(acrylic acid) Produced by RAFT Polymerization. Application as a Very Efficient Dispersant of $CaCO_3$, Kaolin, and TiO_2,* Macromolecules, **2003**, *36*: 3066-3077.

[6] M. Harini, and A. P. Deshpande, *Rheology of Poly(Sodium Acrylate) Hydrogels During Cross-Linking with and Without Cellulose Microfibrils,* Journal of Rheology, **2009**, *53*: 31-47.

[7] D. Sakasegawa, M. Goto, and A. Suzuki, *Adhesion Properties of Physically Crosslinked Elastic Gels of Poly(Sodium Acrylate)–Poly(Acrylic Acid) Mixtures Evaluated by a Point Contact Method,* Colloid Polymer Science, **2009**, *287*: 1281-1293.

[8] W. F. Lee, and Y. C. Chen, *Effect of Intercalated Reactive Mica on Water Absorbency for Poly(sodium acrylate) Composite Superabsorbents,* European Polymer Journal, **2005**: *41*, 1605-1612.

[9] A. S. Sarac, *Redox Polymerization*, Progress in Polymer Science, **1999**, 24: 1149-1204.

[10] X. Chen, and H. J. Schluesener, N*anosilver: A Nanoproduct in Medical Application.* Toxicology Letters, **2008**, *176(1)*: 1-12.

[11] B. Nowack, H. F. Krug, and M. Height, *120 Years of Nanosilver History: Implications for Policy Makers,* Environmental Science and Technology, **2011**, *45*: 1177-1183.

[12] C. Silan, A. Akcali, M. T. Otkun, N. Ozbey, S. Butun, O. Ozay, and N. Sahiner *Novel Hydrogel Particles and their IPN Films as Drug Delivery Systems with Antibacterial Properties*, Colloids Surf B, **2012**, *89*: 248-253.

[13] G. A. Sotiriou, and S. E. Pratsinis, *Antibacterial Activity of Nanosilver Ions and Particles*, Environmental Science and Technology, **2010**, *44*: 5649-5654.

[14] P. A. Zapata, L. Tamayo, M. Páez, E. Cerda, I. Azócar, and F. M. Rabagliati, *Nanocomposites Based on Polyethylene and Nanosilver Particles Produced by Metallocenic "In Situ" Polymerization: Synthesis, Characterization, and Antimicrobial Behavior*, European Polymer Journal, **2011**, *47*: 1541-1549.

[15] S. Khanlari, and M. Kokabi, *Thermal Stability, Aging Properties, and Flame Resistance of NR-Based Nanocomposite*, Journal of Applied Polymer Science, **2011**, *119*: 855-862.

[16] S. Khanlari, G. D. Ashkezari, M . Kokabi, and M. R. Kashani, *Fiber-Reinforced Nanocomposite Seismic Isolators: Design and Manufacturing*, Polymer Composites, **2010**, *31*: 299-306.

[17] D. McShan, P. C. Ray, and H. Yu, *Molecular Toxicity Mechanism of Nanosilver*, Journal of Food and Drug Analysis, **2014**, *22(1)*: 116-127.

[18] W. R. Feairheller, and J. E. Katon, *The Vibrational Spectra of Acrylic Acid and Sodium Acrylate*, Spectrochimica Acta Part A: Molecular Spectroscopy, **1967**, *28A*: 2225-2232.

[19] B. Grabowska, and M. Holtzer, *Structural Examination of the Cross-Linking Reaction Mechanism of Polyacrylate Binding Agents*, Archives of Metallurgy and Materials, **2009**, *54*: 427-437.

[20] A. S. G. Magalhães, M. P. Almeida Neto, M. N. Bezerra, N. M. P. S. Ricardo, and J.P.A. Feitosa, *Application of FTIR in the Determination of Acrylate Content in Poly(sodium acrylate-co-acrylamide) Superabsorbent Hydrogels*, Quimica Nova, **2012**, *35*: 1464-1467.

[21] M. Mamaghani, M. Pishvaei, and B. Kaffashi, *Synthesis of Latex Based Antibacterial Acrylate Polymer/Nanosilver via In Situ Miniemulsion Polymerization*, Macromolecular Research, **2011**, *19(3)*: 243-249.

[22] R. N. Darie, E. Pâslaru, A. Sdrobis, G.M. Pricope, G. E. Hitruc, A. Poiată, A. Baklavaridis , and C. Vasile, *Effect of Nanoclay Hydrophilicity on the Poly(lactic acid)/Clay Nanocomposites Properties*, Industrial and Engineering Chemistry Research, **2014**, *53:*7877-7890.

Chapter 5: Image Processing Techniques for Nanofiller Distribution Quantification

S. Khanlari, A. Gheibi and M. A. Dubé, to be Submitted (2015)

Abstract: In the preparation of nanocomposite polymer materials, it is often desired to homogeneously distribute the nanofiller throughout the polymer matrix. In this work, three different image processing techniques were investigated in order to quantify the homogeneity of nanosilver loading in poly(sodium acrylate)-based nanocomposites using scanning electron microscopy (SEM) images. Nanocomposites with different nanosilver loadings were synthesized and SEM images were taken of films cast from the nanocomposites. After converting the grayscale SEM images to black and white images (i.e., for noise elimination and thresholding), three methods were applied to quantify the distribution and loadings of nanofiller in the polymer matrices. These included the Voronoi Diagram, Euclidean Minimum Spanning Tree (EMST) method and pixel counting. Results showed that pixel counting combined with the EMST method would be most appropriate for nanocomposite morphology quantification.

5.1 Introduction

Polymer-based nanocomposites are a new class of material which are used in many different areas of science and technology. They are products in which a nanofiller, with at least one dimension smaller than 100 nm is dispersed in a polymer matrix [1]. This

usually results in changes to rheological [2, 3], mechanical [4, 5], electrical [6, 7], magnetic [8, 9], optical [10, 11], thermal [1, 12], flammability [1, 13], biological [14, 15] and barrier [16, 17] properties. These properties are known to be driven by one specific feature, the huge interfacial area developed by nanofillers which appears to be strongly related to two main effects: a structural effect (shape, dispersion, and organization of the nanofillers within the material) and an interfacial effect (nature and strength of the filler−filler and filler−matrix interactions) [18]. In order to ensure homogeneous properties throughout the entire product, it is important to have a homogeneous nanofiller distribution in each sample analysis. Normally, in order to judge whether the morphology is reasonably homogeneous or not, researchers rely on the visual judgment of the images taken by scanning electron microscope (SEM) or transmission electron microscope (TEM) methods. On the other hand, even if there is a fairly homogeneous morphology in one sample, it is not obvious whether the expected loading is present in that microscopic shot or not [18]. In other words, despite a homogeneous distribution of nanofiller in one image, a quantified amount of the nanofiller falling below (or above) the expected loading would be an indication of uneven distribution in the product as a whole.

The morphology and distribution of nanofillers in a composite material can be investigated using different methods: e.g., X-ray diffraction (XRD) [1, 19] TEM (2D and 3D) [1, 20], atomic force microscopy (AFM) [21, 22] and SEM [23-26]. Among these, SEM is preferred because it is cost effective and requires a much simpler sample preparation compared to the other methods. While at least one of the aforementioned methods is used in all nanocomposite studies, the quantification of the nanocomposite homogeneity is not frequently reported. Recently, Dalmas *et al*. performed a quantitative

study on the 3D-distribution of grafted silica nanoparticles dispersed in polystyrene, based on observations of the nanocomposite using 3-D transmission electron tomography [18].

In this paper, three different quantitative methods based on image processing techniques are introduced to quantify the nanofiller distribution in a nanocomposite material. The first method employs a Voronoi diagram to partition a 2-D area of an SEM image of a nanocomposite material. The Voronoi diagram is combined with digital image processing techniques. The second method uses an Euclidean minimum spanning tree (EMST), which is a faster, linear approach. The third method relies on a black and white pixel counting method to measure the nanofiller loading accuracy. The methods are compared using images of a poly (sodium acrylate)-nanosilver composite material.

5.2 Experimental Section

5.2.1 Materials

High purity acrylic acid (>99.5%, Acros Organics), sodium hydroxide pellets (NaOH, ≥98%, Sigma Aldrich), ammonium persulfate (APS, >98%, Sigma Aldrich) and potassium disulfite (KDS, Sigma Aldrich) were used without further purification. The solvent was distilled deionized water (DDW). Nano-sized silver powder (Sigma-Aldrich) with an average particle size of <100 nm was used as nanofiller.

5.2.2 Synthesis

Among the methods proposed for nanocomposite preparation [27], in-situ polymerization was selected as the nanocomposite formation method; thus, pre-determined amounts of nanosilver were added to 14.9 g acrylic acid neutralized with sufficient amounts of NaOH dissolved in DDW. The mixture was stirred magnetically at room temperature under full exposure to normal atmosphere. 0.35 g of APS and 0.34 g of PDS, each dissolved in 3 mL of DDW separately, were added to the monomer/nanosilver mixture. Early during the reaction, the mixture viscosity increased significantly and polymer formation was observed. More details about the nanocomposite formation are discussed elsewhere [28]. Table 5.1 shows the composition of the synthesized nanocomposites used in this study.

Table 5.1 Sample identification of the synthesized nanocomposites.

Sample	**NS (wt.%)**	**NS (g)**
PNaNS0.5	0.5	0.075
PNaNS1	1	0.15
PNaNS2	2	0.3
PNaNS3	3	0.46

5.2.3 Characterization

Scanning electronic microscopy (SEM) was performed using a JEOL SEM microscope, (JSM-7500F-Japan) on a nanocomposite film sample mounted on a sample holder using

conductive glue made of graphite. Prior to analysis, the samples were vacuum-coated with a thin layer of gold (thickness ~5 nm) by a Gatan 682 Precision Etching and Coating system. Most of the images were taken at 15 kV unless it was possible to take high resolution images at lower voltages. The image processing analysis was conducted using Matlab™ 7.11.1.

5.3 Results and Discussion

Three different quantitative methods based on image processing techniques were used to quantify the distribution of NS in a poly(sodium acrylate) matrix. These methods, including the Voronoi Diagram method, the Euclidean Minimum Spanning Tree (EMST) method, and a black and white pixel counting method, are described in greater detail below.

Particle detection and localization is the first step in the assessment of particle distribution homogeneity. Template matching, edge detection, intensity comparisons, texture-based methods and neural networks are some of the automatic particle detection methods reviewed by Nicholson and Glaeser [29]. In the present study, the first step towards particle detection, for all cases, was the conversion of grayscale images from the SEM to black and white images. In other words, we located the nanoparticles in the SEM image by differentiating between the particles and signal noise. SEM images are usually noisy and automatic particle detection is not straightforward using gray-scale images (Figure 5.1a). The SEM image was converted to a black and white image using a threshold on the gray-scale pixels and then by applying a closing operation [30]. Figure 5.1b shows the result of conversion of a gray-scale image to black and white. It should be

noted that in the case of high resolution images, this image conversion step would not be necessary, the exception being for the pixel counting method.

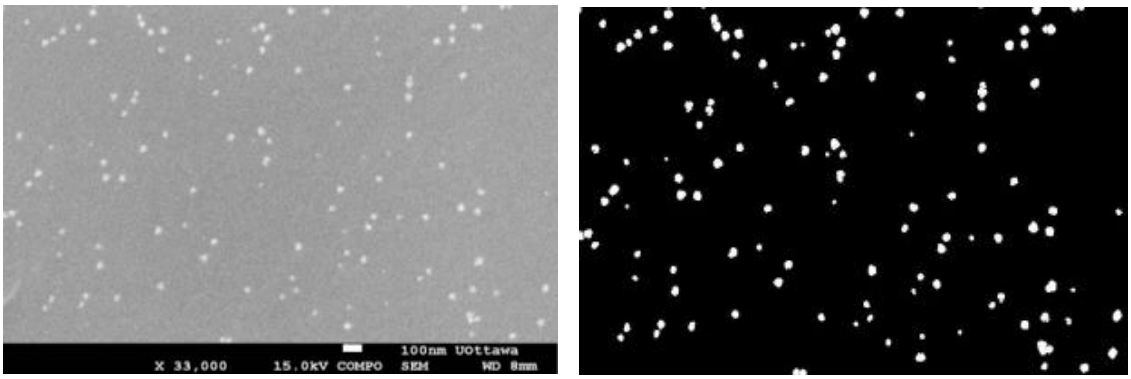

a) b)

Figure 5.1 a) SEM image of PNaA/NS nanocomposite with 3 wt.% nanosilver (gray scale); b) black and white version of part a).

In the Voronoi Diagram and Euclidian Minimum Spanning Tree (EMST) methods, it is important to find the center of mass of the particles and apply the image processing based on a single point. The centers of mass of the particles found in SEM images represent nanoparticles. These points are used to compute Voronoi and EMST diagrams. As each particle consists of several points, the next step in these methods requires the calculation of a representative point for each particle. Herein, the mathematical definition of center of mass was used to find a representative point for each nanoparticle.

5.3.1 The Voronoi Method, (a 2-D Method)

Voronoi diagrams have a long history and often appear in nature. The first known presentation of Voronoi diagrams dates back to the works of Kepler and Descartes, on the

distribution of matter in cosmic regions around the stars [31]. More than 200 years later, Dirichlet formalized the Voronoi cells (also known as Dirichlet cells) in his study of two- and three-dimensional quadratic forms [32]. Around the same time, during the cholera outbreak in London, the father of modern epidemiology, John Snow, superimposed a map of cholera cases and a Voronoi diagram of the city's water pumps. Thus, they were able to identify infected pumps and save thousands of lives [31, 32]. In 1907, Georgy Feodosevich Voronoy, generalized the work of Dirichlet to arbitrary dimensions and proposed the Voronoi diagram that we use today [32]. The Voronoi diagram is likely the most used geometric structure over a broad range of applications, namely in the social sciences, e.g., in the study of dialect variations, demographics, territorial systems, economics, and markets [33-35], to crystallography, especially in the study of space-filling polyhedrons [31, 32]. The Voronoi diagram has been known by many different names due to its reinvention over the years, i.e., Thiessen polygons, area of influence polygons, Wigner-Seitz regions, domain of an atom, Meijering cells, Brillouin zone, maximum likelihood regions, plant polygons in ecology, and capillary domains. Fortunately, constructing Voronoi diagrams is addressed in computational geometry and some efficient and practical algorithms are proposed for this purpose [32].

The Voronoi diagram (see Figure 5.2) is a geometric naturalistic method to partition a space based on the position of particles dispersed in that space, which could be either 2-D or 3-D or any higher dimension. Herein we restrict our discussion to two-dimensional space because our SEM images are two-dimensional. We assume $P = \{p_1, p_2, \dots, p_n\}$ is a set of points in the two-dimensional space, $\mathbb{R}^2$. Each point represents a particle in the set. The Voronoi cell of each point is the area occupied by one point (or

in this case, one particle) and is defined as: $V(p_i) = \{q \in \mathbb{R}^2 | d(q, p_i) \leq d(q, p_j), \forall j \neq i, \}$ where $d(.,.)$ is the Euclidean (i.e., straight-line) distance between two points. The Voronoi diagram is defined as the union of Voronoi regions of particles: $V(P) = \bigcup_{i=1}^{n} V(p_i)$ [31]. It should be noted that Matlab™ 7.11.1 provides a tool to generate the Voronoi diagram for a set of points.

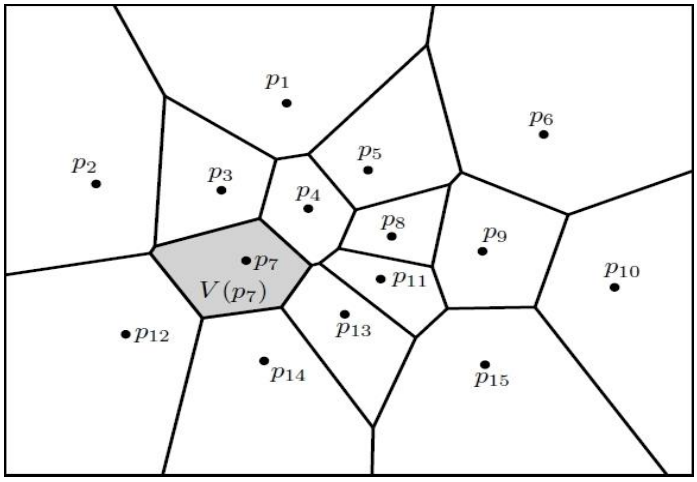

Figure 5.2 Voronoi diagram of 15 points in a plane. The Voronoi cell of one of the points, $\boldsymbol{p_7}$, is identified by a grey polygon.

As shown in Figure 5.2, the Voronoi diagram partitions the 2D image in such a way that each point *x* in $V(p_i)$ is closer to the representative point of the zone, p_i, rather than another zone, p_j, where $j \neq i$. In Figure 5.2, the corresponding Voronoi cells p_1, p_2, p_6, p_{10}, p_{12}, p_{14} and p_{15} are theoretically unbounded (i.e., in some directions there is no limit to the cell boundary), while the corresponding Voronoi cells p_3, p_4, p_5, p_7, p_8, p_{11} and p_{13} are bounded (i.e., in any direction there is a defined cell boundary). It can be concluded that if the Voronoi diagram results in equal-sized cells for all of the points in an image, the points must be homogeneously distributed throughout the whole 2-D image. On the other

hand, if the cells occupy totally/partially different areas, one can conclude that the points are not distributed evenly. In order to illustrate this idea, the Voronoi diagram is applied to three different schematics of different particle distributions (see Figure 5.3). Distributions of the Voronoi cell-sizes are shown as well.

a)

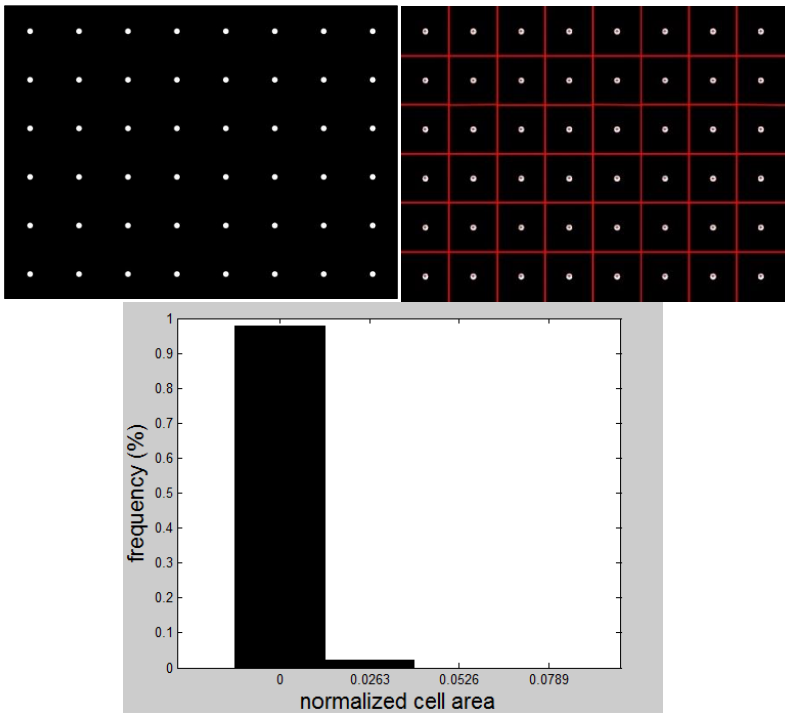

b)

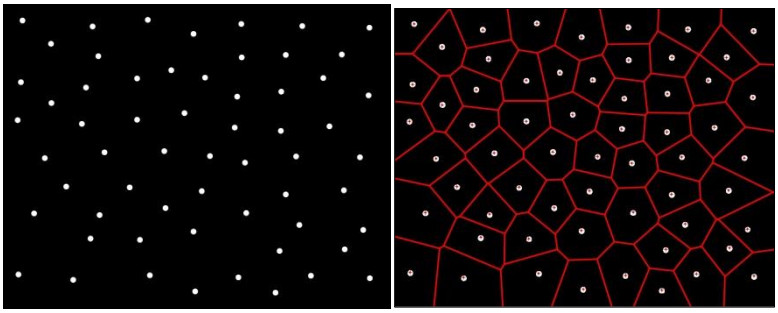

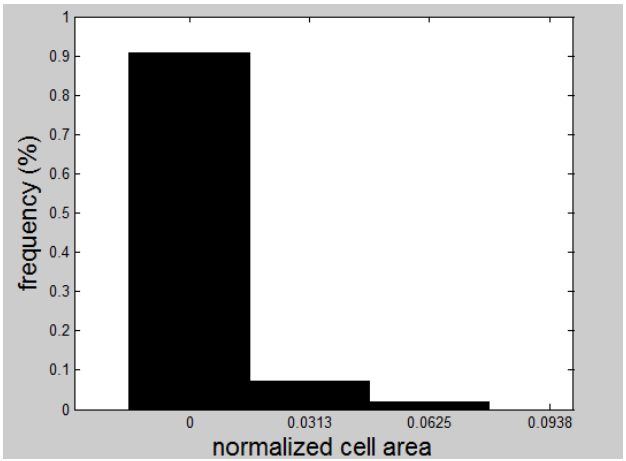

c)

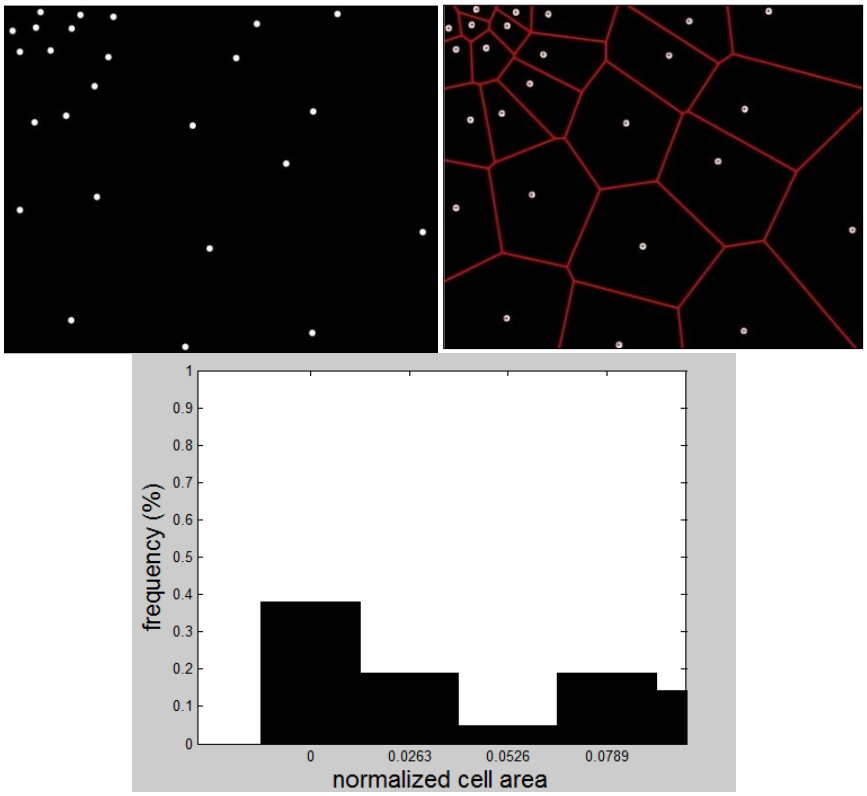

Figure 5.3 Voronoi diagram applied to schematics of different distributions of particles and their associated cell area distribution for a) exaggerated homogeneous, b) random homogeneous, and c) random non-homogeneous distributions.

In Figure 5.3a) a schematic of an exaggerated homogeneous distribution of particles is shown (image on left). This image was manually generated. The Voronoi diagram was applied to that image (image on right) and because the particles were distributed completely homogeneously, the Voronoi diagram produced equal-sized cells. Cell areas were normalized using:

$$normalized\ area = \frac{Cell\ Area}{Maximum\ Cell\ Area} \tag{5.1}$$

where cell area is the internal area of each cell and the maximum area is the area of the largest cell. The areas were then plotted as a frequency chart (see Figure 5.3a). It was expected that all areas would have been captured in one bin. However, due to slight errors in the manual preparation of the image, an extra bin was generated. This reveals that in practice, after image processing steps, a slight difference in point location could change the cell area. In the case of the points in Figure 5.3a, a slight change in the position of the points could make an unbounded region bounded. That is why we have very large bounded region for the outermost points, while in theory, those regions should be unbounded. Figure 5.3b shows a schematic of random homogeneous particles distributed and its Voronoi diagram. In the distribution diagram, it can be seen that ~90% of the cells are located in one bin size. This implies a 90% homogeneity of the particle distribution. In the final schematic (Figure 5.3c), an image of a non-homogeneous distribution of particles was generated. The distribution diagram shows a broad number of bins, as would be expected. Figure 5.4 shows the Voronoi diagram method applied to SEM images taken from two different NS distributions in poly(sodium acrylate). In both cases, the distribution of particles is close to homogeneous as the relative areas of the Voronoi cells are almost equal.

a)

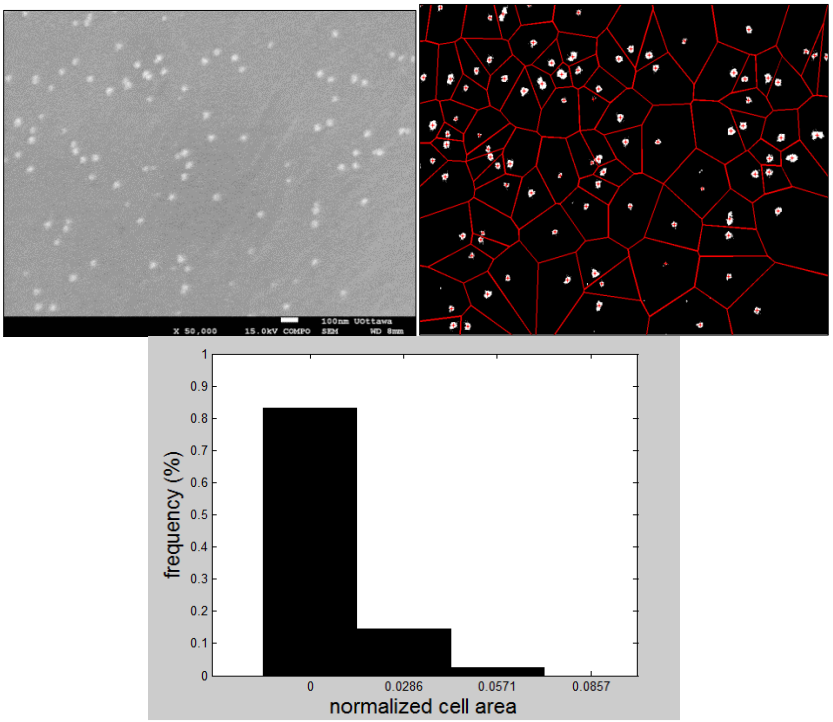

b)

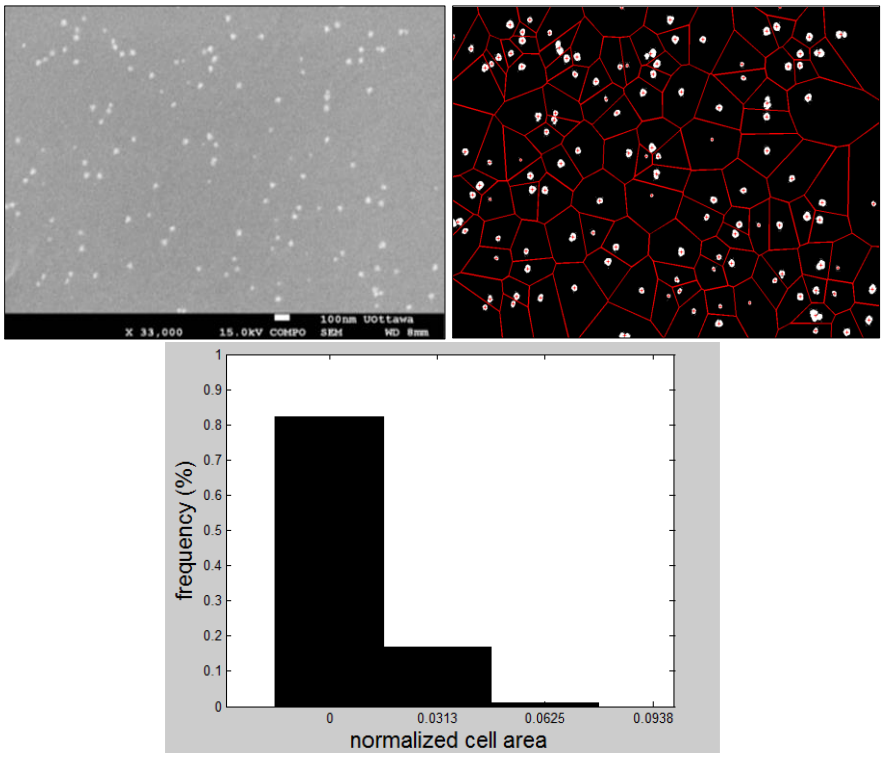

Figure 5.4 Voronoi diagram method applied to distributions of nanosilver in PNaA matrix; a) PNaANS2, b) PNaANS3.

In other words, the frequency of relative areas has a peak greater than 75%, which means that at-least 75% of the cells are of the same area, i.e., at least 75% of the particles are the same distance from each other. Consequently, it can be concluded that both SEM images depict homogeneously dispersed nanoparticles.

5.3.2 Euclidean Minimum Spanning Tree Method (a 1-D method)

In the (EMST) method, a set of points in a plane are connected to each other by lines, subject to two conditions: a) The total length of the lines is minimized; and b) any point can be reached from any other point by following the lines [36, 37]. The word "tree" implies a branched structure as opposed to the formation of loops. Figure 5.5 depicts the EMST method applied to the same set of the points used in Figure 5.2. As was the case for the Voronoi diagram, a Matlab™ 7.11.1 tool is available to generate the EMST diagram.

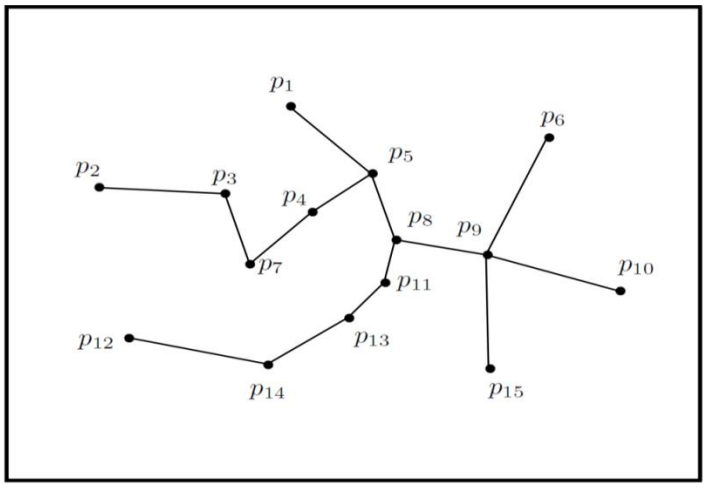

Figure 5.5 Euclidean minimum spanning method diagram of 15 points in a plane.

a)

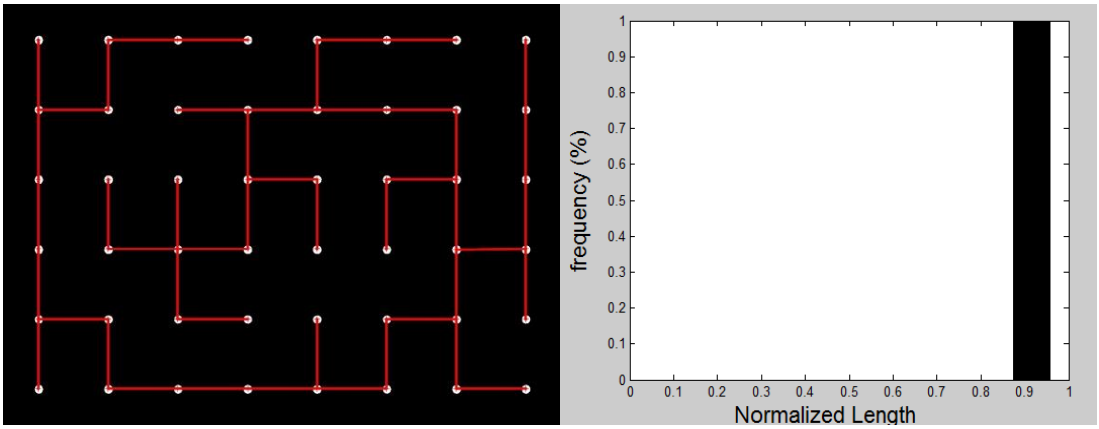

b)

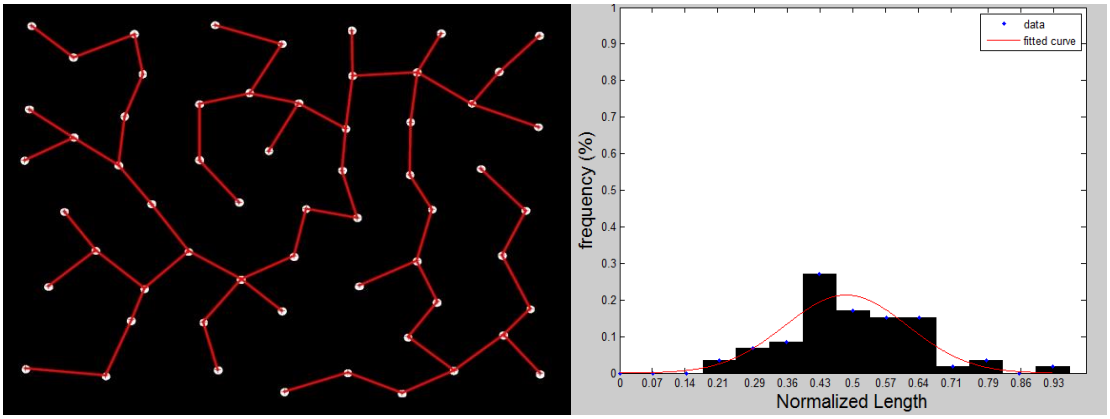

c)

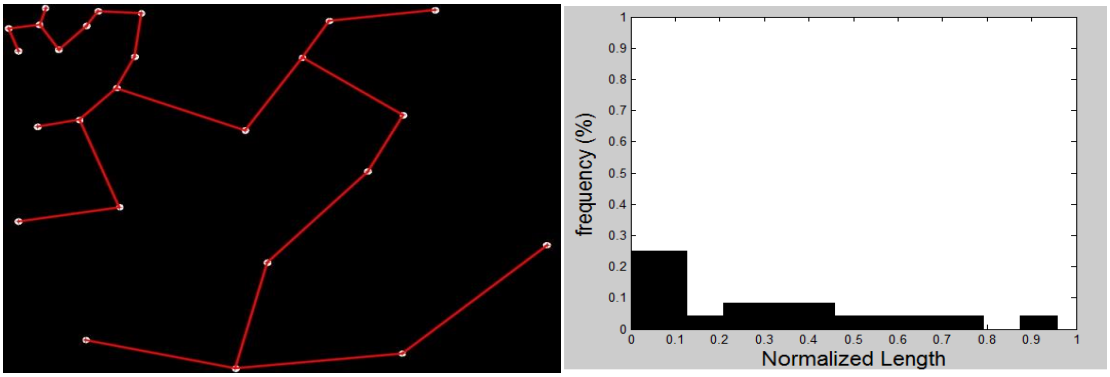

Figure 5.6 The EMST method applied to schematics of different distributions of points and their associated line length distribution; a) exaggerated homogeneously distributed, b) random homogeneously distributed, and c) non-homogeneously distributed.

The EMST method is commonly used for designing cost-effective transportation, piping or wiring networks, assuming a constant price per unit length of the services being networked.

To our knowledge, the EMST method has never been used for nanocomposite morphology studies. The EMST method was applied to the three different schematic distributions used to illustrate the Voronoi diagram method earlier. (It is shown in Figure 5.6.)

In Figure 5.6a, results of the application of EMST to a set of exaggerated homogeneously distributed points are shown. Also shown is the distribution of EMST segments' normalized lengths. The normalized lengths are calculated from:

$$normalized\ length = \frac{edge\ length}{longest\ edge\ length} \tag{5.2}$$

where the numerator is the length of every segment line drawn between the particles and the denominator is the longest among them.

The narrow distribution of segment lengths for Figure 5.6a reflects the homogeneous distribution of points in the schematic image. A Gaussian model was fitted to the distribution plots in Figure 5.6b and 5.6c. Results reveal a normal distribution for the random homogeneous case (Figure 5.6b) while it was not possible to fit the Gaussian model to the results of the non-homogeneous distribution case (Figure 5.6c). The Gaussian model (single pick) used for curve fitting followed equation 5.3:

$$f(x) = a_1 \exp\left(-\left(\frac{x-b_1}{c_1}\right)^2\right) \tag{5.3}$$

For Figure 5.6b, the model parameters were calculated as a_1 = 0.24973, b_1 = 0.47923, and c_1 = 0.19659. The "Trust-Region-Reflective Least Squares" algorithm [38]

in Matlab™ 7.11.1 was used to fit the Gaussian curve. An R^2 = 0.92 for the model suggests a reasonable fit for the data in Figure 5.6b,

The application of the EMST method to real SEM images taken from PNaA based nanocomposites containing 2 and 3% NS are shown in Figure 5.7. The Gaussian models fitted to the distributions revealed a more or less homogeneous distribution. Table 5.2 summarizes the Gaussian model parameters for the two samples. R^2 values of 0.78 and 0.77 for PNaANS2 and PNaANS3, respectively, were calculated, implying a non-Gaussian fit to the data.

a)

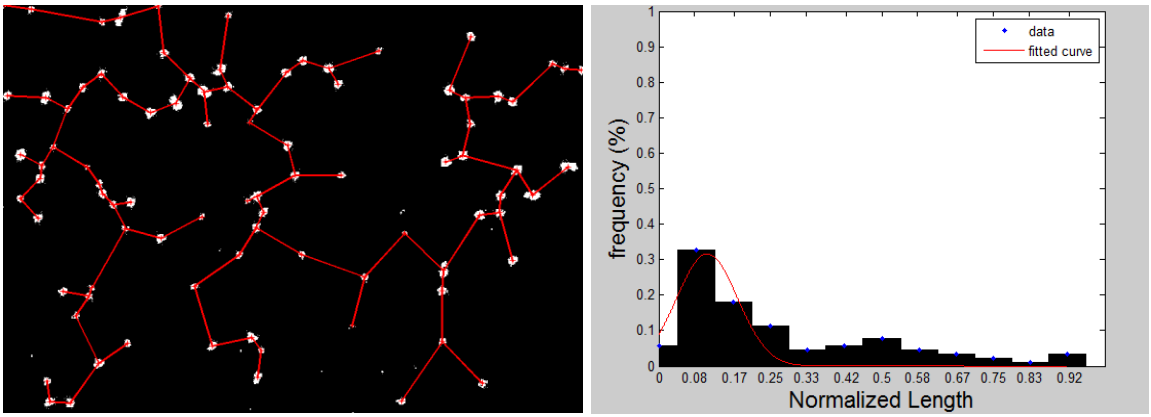

b)

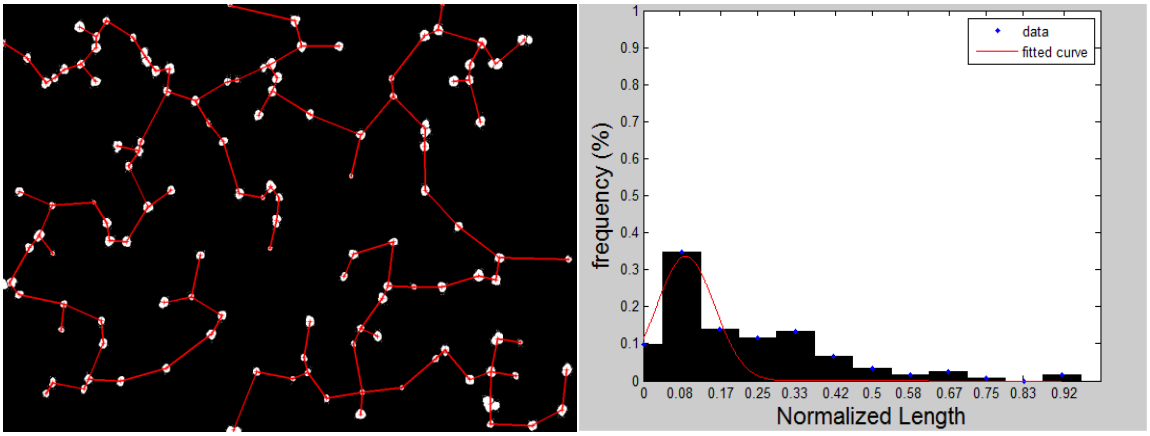

Figure 5.7 EMST method applied to SEM images for nanocomposites a) PNaANS2 and b) PNaANS3.

Table 5.2 Gaussian model parameters calculated for the synthesized nanocomposites.

Sample	a_1	b_1	c_1
PNaNS2	0.3078	0.11168	0.1098
PNaNS3	0.3523	0.093399	0.090808

5.3.3 Pixel Counting Method (a 0-D Method)

The Voronoi diagram method serves to examine the distribution of the particles in the SEM image area regardless of the percent nanofiller loading present in the image. In order to make a comprehensive judgment about nanocomposite homogeneity, it is also important to examine the accuracy of nanofiller loading in all microscopic shots. In other words, we wish to verify that the percent nanofiller present in the SEM image is equal to that loaded during nanocomposite synthesis. If this is not the case, it could imply poor mixing or that aggregation of nanoparticles may have occurred outside of the sample scanning area. This is very important in nano-sized medicine in which nanoparticles of a drug are distributed in a matrix and a homogeneous dosage throughout the whole product is vital.

After conversion of the SEM image to black and white, the matrix of pixels in the digital image is converted to a matrix in which every element is either 1 for the white pixels (nanofiller) or 0 for the black ones (polymer matrix) using Matlab™ 7.11.1. The nanofiller percentage in each SEM image was calculated according to Equation 5.4, where m and n are the number of rows and columns of pixels in the image, i.e., the order of the matrix is the pixel size of the SEM image:

$$nanofiller\ (\%) = \frac{\sum_{j=1}^{m}\sum_{i=1}^{n} x_{ij}}{m \times n} \times 100 \qquad (5.4)$$

where x_{ij} represents any component of the matrix made by the pixels of the SEM image (with the value of either 1 or 0). In equation 5.4, the numerator represents the number of white cells (the number of "ones") because the values of the black pixels are zero; the denominator represents the total number of cells.

Figure 5.8 illustrates a hypothetical application of the pixel counting method. According to the method, the calculated percentage of nanofiller in Figure 5.8a, from the matrix presented in Figure 5.8b using equation 5.4 is 20% (which is obviously beyond the expected loading percent normally found in nanocomposites, <10%). This method was then applied to a number of SEM images from the PNaA/NS samples produced in this study. Figure 5.9 shows gray-scale images of these samples with different nanosilver loadings. After conversion to black and white, the pixel counting method yielded results of 0.506 and 0.86 wt.% for nanofiller loadings of a) 0.5 and b) 1 wt.%, respectively.

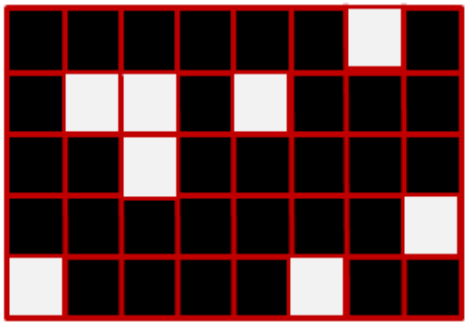

a)

$$\begin{bmatrix} 0 & 0 & 0 & 0 & 0 & 0 & 1 & 0 \\ 0 & 1 & 1 & 0 & 1 & 0 & 0 & 0 \\ 0 & 0 & 1 & 0 & 0 & 0 & 0 & 0 \\ 0 & 0 & 0 & 0 & 0 & 0 & 0 & 1 \\ 1 & 0 & 0 & 0 & 0 & 1 & 0 & 0 \end{bmatrix}$$

b)

Figure 5.8 a) Schematic diagram of pixelated image b) The matrix associated with the image of part a.

a)

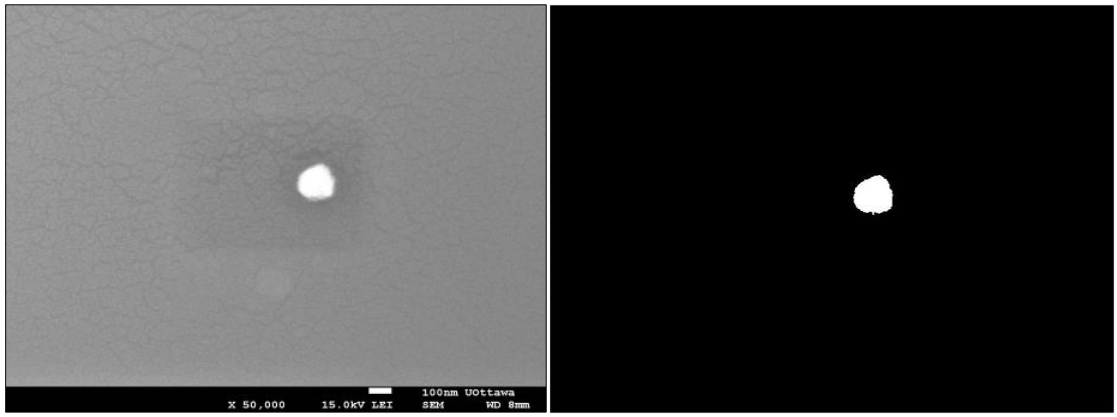

b)

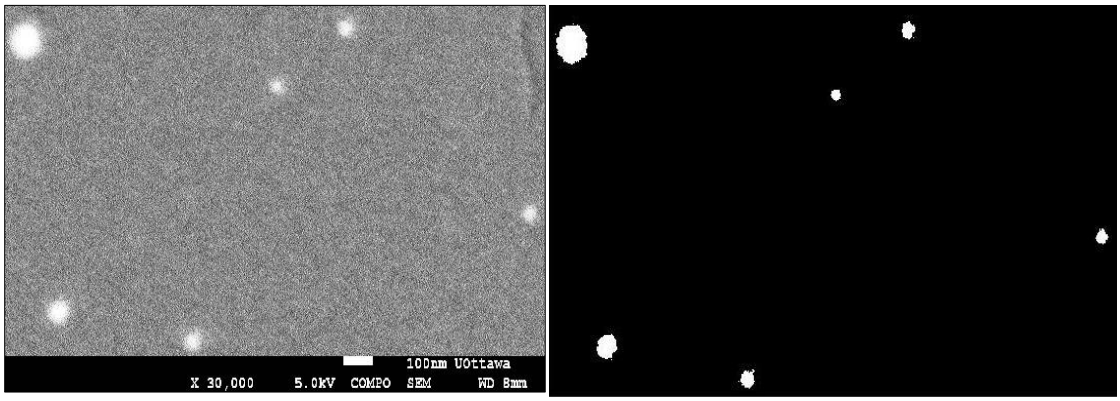

Figure 5.9 SEM images of a) PNaNS0.5 and b) PNaNS1.

The results of the pixel counting method for the SEM images of PNaA/NS samples shown earlier in Figure 5.4, yielded 2.09±0.11 and 2.92±0.14 wt.% for nanofiller loadings of 2 and 3 wt.%, respectively, which are close to the expected amounts. The pixel counting method was applied to several SEM images taken from different parts of the nanocomposite samples for each of the different nanofiller loadings. As the percent of the nanofillers in each image was consistent with the percent nanofiller loaded initially, one can conclude that the distribution of the nanofiller in the entire polymer matrix was

homogeneous. The nanofiller loading accuracy could be assessed in other ways such as via thermogravimetric analysis, but for the case where the nanofiller is organic (e.g., nano-starch or nano-cellulose) the thermogravimetric method would not be applicable.

It should further be noted that the pixel counting method, due to its nature, is independent of particle shape and geometry, for all isotropic fillers, and is therefore broadly applicable to many other composite materials. More importantly, beside its simple coding algorithm, in cases of very low nanoparticle loadings (e.g., Figure 5.9) in which the nanofiller doesn't show any distribution and there might be a few (one or two) particles in each microscopic shot, none of the distribution based methods can be used and the pixel counting method is highly effective.

5.4 Conclusion

PNaA based nanocomposites were synthesized and characterized for nanoparticle distribution and loading using image processing techniques combined with the Voronoi diagram, Euclidean minimum spanning tree and pixel counting methods. We proposed quantitative measures for evaluation of the homogeneity of nanofiller loading in nanocomposites. The results showed that all of the proposed methods are reliable but that the Voronoi diagram method can be subject to mathematical instability. It is worth mentioning that none of the aforementioned methods are limited to composites containing nano-sized fillers and could be used in higher ranges of fillers including microfillers; moreover, the methods are applicable to images taken from nanocomposites using a 2D TEM or microcomposites using an optical microscope. In addition, at very low filler loadings where one would observe, say, <5 nanoparticles in an image, evidently

the two distribution based methods would be inappropriate. The pixel counting 0-D method does not suffer from this constraint and can be used for very low filler loadings. Thus, to completely characterize nanofiller loading and distribution, we suggest the use of the pixel counting method to quantify nanofiller loadings along with the EMST method to quantify nanofiller distribution.

5.5 Acknowledgements

The authors gratefully acknowledge the financial support of the Natural Sciences and Engineering Research Council (NSERC) of Canada.

5.6 References

[1] S. Khanlari, and M. Kokabi, *Thermal Stability, Aging Properties, and Flame Resistance of NR-Based Nanocomposite*, Journal of Applied Polymer Science, **2011**, *199(2)*: 855-862.

[2] H. C. Kuan, C. C. M. Ma, W. P. Chang, S. M. Yuen, H. H. Wu, and T. M. Lee, *Synthesis, Thermal, Mechanical and Rheological Properties of Multiwall Carbon Nanotube/Waterborne Polyurethane Nanocomposite,* Composite Science and Technology, **2005**, *65(11–12)*: 1703-1710.

[3] P. Manivel, S. Kanagaraj, A. Balamurugan, N. Ponpandian, D. Mangalaraj, and C. Viswanathan, *Rheological Behavior and Electrical Properties of Polypyrrole/Thermally Reduced Graphene Oxide Nanocomposite,* Colloids and Surfaces A: Physicochemical and Engineering Aspects, **2014**, *441(0)*: 614-622.

[4] J. Xu, W. Hu, Y. Yong, X. Lu, P. Munroe, and Z. H. Xie, *Microstructure and Mechanical Properties of a Mo-toughened Mo_3Si-based In Situ Nanocomposite,* Vacuum**,** **2014**, *109(0)*: 112-119.

[5] M. A. Rafiee, J. Rafiee, Z. Wang, H. Song, Z. Z. Yu, and N. Koratkar, *Enhanced Mechanical Properties of Nanocomposites at Low Graphene Content*, ACS Nano Letter, **2009**, *3(12)*: 3884-3890.

[6] J. B. Marroquin, K.Y. Rhee, and S. Park, *Chitosan Nanocomposite Films: Enhanced Electrical Conductivity, Thermal Stability, and Mechanical Properties,* Journal of Carbohydrate Polymers, **2013**, *92(2)*: 1783-1791.

[7] N. A. N. Azmy, H. Abdullah, N. M. Naim, A. A. Hamid, S. Shaari, and W. H. Mokhtar, *Gamma Irradiation Effect on the Structural, Morphology and Electrical Properties of ZnO–CuO Doped PVA Nanocomposite Thin Films for Escherichia Coli Sensor*, Radiation Physics and Chemistry, **2014**, *103(0)*: 108-113.

[8] K. Mandel, F. Hutter, C. Gellermann, and G. Sextl, *Stabilisation Effects of Superparamagnetic Nanoparticles on Clustering in Nanocomposite Microparticles and on Magnetic Behaviour,* Journal of Magnetism and Magnetic Materials, **2013**, *331(0)*: 269-275.

[9] F. Song, X. Shen, M. Liu, and J. Xiang, *Preparation and Magnetic Properties of $SrFe_{12}O_{19}/Ni_{0.5}$ $Zn_{0.5}Fe_2O_4$ Nanocomposite Ferrite Microfibers via Sol–Gel Process,* Materials Chemistry and Physics, **2011**, *126(3)*, 791-796.

[10] I. Naydenova, E. Leite, T. Babeva, N. Pandey, T. Baron, T. Yovcheva, S. Saino, S. Martin, S. Mintova, and V. Toal, *Optical Properties of Photopolymerizable*

Nanocomposites Containing Nanosized Molecular Sieves, Journal of Optics, **2011**, *13*: 1-10.

[11] M. Halajan, M. J. Torkamany, and D. Dorranian, *Effects of the ZnSe Concentration on the Structural and Optical Properties of ZnSe/PVA Nanocomposite Thin Film,* Journal of Physics and Chemistry of Solids, **2014**, *75(11)*: 1187-1193.

[12] S. S. Ray, J. Bandyopadhyay, and M. Bousmina, *Thermal and Thermomechanical Properties of Poly[(butylene succinate)-co-adipate] Nanocomposite,* Polymer Degradation and Stability, **2007**, *92(5)*: 802-812.

[13] G. Beyer, *Flame Retardant Properties of EVA-nanocomposites and Improvements by Combination of Nanofillers with Aluminium Trihydrate,* Fire and Materials, **2001**, *25*: 193-197.

[14] V. Alt, T. Bechert, P. Steinrucke, M.Wagener, P. Seidel, E. Dinqelein, E. Domann, and R.Schnettler, *An in Vitro Assessment of the Antibacterial Properties and Cytotoxicity of Nanoparticulate Silver Bone Cement,* Biomaterials, **2004**, *25(18)*: 4383-4391.

[15] M. Mamaghani, M. Pishvaei, and B. Kaffashi, *Synthesis of Latex Based Antibacterial Acrylate Polymer/Nanosilver via in Situ Miniemulsion Polymerization,* Macromolecular Research, **2011**, *19(3)*: 243-249.

[16] A. Khan, R. A. Khan; S. Salmieri, C. L. Tien, B. Riedl, J. Bouchard, G. Chauve, V. Tan, M. R. Kamal, and M. Lacroix, *Mechanical and Barrier Properties of Nanocrystalline Cellulose Reinforced Chitosan Based Nanocomposite Films, Carbohydrate Polymers,* **2012**, *90(4)*: 1601-1608.

[17] R. Pantani, G. Gorrasi, G. Vigliotta, M. Murariu, and P. Dubois, *PLA-ZnO Nanocomposite Films: Water Vapor Barrier Properties and Specific end-use Characteristics*, European Polymer Journal, **2013**, *49(11)*: 3471-3482.

[18] F. Dalmas, N. Genevaz, M. Roth, J. Jestin, and E. Leroy, *3D Dispersion of Spherical Silica Nanoparticles in Polymer Nanocomposites: A Quantitative Study by Electron Tomography*, Macromolecules, **2014**, *47(6)*: 2044-2051.

[19] N. Misra, V. Kumar, J. Bahadur, S. Bhattacharya, S. Mazumder, and L. Varshney, *Layered Silicate-Polymer Nanocomposite Coatings via Radiation Curing Process for Flame Retardant Applications*, Progress in Organic Coatings, **2014**, *77(9)*: 1443-1451.

[20] S. Kohjiya, A. Kato, and Y. Ikeda, *Visualization of Nanostructure of Soft Matter by 3D-TEM: Nanoparticles in a Natural Rubber Matrix*, Progress in Polymer Science, **2008**, *33(10)*: 979-997.

[21] M. K. Jaiswal, and R. Kumar, *Dense Electronic Excitation Induced Modification in TiO_2 Doped SnO_2 Nanocomposite Films*, Journal of Alloys and Compounds, **2014**, *610*: 651-658.

[22] W. Chen, C. M. Li, L.Yu, Z. Lu, and Q. Zhou, *In situ AFM Study of Electrochemical Synthesis of Polypyrrole/Au Nanocomposite*, Electrochemistry Communications, **2008**, *10(9)*: 1340-1343.

[23] S. B. Subramanian, A. P. Francis, and T. Devasena, *Chitosan–Starch Nanocomposite Particles as a Drug Carrier for the Delivery of Bis-desmethoxy Curcumin Analog*, Carbohydrate Polymers, **2014**, *114(0)*: 170-178.

[24] R. H. Upadhyay, and R. R. Deshmukh, *Investigation of Dielectric Properties of Newly Prepared β-phase Polyvinylidene Fluoride–Barium Titanate Nanocomposite Films*, Journal of Electrostatics, **2013**, *71(5)*: 945-950.

[25] A. Konwar, G. Neelam, M. Gitanjali, and C. Devasish, *Green Chitosan–Carbon Dots Nanocomposite Hydrogel Film with Superior Properties*, Carbohydrate Polymers, **2015**, *115(0)*: 238-245.

[26] M. Monti, M. Rallini, D. Puglia, L. Peponi, L. Torre, and J. *M.* Kenny, *Morphology and Electrical Properties of Graphene–Epoxy Nanocomposites Obtained by Different Solvent Assisted Processing Methods,* Composites Part A, **2013**, *46(0)*: 166-172.

[27] P. H. C. Camargo, K. G. Satyanarayana, and F. Wypych, *Nanocomposites: Synthesis, Structure, Properties and New Application Opportunities,* Materials Research, **2009**, *12(1)*: 1-39.

[28] S. Khanlari, and M. A. Dubé, *In situ Poly(Sodium Acrylate)-Based Nanocomposite Formation by Redox-Initiated Solution Polymerization,* Polymer Engineering and Science, **2015**, *55(6)*: 1230-1236.

[29] W. V. Nicholson, and R. M. Glaeser, *Review: Automatic Particle Detection in Electron Microscopy*, Journal of Structural Biology, **2001**, *133(2–3)*: 90-101.

[30] V. Hergault, P. Frey, and F. Métivier, *Image Processing for the Study of Bedload Transport of Two-Size Spherical Particles in a Supercritical Flow,* Experiments in Fluids, **2010**, *49(5)*: 1095-1107.

[31] T. M. Liebling, and L. Pournin, *Voronoi Diagrams and Delaunay Triangulations: Ubiquitous Siamese Twins*, Documenta Mathematica, **2012**, Extra Volume: *419-431*.

[32] L. Ju, T. Ringler, and M. Gunzburger, *Voronoi Tessellations and Their Application to Climate and Global Modeling*, Lecture Notes in Computational Science and Engineering, **2011**, *80*: 313-342.

[33] S. Teerarojanarat, K. Tingsabadh, S. T. A. K. Tingsabadh, *A Gis-Based Approach For Dialect Boundary Studies*, Dialectologia, **2011**, *6:* 55-75.

[34] B. Boots, and R. South, *Modeling Retail Trade Areas Using Higher-Order, Mukiplicatively Weighted Voronoi Diagrams*, Journal of Retailing, **1997**, *73*: 519-536.

[35] P. J. Halls, M. Bulling, P. C. L. White, L. Garland, and S. Harris, *Dirichlet Neighbours: Revisiting Dirichlet Tessellation for Neighbourhood Analysis*, Computers, Environment and Urban Systems, **2001**, *25*: 105-117.

[36] W. B. March; P. Ram, and A. G. Gray, *Fast Euclidean Minimum Spanning Tree: Algorithm, Analysis, and Applications, in Proc. 16th ACM SIGKDD (KDD '10),* **2010**, New York, NY, USA: 603-613.

[37] S. C. Wieland, J. S. Brownstein, B. Berger, and K. D. Mandl, *Density-Equalizing Euclidean Minimum Spanning Trees for the Detection of all Disease Cluster Shapes, Proceeding of the National Academy of Science of the United States of America,* **2007**, *104(22)*: 9404-9409.

[38] J. J. Moré, and D. C. Sorensen, *Computing a Trust Region Step,* SIAM Journal on Scientificand Statistical Computing, **1983**, *3*: 553-572.

Chapter 6: Reaction Monitoring of In-Situ Formation of Poly(sodium acrylate) based Nanocomposite Using ATR-FTIR Spectroscopy

S. Khanlari and M. A. Dubé, *Industrial and Engineering Chemistry Research* (2015), Volume 54, pages 5598−5603.

Abstract: The in situ formation of poly(sodium acrylate)-based nanocomposites was monitored in-line using an attenuated total reflectance/Fourier transform infrared (ATR-FTIR) spectroscopic probe. Results were compared with conversion measurements using an off-line gravimetric method. A multivariate statistical data treatment based on the on-line data for the nanocomposite containing 0.5 wt.% of nanosilver was used to calibrate the ATR-FTIR spectroscopic probe. The ATR-FTIR method was shown to be reliable based on 95% confidence intervals for monitoring the production of polymers synthesized in the presence of different amounts of nanosilver over the full range of monomer conversion.

6.1 Introduction

Sensor technologies for polymerization reaction monitoring have seen significant growth during the past years. Online monitoring of polymerization reactions is crucial to the production of polymers with pre-determined properties because it provides information on the state and evolution of the on-going reaction [1]. Sensor-based online monitoring

has some advantages over traditional off-line monitoring; for example, online monitoring is typically much faster than off-line methods, thus enabling more frequent measurements with less effort. Moreover, effective on-line measurement methods do not involve complicated sample workup and allow for a quick response to rapidly changing reaction conditions for the purposes of process control [1, 2].

Attenuated total reflectance Fourier Transform infrared (ATR-FTIR) spectroscopy is a method for which robust, reliable sensors are commercially available (e.g., ReactIR™ from Mettler-Toledo). ATR-FTIR probes can be used as immersion probes to provide continuous data transmission in real-time. This permits one to implement closed-loop control strategies on various reaction conditions and polymer properties. This eventually leads to more consistent product quality. In the case of process investigations, in-line sensors such as ATR-FTIR spectroscopy probes permit an enhanced understanding of the underlying phenomena in polymerization reactions that might be overlooked with off-line analysis [1].

A number of polymerizations have been successfully monitored using the ReactIR 1000™ probe (Mettler-Toledo) and later models [3, 4]. These examples provide continuous conversion and polymer composition data under a wide range of reaction conditions. For some systems, a non-calibrated univariate method was sufficient to calculate individual monomer conversions by monitoring the peak height of characteristic IR absorbances for each monomer [2]. An alternative, calibrated method using multivariate partial least squares (PLS) regression to relate the IR spectral changes to monomer concentration was necessary in other cases [4]. One challenge often faced by users of infrared spectroscopy as a quantitative tool, is the presence of water. This has

been overcome using spectral subtraction of the water absorbances with good success [3-5]. In any case, ATR-FTIR real-time monitoring has been used in many fields other than polymer reaction engineering [6-10]. To our knowledge, there are no reports of online ATR-FTIR monitoring in the production of nanocomposite materials, which is the focus of the current work.

Nanofillers may be added to polymer matrices to modify mechanical properties, hydrophilicity, adhesive properties, among many others. Interestingly, due to their high surface to volume ratio, nanofillers are typically added to the polymer matrices at very low loadings [11]. Nanosilver is one nanomaterial that is under high scrutiny today and its effects are studied widely. Nanosilver particles are not perfectly spherical and have a characteristic dimension less than 100 nm. These particles generally contain 20-15,000 silver atoms [12]. Products containing nanosilver particles have been commercially available for over 100 years and were used in applications as diverse as pigments, in photography, wound treatment, conductive/antistatic composites, catalysts, and as a biocide [13]. Nanosilver has received particular attention due to its anti-bacterial properties [12, 14-17].

In situ polymerization is one of three conventional methods used to produce polymer-based nanocomposites; the others being solution blending and melt mixing. In situ polymerization involves simultaneous dispersion of nanoparticles during a polymerization reaction. This results in an enhanced dispersion of the inorganic nanoparticles and is the reason why this technique is considered one of the most promising for polymer nanocomposite production [18].

Poly(sodium acrylate) (PNaA) is a material finding increased use as a bioadhesive [19] and superabsorbent [20]. It is produced through the polymerization of acrylic acid monomer neutralized by sodium hydroxide (see Figure 6.1). PNaA bioadhesives can be modified to enhance their antiseptic properties by combining them with nanosilver [15, 21-23].

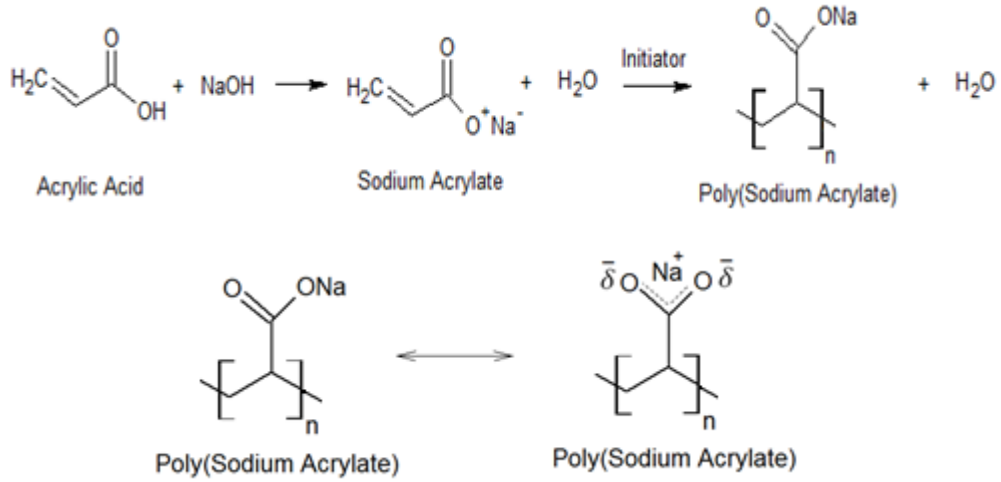

Figure 6.1 Poly (sodium acrylate) synthesis.

In a previous study, we reported the properties of PNaA based polymers synthesized in the presence of different amounts of NS; the monomer conversion was calculated using an off-line water removal gravimetric method [16]. In this work, the free radical aqueous solution in-situ polymerization of sodium acrylate in the presence of nanosilver (NS) using a redox initiation system was monitored via ATR-FTIR spectroscopy. Monomer conversion from the ATR-FTIR spectroscopy was compared to the off-line gravimetric method.

6.2 Experimental

6.2.1 Materials

Acrylic acid (>99.5%, Acros Organics), NaOH pellets (Sigma Aldrich), ammonium persulfate (APS, 98%+, Sigma Aldrich) and potassium disulfite (KDS, Sigma Aldrich) were used without further purification. The solvent used was distilled deionized water (DDW) and hydroquinone (JT Baker Chemicals) was used to short-stop the reaction. Nanosilver powder (Sigma-Aldrich) with an average particle size of <100 nm was used as nanofiller.

6.2.2 Synthesis

Pre-determined amounts of nanosilver were added to 14.9 g acrylic acid neutralized to pH 7 with sufficient amounts of NaOH dissolved in DDW in a 200 mL beaker. The mixture was stirred magnetically while exposed to normal atmospheric conditions (open to air at 22 ^{o}C). 3 mL each of APS and PDS aqueous solutions containing 0.35 and 0.34 g, respectively, were added to the monomer/nanoparticle mixture. Reactions exhibited a significant exotherm with temperature rising to as high as 94^{o}C, in some cases. More details about the synthesis are discussed elsewhere [16]. Table 6.1 summarizes the amounts of nanofiller used in each nanocomposite produced.

Table 6.1 Sample identification and nanoparticle loading.

Run	Sample	Nanosilver (wt.%)	Nanosilver (g)
1	PNaANS0	0	0
2	PNaANS0.5	0.5	0.075
3	PNaANS1	1	0.15
4	PNaANS2	2	0.3
5	PNaANS3	3	0.46

The polymerization reaction was terminated at pre-determined intervals to measure a conversion trajectory. Termination of the polymerization was accomplished using 0.17 g hydroquinone solution/g of sample to short-stop the reaction. The hydroquinone solution concentration was 0.4 g hydroquinone/g DDW.

6.2.3 Characterization

Monomer conversion was measured off-line using a standard gravimetric water removal method as well as in-line using ATR-FTIR spectroscopy. For the gravimetric method, the conversion (x in wt.%) was measured based on total dried polymer weight:

$$x(\%) = \frac{\%\ Solids - Nanoparticle\ wt.\% - Other\ Solids\ wt.\%}{Initial\ monomer\ weight\ \%} \times 100 \qquad (6.1)$$

where

$$\%\ Solids = \frac{Dry\ sample}{Initial\ sample} \times 100 \tag{6.2}$$

The polymer was dried under vacuum at room temperature for a minimum of 24 h until a constant weight was achieved. The "Other Solids" in equation 1 accounts for the initiator and hydroquinone added to the reaction mixture. The gravimetric (off-line) mass-based conversions were converted to molar conversions using the molar mass of sodium acrylate (94 g/mol).

In-line data were collected using an ATR-FTIR spectroscopic fibre optic probe (ReactIR45™, Mettler Toledo) immersed in the reaction mixture to track polymer formation and monomer consumption. Spectra were obtained within the frequency range 3000–650 cm^{-1}. Because all of the reactions achieved full conversion within a few minutes, ATR-FTIR data were collected every 5 s, which is the shortest possible interval using the ReactIR45™. Data analysis was accomplished via both a univariate method and a multivariate method. For the univariate method, molar conversions were calculated using the height of the monomer peak at the beginning of the reaction, and the height of the peak at time *t* with [4, 24]:

$$x\ (mol\%) = \frac{Peak\ height\ at\ time\ 0 - Peak\ height\ at\ time\ t}{Peak\ height\ at\ time\ 0} \times 100 \tag{6.3}$$

Equation 6.3 is equivalent to the basic definition of conversion:

$$x\ (mol\%) = \frac{[M]_0 - [M]_t}{[M]_0} \times 100 \tag{6.4}$$

where $[M]_0$ is the initial concentration of the monomer and $[M]_t$ is the concentration of the monomer at time *t*. A number of different peaks were evaluated as part of the univariate approach.

The multivariate method for data analysis comprises a linear combination of several peaks:

$$\begin{gathered}\alpha_1 S_1^1 + \alpha_2 S_2^1 + \cdots \ldots \ldots . . + \alpha_n S_n^1 = O_1 \\ \alpha_1 S_1^2 + \alpha_2 S_2^2 + \cdots \ldots \ldots + \alpha_n S_n^2 = O_2 \\ \vdots \\ \alpha_1 S_1^n + \alpha_2 S_2^n + \cdots \ldots \ldots + \alpha_n S_n^n = O_n\end{gathered} \tag{6.5}$$

where S_i^j is the value of peak *i* at time *j*, and O_i is the conversion calculated by the off-line gravimetric method (equations 1 and 2) at the same time, *j*. Different peaks from different runs were used to develop a more comprehensive model. The α_i parameters were calculated to form a calibration equation and then used to predict conversion. This process was automated using a function in the QUANTIR ("iC IR 4.3") software provided with the ReactIR45™. Several calibrations were performed under the constraint that samples (and runs) used for calibration were different from those used for validation of the method. Thus, a set of reactions was selected to first develop and then validate the PLS models.

6.3 Results and Discussion

In order to study the effect of nanoparticles on the polymerization mechanism it was necessary to first ensure that the nanocomposite has formed successfully. Scanning electron microscopy showed no evidence of agglomeration and a fairly homogeneous distribution of nanoparticles was achieved throughout the polymer matrix, as discussed elsewhere [16, 25].

Several conditions must be met to assess the applicability of ATR-FTIR spectroscopy to monitor a reaction. These include an acceptable signal to noise intensity ratio, the absence of fouling on the probe tip, and the use of an appropriate background spectrum [2, 4]. In our experiments, all three conditions were satisfied. In other words, no fouling was observed on the probe tip, the signal to noise ratio was high enough to clearly distinguish smooth peaks (these are all clearly illustrated in Figure 6.2 for run PNaANS1) and because of broad signal overlap, the solvent (i.e., water) spectrum was subtracted from all of the reaction spectra. At any time during the polymerization reaction, polymer, monomer and water were present in the reaction mixture. Figure 6.2 also shows how the spectra changed during the polymerization. One can clearly observe absorbance peaks that decrease with time, which are attributable to the consumption of acrylic acid (i.e., sodium acrylate) monomer. Other peaks increasing with time relate to the production of poly(sodium acrylate). Assignment of important peak locations to specific monomer and polymer microstructure is given in Table 6.2 and in greater detail elsewhere [16].

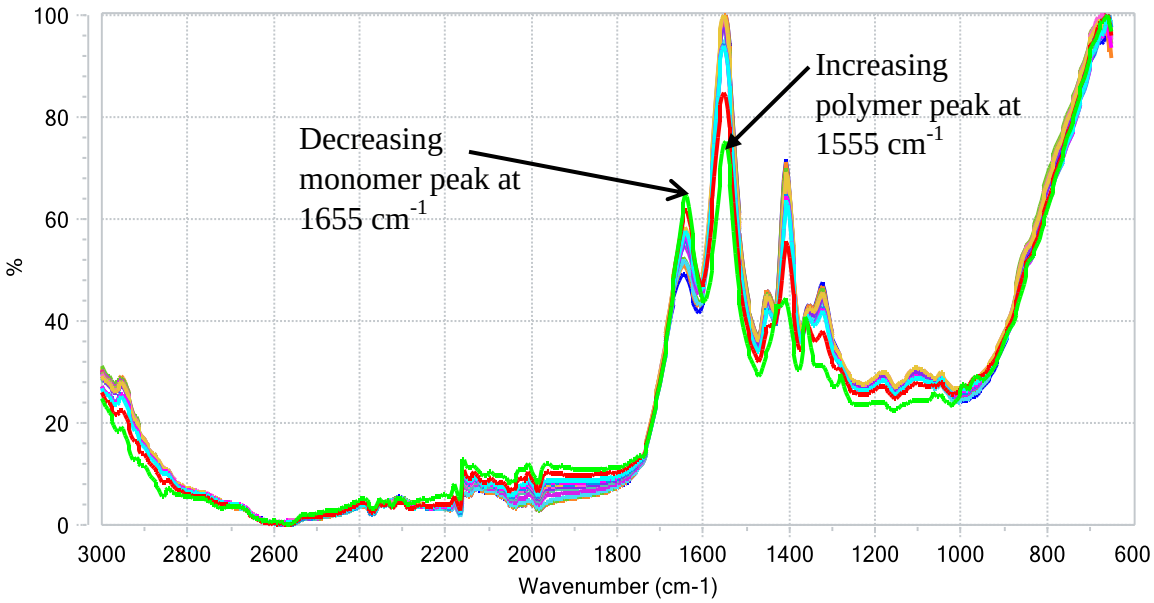

Figure 6.2 Typical ATR-FTIR spectra of the polymerization of sodium acrylate (PNaANS1), after solvent subtraction.

Table 6.2 Peak absorbance values and assignments.

Peak absorbance (cm^{-1})	**Assignment**
1077	O-Na out of plane bending
1112	C-CH_2 stretching
1331	C-O stretching
1409	CH_2 bending
1458	CO_2 (strong)
1555	O=C-O
1655	C=C stretching (monomer)

The nanosilver particles do not absorb in the IR range of 4000-450 cm^{-1}. As a result, they may only possibly exert some influence on the intensity of absorbance peaks

[26]. Thus, because of their low loading and the absorbance frequency being outside of the range of the equipment, the nanosilver particles could not be detected using ATR-FTIR.

The applicability of the ATR-FTIR method for monitoring conversion was examined first using a univariate method. For this purpose, the absorbance of different functional groups in the polymerization mixture (see Table 6.2), which could be either monomer (decreasing peaks) or polymer (increasing peaks), was monitored versus time. Each moiety is observed as a characteristic peak and its intensity, which could be measured as a peak height, is proportional to its concentration according to Beer's law [4]. It should be noted that the absolute value of the numerator of equation 6.3 was used to account for a decreasing peak height (for monitoring monomer consumption) or for an increasing peak height (for monitoring polymer generation).

By applying the peak assignments in Table 6.2 using a univariate approach, no single peak provided an accurate representation of the reaction progress when compared to the off-line gravimetric results. The basis of using equation 6.3 is that the only function affecting the peak's height (peak intensity) is concentration. However, according to Olya et al. the presence of nanosilver may also affect peak height [26]. This was the case for runs #1 through #4. It should be noted that, due to significant temperature rise during the reactions (>30 ^{o}C) a temperature correction was also attempted, but was unsuccessful. Thus, a multivariate (partial least squares (PLS)) approach was attempted next.

For the multivariate PLS approach, among the total number of spectra selected for the calibration, a smaller number of key spectra, which are called *factors*, are selected in such a way that when used as a linear combination, they minimize the predicted residual

error sum of squares (PRESS). The PRESS analysis is used to find the optimum number of factors for which the linear combination of spectra is most precise, i.e., the maximum correlation coefficient, R^2, when comparing predicted to actual (off-line) data. Factors are composed of several peaks within the same spectral region [4]. Figure 6.3a shows a PRESS analysis for the model trained using on-line data from Run#2 (PNaANS0.5) and calibrated using the same sample's off-line conversion data. As the number of factors containing useful information increases, the PRESS value decreases, which implies an improvement to the fit of the PLS calibration model. At some point, the factors added to the PLS model convey noise or other information irrelevant to the conversion and therefore the PRESS value increases significantly. The number of factors for which a minimum PRESS and Root Mean Square Error of Calibration (RMSEC) values were achieved, was used to build the calibration model. RMSEC analysis for the developed models is shown in Figure 6.3b. Figure 6.3a illustrates that by applying 8 factors in developing the multivariate PLS model, the PRESS value is at a desirable minimum. The RMSEC analysis in Figure 6.3b shows that by increasing the number of factors from 8 to 15 no significant change to the RMSEC, which is consistent with the PRESS analysis. In other words, the PLS multivariate calibration model was developed based on 8 factors for which the value of R^2 rendered the closest possible value to 1.

In some studies, the effect of temperature was negligible [4] but in this study, because of the highly exothermic nature of the reaction, temperature increases of greater than 30 ^{o}C were encountered. Figure 6.4 shows the temperature profile for each reaction. In this plot, time zero corresponds to the moment when the redox initiator was added to the reaction mixture. The extent of the temperature rise was dependent on the nanosilver

loading. This dependence was due to the interaction of the nanosilver with the redox initiation system, as discussed in greater detail elsewhere[16]. Therefore, in addition to the spectral peaks, the effect of temperature was included in the PLS calibration model.

a)

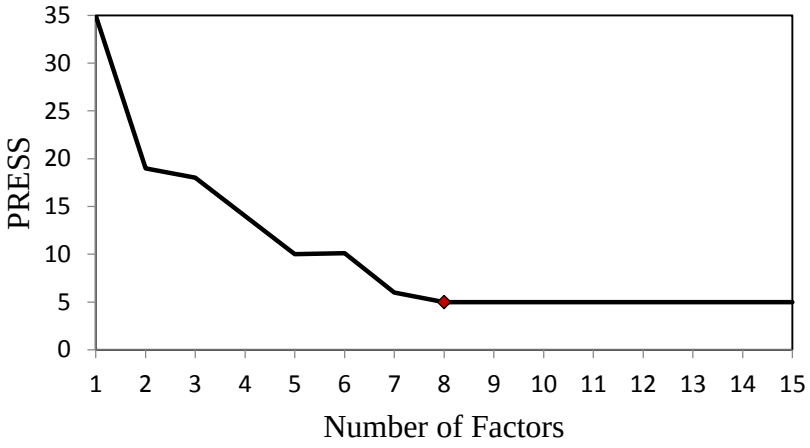

b)

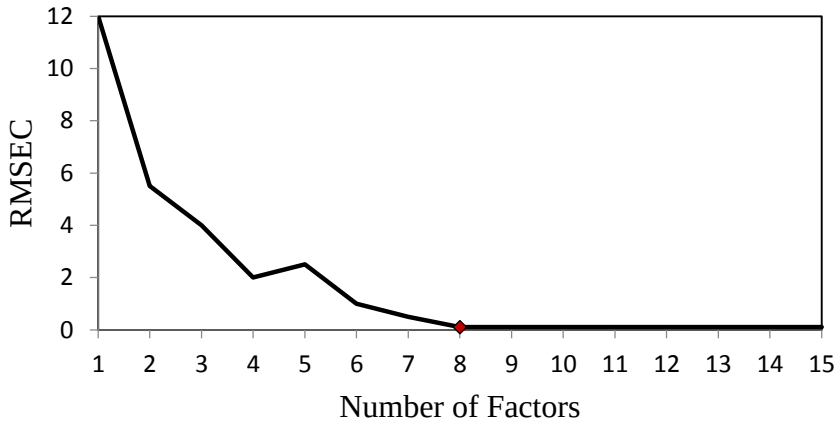

Figure 6.3 a) PRESS analysis b) RMSEC analysis for the multivariate PLS model.

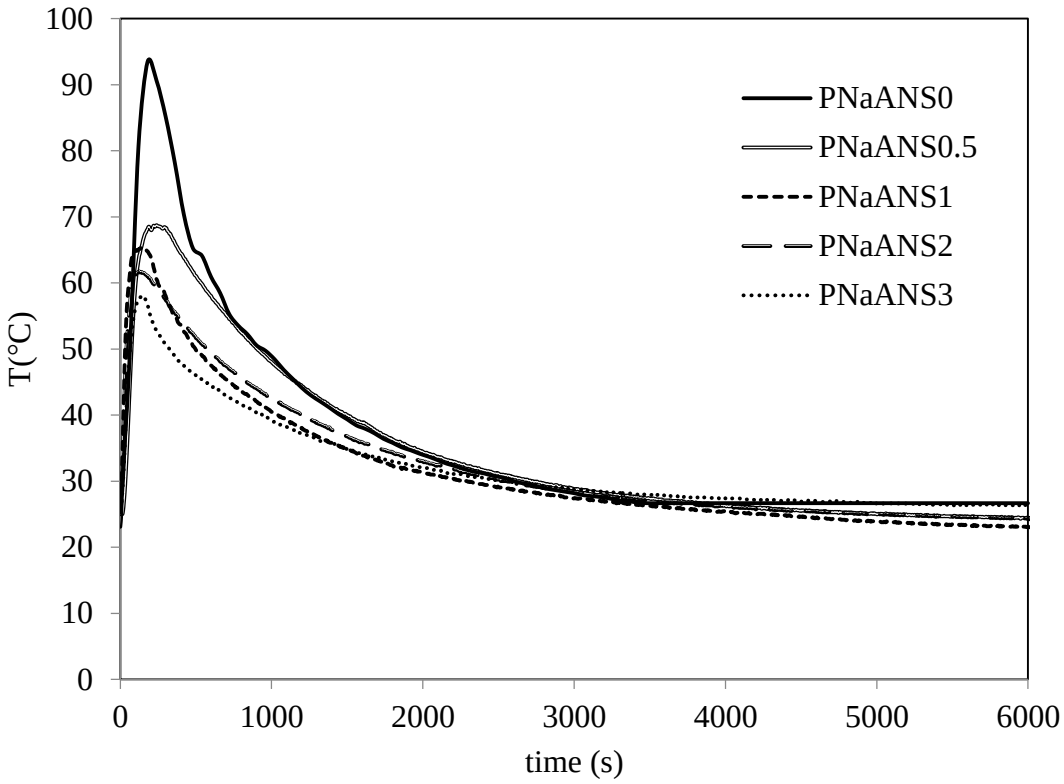

Figure 6.4 Temperature rise for PNaANS0, PNaANS0.5, PNaANS1, PNaANS2 and PNaANS3.

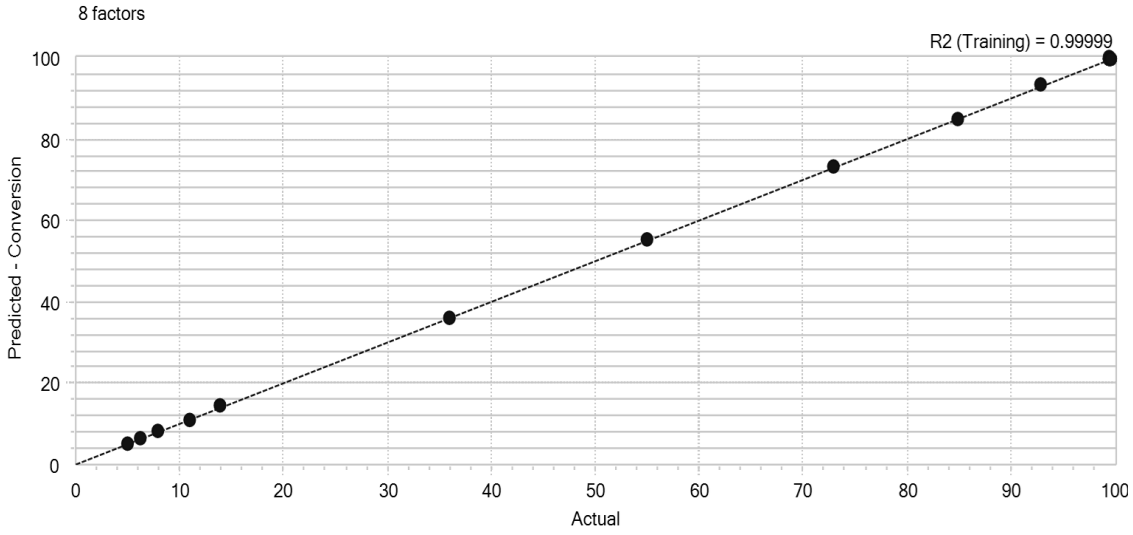

Figure 6.5 Actual versus predicted conversion for model developed using online data from run PNaANS0.5.

Figure 6.5 illustrates the quality of the calibration curve developed from the 8 factors based on the PRESS and the RMSEC analysis; the coefficient of determination, R^2, was 0.9999.

In order to validate the developed PLS multivariate model's accuracy and applicability to other reaction conditions, the on-line data were treated using the calibration model for runs 1, 3, 4 and 5. The results are shown in Figure 6.6; the error expected from the ReactIR45 was ± 3 wt% [27]. According to Figure 6.6, the prediction of the reaction conversion, validated using the off-line gravimetric data, is excellent over the full conversion range. A paired comparison was carried out between the monomer conversion obtained by off-line data calculated via water removal gravimetry and the PLS multivariate model predictions. 95% confidence intervals for the paired comparisons were [-2.0446, 0.7011] (mol. %) for PNaANS0, [-1.2312, 1.1099] (mol. %) for PNaANS1, [-2.5139, 0.5611] (mol. %) for PNaANS2 and [-1.0110, 0.7083] (mol.%) for PNaNS3. Each of these intervals contains zero and therefore implies that no significant difference between the in-line and off-line data exists.

a)

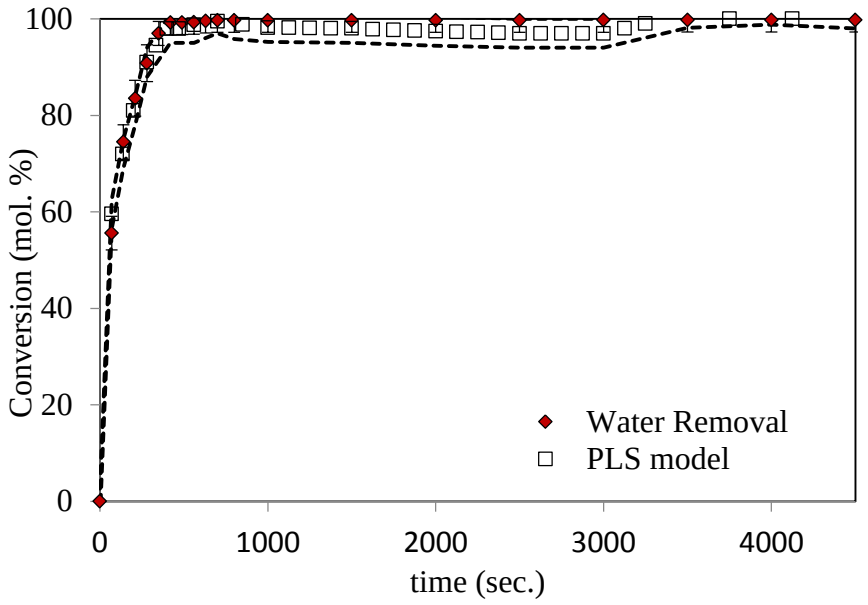
100
80
60
40
20
0
Conversion (mol. %)
0
1000
2000
3000
4000
time (sec.)
Water Removal
PLS model

b)

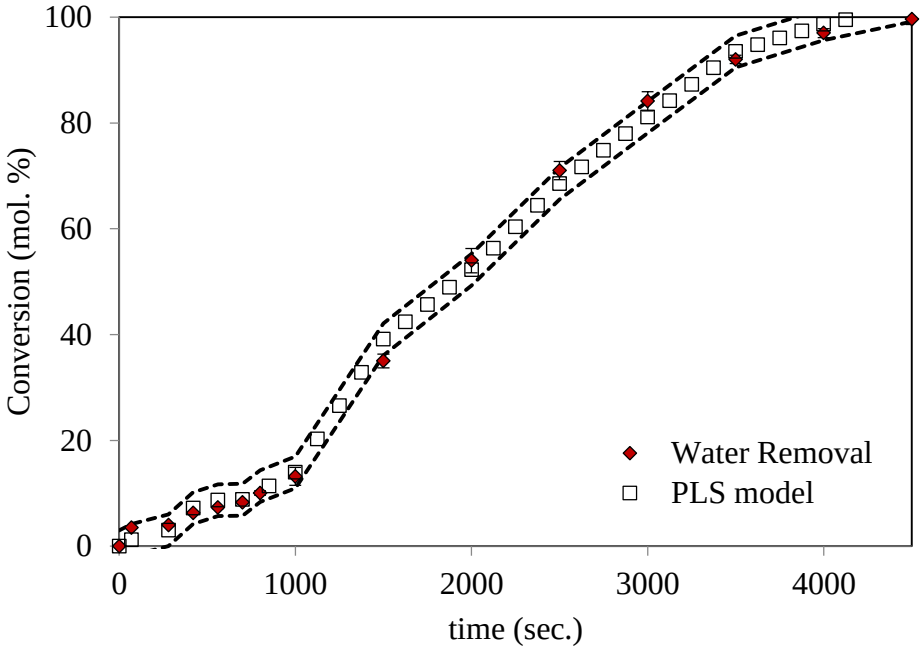
100
80
60
40
20
0
Conversion (mol. %)
0
1000
2000
3000
4000
time (sec.)
Water Removal
PLS model

c)

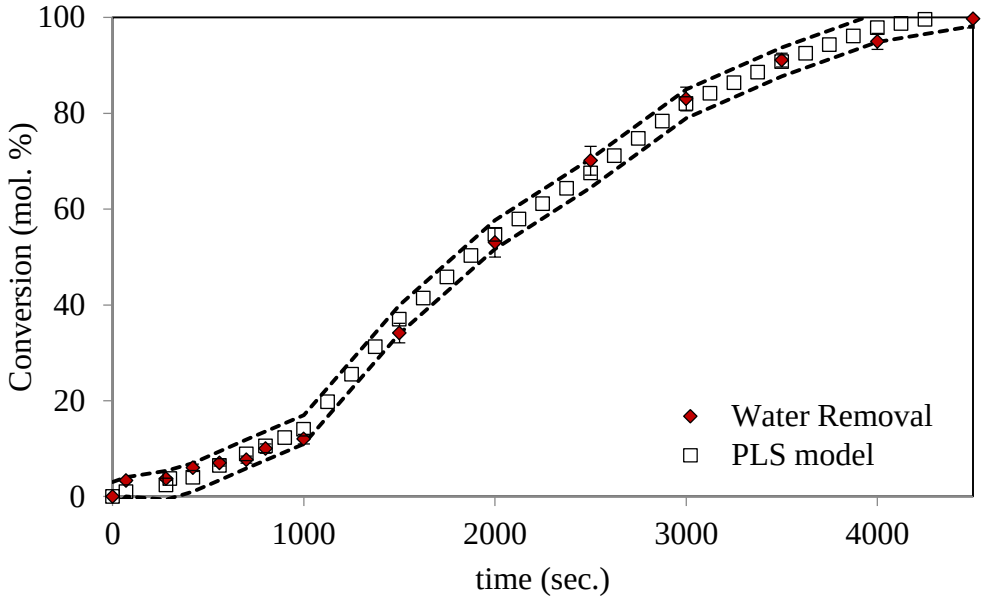

d)

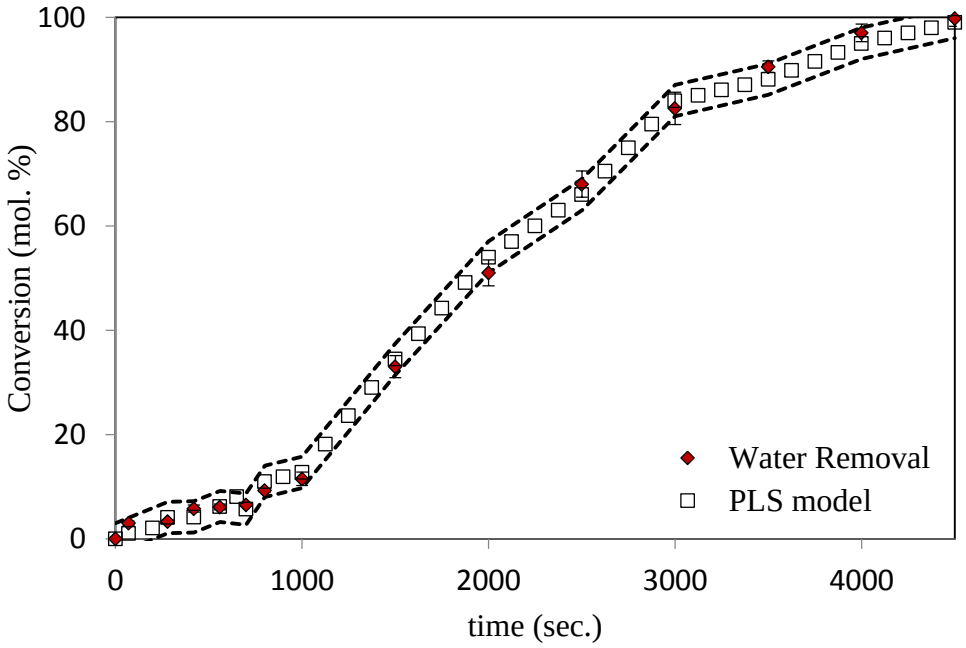

Figure 6.6 Model validations for a) PNaANS0 b) PNaANS1 c) PNaANS2 d) PNaANS3.

6.4 Conclusion

A series of NaA/NS in-situ polymer nanocomposites were produced. The conversions were measured off-line with a water removal gravimetric method, and in-line monitoring was performed using ATR–FTIR spectroscopy. No probe fouling was observed and the water background and the signal-to-noise ratio were both appropriate. A multivariate PLS method using the full spectrum of the PNaANS0.5 run and a temperature compensation term showed that no significant difference existed between the in-line and off-line data. This confirms that the ATR-FTIR can be used for the monitoring of reaction progress in nanocomposite formation.

6.5 Acknowledgements

The authors gratefully acknowledge the financial support of the Natural Sciences and Engineering Research Council (NSERC) of Canada. The authors also wish to acknowledge Stéphane Roberge for helpful discussions.

6.6 References

[1] G. E. Fonseca, M. A. Dubé and Alexander Penlidis, *A Critical Overview of Sensors for Monitoring Polymerizations*, Macromolecular Reaction Engineering, **2009**, *3(7)*: 327-373.

[2] S. Salehpour and M. A. Dubé, *Reaction Monitoring of Glycerol Step-Growth Polymerization Using ATR-FTIR Spectroscopy*, Macromolecular Reaction Engineering, **2012**, *6(2-3)*: 85-92.

[3] R. Jovanović and M. A. Dubé, *In-Line Monitoring of Butyl Acrylate/Vinyl Acetate Emulsion Copolymerizations Using ATR–FTIR Spectroscopy,* Polymer Reaction Engineering, **2003**, *11(3)*: 233-257.

[4] S. Roberge and M. A. Dubé, *Inline Monitoring of Styrene/Butyl Acrylate Miniemulsion Polymerization with Attenuated Total Reflectance/Fourier Transform Infrared Spectroscopy,* Journal of Applied Polymer Science, **2007**, *103(1)*: 46-52.

[5] M. A. Dubé and L. Li, *In-Line Monitoring of SBR Emulsion Polymerization Using ATR-FTIR Spectroscopy,* Polymer-Plastics Technology and Engineering, **2010**, *49(7)*: 648-656.

[6] O. Abbas, C. Rebufa, N. Dupuy, and J. Kister, *FTIR—Multivariate Curve Resolution Monitoring of Photo Fenton Degradation of Phenolic Aqueous Solutions: Comparison with HPLC as a Reference Method,* Talanta, **2008**, *77(1)*: 200-209.

[7] S. Briza, A. J. de Castrob, S. Dı´eza, F. Lo´pezb, and K. Schafer, *Remote Sensing by Open-Path FTIR Spectroscopy, Comparison of Different Analysis Techniques Applied to Ozone and Carbon Monoxide Detection,* Journal of Quantitative Spectroscopy and Radiative Transfer, **2007**, *103(2)*: 314-330.

[8] S. Grassi, J. Manuel Amigo, C. B. Lyndgaard, R. Foschino, and E. Casiraghi, *Assessment of the Sugars and Ethanol Development in Beer Fermentation with FT-IR and Multivariate Curve Resolution Models,* Food Research International, **2014**, *62(0)*: 602-608.

[9] E. Ziemons, N. Wandji Mbakop, E. Rozet, R. Lejeune, L. Angenot, L. Thunus, and Ph. Hubert, *Optimisation of SFE Method on-line Coupled to FT-IR Spectroscopy for the*

Real-time Monitoring of the Extraction of Tagitinin C in T. Diversifolia, The Journal of Supercritical Fluids, **2007**, *40(3)*: 368-375.

[10] R. K. Sahu, U. Zelig, M. Huleihel, N. Brosh, M. Talyshinsky, M. B. Harosh, S. Mordechai, and J. Kapelushnik, *Continuous Monitoring of WBC (biochemistry) in an Adult Leukemia Patient Using Advanced FTIR-Spectroscopy*, Leukemia Research, **2006**, *30(6)*: 687-693.

[11] S. Khanlari and M. A. Dubé, *Bioadhesives: A Review*, Macromolecular Reaction Engineering, **2013**, *7(11)*: 573-587.

[12] X. Chen and H. J. Schluesener, *Nanosilver: A Nanoproduct in Medical Application*, Toxicology Letters, **2008**, *176(1)*: 1-12.

[13] B. Nowack, H. F. Krug, and M. Height, *120 Years of Nanosilver History: Implications for Policy Makers*, Environmental Science & Technology, **2011**, *45(4)*: 1177-1183.

[14] C. Silan, A. Akcali, M. T. Otkun, N. Ozbey, S. Butun, O. Ozay, and N. Sahiner, *Novel Hydrogel Particles and their IPN Films as Drug Delivery Systems with Antibacterial Properties*, Colloids and Surfaces B: Biointerfaces, **2012**, *89(0)*: 248-253.

[15] G. A. Sotiriou and S. E. Pratsinis, *Antibacterial Activity of Nanosilver Ions and Particles*, Environmental Science & Technology, **2010**, *44(14)*: 5649-5654.

[16] S. Khanlari and M. A. Dubé, *In situ Poly(sodium acrylate)-Based Nanocomposite Formation by Redox-Initiated Solution Polymerization*, Polymer Engineering and Science, **2015**, *55(6)*: 1230-1236.

[17] M. A. Habeeb, *Effect of Nanosilver Particles on Thermal and Dielectric Properties of (PVA-PVP) Films,* International Journal of Applied and Natural Sciences (IJANS), **2013**, *2(4)*: 103-108.

[18] P. A. Zapata, L. Tamayo, M. Páez, E. Cerda, I. Azócar, and F. M. Rabagliati, *Nanocomposites Based on Polyethylene and Nanosilver Particles Produced by Metallocenic "In Situ" Polymerization: Synthesis, Characterization, and Antimicrobial Behavior,* European Polymer Journal, **2011**, *47(8)*: 1541-1549.

[19] D. Sakasegawa, M. Goto, and A. Suzuki, *Adhesion Properties of Physically Crosslinked Elastic Gels of Poly(sodium acrylate)–poly(acrylic acid) Mixtures Evaluated by a Point Contact Method,* Colloid and Polymer Science, **2009**, *287(11)*: 1281-1293.

[20] W. F. Lee, and Y. C. Chen, *Effect of Intercalated Reactive Mica on Water Absorbency for Poly(Sodium Acrylate) Composite Superabsorbents,* European Polymer Journal, **2005**, *41(7)*: 1605-1612.

[21] V. Alt, T. Bechert, P. Steinrücke, M. Wagener, P. Seidel, E. Dingeldein, E. Domann, and R. Schnettler, *An In Vitro Assessment of the Antibacterial Properties and Cytotoxicity of Nanoparticulate Silver Bone Cement,* Biomaterials, **2004**, *25(18)*: 4383-4391.

[22] H. J. Lee, S. Y. Yeo, S. H. Jeong, *Antibacterial Effect of Nanosized Silver Colloidal Solution on Textile Fabrics,* Journal of Materials Science, **2003**, *38*: 2199-2204.

[23] M. Y. Mamaghani, M. Pishvaei, and B. Kaffashi, *Synthesis of Latex Based Antibacterial Acrylate Polymer/Nanosilver via In Situ Miniemulsion Polymerization,* Macromolecular Research, **2011**, *19(3)*: 243-249.

[24] H. Hua, T. Rivard, and M. A. Dubé, *Off-line Monitoring of Styrene/Butyl Acrylate Copolymerizations in Toluene Using ATR-FTIR Spectroscopy*, Polymer, **2004**, *45(2)*: 345-354.

[25] S. Khanlari, A. Gheibi, and M. A. Dubé, *Image Processing Techniques for Nanocomposite Distribution Quantification,* to be Submitted **2015**.

[26] M. Akbarian, M. E. Olya, M. Ataeefard, M. Mahdavian, *The Influence of Nanosilver on Thermal and Antibacterial Properties of a 2K Waterborne Polyurethane Coating*, Progress in Organic Coatings, **2012**, *75(4)*: 344-348.

[27] H. Hua and M. A. Dubé, *In-line Monitoring of Emulsion Homo- and Copolymerizations Using ATR-FTIR Spectrometry*, Polymer Reaction Engineering, **2002**, *10(1-2)*: 21-39.

Chapter 7: Bioactivity of Nanocomposites Synthesized as Bioadhesives

S. Khanlari, M. A. Dubé, J. Tang, and K. Kirkwood, to be submitted (2015)

Abstract: Poly(sodium acrylate) (PNaA) based nanocomposites were synthesized using different nanosilver loadings via redox solution polymerization at room temperature and under full exposure to the atmosphere. The nanocomposites were shown to possess increasing antibacterial activity with increased nanosilver content. Biocompatibility was determined using an MTT assay; no significant cytotoxicity was observed at the examined nanosilver loadings. Finally, adhesion was measured using a tensile test and stress versus strain showed an acceptable stress developed in the model tissue adhered using the synthesized bioadhesive containing 2 wt. % of nanosilver. Results also showed that introducing a second more degradable polymer to the system in the form of an interpenetrating polymer network tuned the degradation rate of the bioadhesive.

7.1 Introduction

Infection occurring after injury is one of the leading causes of fatality for those initially surviving a natural disaster [1]. In such instances, immediate surgery may not be possible and alternatives to suturing to join damaged tissues that ensure prevention of infection and encourage healing are needed. Materials such as polymeric bioadhesives are well suited for such cases [2].

Although suturing remains the most common method for closing wounds, topical skin adhesives are increasingly being used by health professionals to replace sutures, staples and adhesive strips in the fields of trauma, plastic and other surgeries, emergency medicine and pediatrics [3]. Bioadhesion may be defined as the state in which two materials, at least one of which is biological in nature, are held together for extended periods of time by interfacial forces [4, 5] and it is used for many hard- and soft-tissue applications [6]. Bioadhesives have some advantages compared with traditional suturing. They provide a needle-free method of wound closure and do not require local anesthetics. They can accomplish other tasks, such as haemostasis (i.e., cessation of bleeding) and the ability to seal air leakages and have the potential to serve as drug-delivery systems. Another advantage of bioadhesives is the fact that they usually provide excellent cosmetic results [3, 7]. Tissue adhesives also present the potential to serve as delivery systems and can be engineered for slow, localized release of medications, such as pain treatment drugs, antibiotics, chemotherapy treatment or as a vehicle to growth factors and actual cell lines to assist in healing, namely, in poor healing tissues like cartilage [8]. Although the cost of tissue adhesives is higher than conventional sutures, follow-up visits for suture removal are not needed, reducing medical service time during the wound check visit [7].

Nanocomposites are a class of composite materials that are particle-filled polymers for which at least one dimension of the dispersed particles is in the nanometer range [9]. Nanofillers may be added to bioadhesive matrices to change hydrophilicity, mechanical properties, and adhesive properties as well as to impart other properties that may improve wound healing.

A series of nanocomposite hydrogels used for bioadhesives was prepared by Lee et al. from acrylic acid, poly(ethylene glycol), methyl ether acrylate, and intercalated hydrotalcite (HT) using photopolymerization. The results showed that the swelling ratio for these nanocomposite hydrogels increased with an increase in HT, but the gel strength and adhesive force for these gels decreased. The drug-release behavior for these gels was also examined [6].

The effect of silica nanofillers and silver nanoparticles in orthodontic adhesives was investigated by Lim et al. to analyze surface characteristics, physical properties and antibacterial activity against cariogenic streptococci [10]. They found that incorporation of silver nanoparticles into bonding adhesives was possible on both the physical and antimicrobial level.

Paksujarit et al. published their research on rice starch hydroxyapatite (HA) nanocomposites. In that work, they investigated the adhesive properties of the final product and concluded that the nanocomposite bioadhesive had a high water resistance (i.e., the bioadhesive dissolved only after 7 days) that could be useful in the human body. Moreover, their bioadhesive could provide direct bonding immediately on a glass surface in water for a long time, was biocompatible, bioabsorbable, of low cost, and was eco-friendly [11]. They also prepared gelatin/nanocarbon nanocomposites and showed that with the addition of 0.3 wt% carbon nanopowder, the maximum bonding strength of this adhesive to porcine muscle tissue was 0.06 ± 0.005 MPa, which is greater than that of bioadhesives without nanofillers [12].

Silver nanoparticles (nanosilver) are clusters of silver atoms that range in diameter from 1 to 100 nm, contain 20–15,000 silver atoms, and are attracting interest as long-

term antibacterial, antimicrobial and antifungal agents for applications in medicine [13-15]. No side effects or toxicity on human cells and tissues were observed when using biomaterials based on metallic nano-silver in clinical trials [15, 16]. While only a few nanoproducts are currently in use for medical purposes, the most prominent nanoproduct is nanosilver. Due to its strong antibacterial activity, nanosilver coatings are used on various textiles [17] and as coatings [18] on certain implants as well as in medical applications [19]. Furthermore, nanosilver is used for the treatment of wounds and burns and is marketed as a water disinfectant and room spray. Nanosilver has shown accelerated burn healing [20]. Thus, the use of nanosilver is becoming more widespread in medicine and related applications in recent years; for example in antimicrobial polypropylene (PP) based sutures [21], antibacterial chitin-based wound dressings [22], burn dressings [20] and bone cement [23].

The mechanism of antimicrobial activity of nanosilver is not well-known yet can be explained as follows:

a) Generally, Ag^+ metal ions destroy or pass through the microorganism's membrane and bond to the −SH group of cellular enzymes. The consequent critical decrease of enzymatic activity causes the micro-organisms' metabolism to change and inhibits their growth, up to the cell's death. The Ag^+ metal ions also catalyze the production of oxygen radicals that oxidize the molecular structure of bacteria. The antibacterial-antimicrobial-antifungal mechanism of silver nanoparticles has been attributed to the presence of water and oxygen. Elemental silver particles are released in the form of silver ions. The formation of active oxygen occurs according to the chemical reaction:

$$H_2O + \frac{1}{2}O_2 \xrightarrow{Silver\ Ions} H_2O_2 \rightarrow H_2O + (\dot{O}) \quad (7.1)$$

Such a mechanism does not need any direct contact between the anti-microbial agent and the bacteria, because the produced active oxygen (oxygen radical) diffuses from the nanocomposite to the surrounding environment. Therefore, the Ag^+ metal ions inhibit the multiplication of micro-organisms. Bacteria are not permanently exposed to oxygen radicals and thus, the ionic additive does not seem to facilitate the selection of resistant strains [24].

b) Another mechanism for the antibacterial activity of nanosilver proposed by Kumar and Munstedt stated that the silver cation, Ag^+, binds strongly to electron releasing groups in biological molecules containing sulfur, oxygen, or nitrogen, present in bacteria. This may result in defects of the cytoplasmic membrane or its detachment from the cell, and as a result, DNA molecules become condensed and lose their ability to replicate [25].

Li et al. observed that the surface of *Staphylococcus aureus* grown on a polymer membrane was smoother than that grown on polymer/nanosilver media. This morphological change of the bacterial growth implies that nanosilver may affect the structure of the bacterial membrane, thereby causing the defunctionalization of the bacteria. The mechanism of antibacterial activity of nanosilver membranes requires further study [26].

Hydrophilicity is a key characteristic for biomaterials as there is a direct correlation between hydrophilicity and biocompatibility of polymeric biomaterials [27]. Rather than designing a new polymer to achieve required properties, one can combine the properties

of two separate polymers via the synthesis of interpenetrating polymer networks (IPNs). IPNs comprise two or more independent polymer networks that are formed in the presence of one another [28]. IPN formation is a popular alternative to synthesizing new polymers. In other words, rather than designing a new copolymer to achieve required application properties, one can combine the properties of two separate polymers via the synthesis of IPNs. The IPNs behave like composite materials and reflect a combination of the properties of its components. Depending on the network composition, the degradation and drug-release behavior of IPNs can be varied from a few days to over a year without losing strength [29].

IPNs may be synthesized in a variety of ways, and the mode of synthesis is used as a convenient way of subdividing IPNs into various classes. These classes include sequential IPNs, simultaneous IPNs, and latex IPNs [30]. Koul et al. produced IPN hydrogels based on poly(acrylic acid) and gelatin (Ge). They evaluated the hydrogels for in vitro and in vivo biodegradation and in vivo release of gentamicin sulphate. In vitro and in vivo degradation studies demonstrated that with the increase of acrylic acid content in the IPN, the rate of degradation decreased while the opposite was observed with increasing Ge content [29].

In this study, poly(sodium acrylate) (PNaA)-based nanocomposites were synthesized in the presence of nanosilver, which is an antibacterial agent, at different nanosilver loadings. The antibacterial activity and biocompatibility of the samples were tested. Moreover, the effect of IPN formation using a second, more hydrophilic polymer on hydrophilicity and degradation rate of PNaA-based IPNs was investigated.

7.2 Experimental

7.2.1 Materials

Acrylic acid (AA) from Acros Organics, sodium hydroxide (NaOH) pellets, ammonium persulfate (APS) and potassium disulfite (KDS), all from Sigma Aldrich, were used without further purification. The solvent used was distilled deionized water (DDW). Nanosilver powder, purchased from Sigma-Aldrich, with an average particle size of <100 nm was used as nanofiller. SEM analysis demonstrated that the dimensions of the nanosilver particles were in the nanometer range (see Figure 7.1).

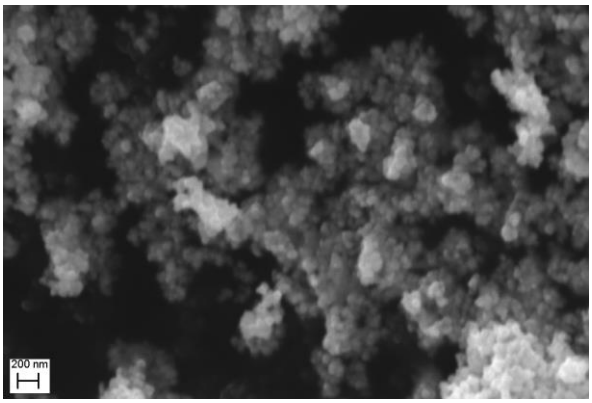

Figure 7.1 SEM image of nanosilver used in this project.

Bovine gelatin (Ge) and poly(vinyl alcohol) (PVA) (Sigma-Aldrich™) were used as the second, more degradable polymers to form the IPN. Phosphate buffered saline (PBS) solution was purchased from Fisher Scientific. Photoinitiator and crosslinker, diethoxyacetophenon (DEAP) and ethylene glycol dimethacrylate (EGDMA), respectively, and Lysogeny Broth (LB) were all purchased from Sigma Aldrich. Dulbecco's Modified Eagle's Medium (DMEM) and fetal bovine serum were purchased from Hyclone and the MTT assay kit was purchased from Life Technologies.

7.2.2 Nanocomposite Synthesis and Characterization

Metallic silver is insoluble in water, but metallic salts such as silver nitrate ($AgNO_3$) and silver chloride (AgCl) are soluble in water (hydrophilic) [31]. An innovative method has been developed by Tien et al. in which nanosilver particles with the ability of being suspended in pure water are produced directly via an arc-discharge method [16]. In this study, predetermined amounts of nanosilver (0.5, 1, 2 and 3 wt.% based on monomer weight) was added to 14.9 g AA which was already neutralized with a sufficient amount of NaOH dissolved in DDW. 0.34 and 0.35 g of APS and PDS were each dissolved in 3 g of DDW and were added to the reaction mixture to start the polymerization. More details about the polymerization was discussed elsewhere [32].

Before adding the initiator and at the very start of the reaction, the viscosity was low, therefore, a high agitation rate (using a magnetic stir bar) permitted the even dispersal of the nanosilver in the reaction mixture [33]. However, the rapid increase in viscosity eventually prevented further agitation. Nonetheless, this increased viscosity also prevented gravitational settling of the nanosilver. Thus, the hydrophobicity of the nanosilver particles was not an issue in our case. A sample with no nanosilver was also prepared as a control sample. Table 7.1 lists the sample formulations.

The polymer chemical structure was verified using attenuated total reflectance Fourier transform infrared (ATR-FTIR) spectroscopy with the ReactIR45™ (Mettler Toledo).

Table 7.1 Sample identification and nanoparticle loading.

Run #	Sample name	Nanosilver (wt. %)	Nanosilver (g)
1	PNaANS0	0	0
2	PNaANS0.5	0.5	0.075
3	PNaANS1	1	0.15
4	PNaANS2	2	0.3
5	PNaANS3	3	0.46

7.2.3 Antibacterial Property of the Nanocomposites

The antibacterial activity of the synthesized nanocomposites was studied using *Escherichia coli*, also known as E-coli, W3110 (ATCC27325). Initially, the bacteria were transferred to an LB medium, consist of 25 g LB and dissolved in 1 L of DDW, which was already autoclaved at 120 °C, and then incubated at 37 °C overnight. After a night of incubation, 50 µL of the liquid bacterial culture was transferred to vials of solution of LB each one containing 0.5 g of nanocomposite bioadhesive. After 24 h incubation in the presence of the nanocomposite bioadhesives at 37º C, optical densities (OD) of the cultures were measured at the wavelength of 600 nm using a spectrophotometer (Thermo Electron Corporation). Three samples were used for each experiment for statistical purposes.

7.2.4 Biocompatibility

Cytotoxicity is defined as the cell-killing ability of a compound (such as a food, cosmetic, or pharmaceutical). Cytotoxicity assays are widely used by the pharmaceutical industry as a means to assess biocompatibility (i.e., no cytotoxicity) which is necessary for all products to be used in contact with the human body. To assess the cytotoxicity, which reveals the biocompatibility of the samples, the cells were transferred to cell-growth media saturated by the samples and after an interval, the cell viability was measured based on an MTT (3-(4,5-Dimethylthiazol-2-Yl)-2,5-Diphenyltetrazolium Bromide) assay. Details of these tests follow:

7.2.4.1 Cell Culture 3T3 mouse fibroblasts, which were preserved in our lab, were incubated in a 25 mL flask at 37°C and 5% CO_2 environment until a sufficient cell count is achieved. The cells were grown to around 90% confluence, then digested with trypsin-EDTA. Digestion was stopped with DMEM. The cells were then suspended with 10% fetal bovine serum (FBS), counted and then cultured in 25 μL flasks at 2×10^5 cells per flask.

7.2.4.2 Cytotoxicity Test The PNaA/nanosilver nanocomposites were dissolved in DMEM to saturation and then sterilized in an autoclave. 3T3 fibroblasts were seeded in a 96-well plate. Each well had 1×10^4 cells and 0.5 mL of DMEM were supplemented with 10% FBS, gentamycin, penicillin (100 units/mL) and streptomycin (100 μg/mL). The cells were incubated at 37 °C in a humidified atmosphere of 5% CO_2 for 2 h. Afterwards, the original medium was removed carefully and replaced with the sample-dissolved medium (200 μL per well). After 24 h incubation, 10 μL MTT stock solution (12 mM) was added to each well; including a negative control of 10 μL of MTT stock solution

added to 200 µL medium. The next step was incubation at 37 °C for 4 h, followed by careful removal of the supernatant from each well and a final addition of 50 µL dimethyl sulfoxide (DMSO) to each well to dissolve precipitated crystals. Each solution was mixed thoroughly with a pipette and incubated at 37 °C for 10 min. Each sample was mixed again and the absorbances were read at a wavelength of 570 nm with a microplate reader (Bio-Rad).

7.2.5 Bioadhesion

The force required to detach two tissue sections with the nanocomposite bioadhesive sandwiched between them is considered as a good measure of bioadhesion; this force was determined using an Instron tester. The force detection system consists of a precision load cell and the tensile strength is determined with a constant speed of 30 mm/min and the force required to fracture the adhesive bond or detach the bioadhesive from the tissue is recorded [34]. At the end of the test, if the specimen is torn from the glued joining point, the energy consumed is deemed to have been mostly used to tear the adhesive, but if the specimen is torn from other parts, i.e., from the tissue, it implies that the mechanical strength of the bioadhesive is higher than that of the tissue. Figure 7.2 depicts the method to quantify the adhesion property. Porcine tissue was used as a model for soft tissue. A sufficient amount of bioadhesive (thickness ~ 1mm) was applied between two tissue pieces and after cross-link formation by UV radiation (30 s) using a handheld UV lamp (UVGL-58, 254 nm, 115 V ~60 Hz), the specimen was tested using a tensile test as described earlier.

7.2.6 IPN Formation and Characterization

Predetermined amounts of Ge and PVA were dissolved in 14.9 g AA and then neutralized with NaOH dissolved in distilled deionized water and stirred at room temperature. 0.35 g of APS and 0.34 g of PDS, each dissolved in 3 mL of DDW, were added to the mixture and polymerization occurred. Table 7.2 shows details about the formulation used in this part.

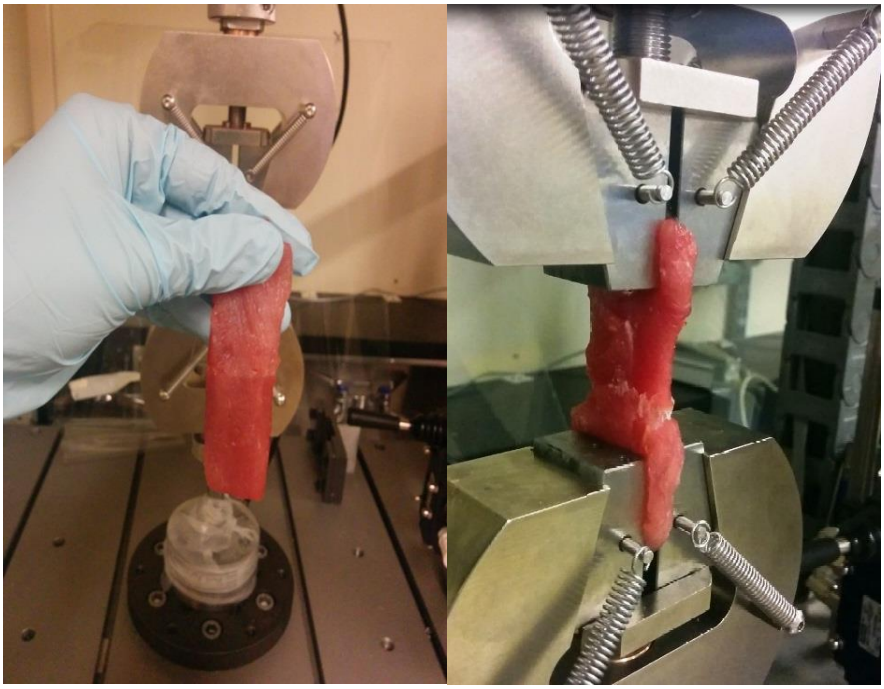

Figure 7.2 Bioadhesion property measurement method.

To determine the degradation rate of the crosslinked bioadhesive, a mixture of PNaA hydrogel (i.e., PNaA dissolved in a sufficient amount of water), crosslinker and photoinitiator was transferred to a cylindrical mould. To prepare the mixture, the polymer was dissolved in solvent (i.e., water) and then, initiator and crosslinker were added while stirring using a magnetic stirrer. Another option could have been to cast the mixture as a sheet on a glass plate, followed by solvent evaporation in a vacuum oven at room

temperature. The resulting sample served as a test specimen to determine the degradation rate in PBS solution and the amount of degradation was calculated by submerging the specimen in PBS solution at 37 ºC using:

$$Remaining\ weight\ (\%) = \frac{m_t}{m_0} \times 100 \quad (7.2)$$

where m_0 and m_t indicate initial and final sample mass. Hydrophilicity was determined by water contact angle measurements using a Sessile drop method with a 2 µL distilled water droplet using a VCA-Optima setup.

Table 7.2 Sample identification and IPN formulations.

Run #	Sample name	Ge (wt.%)	Ge (g)	Run #	Sample name	PVA (wt.%)	PVA (g)
1	PNaA	0	0	6	PNaA	0	0
2	PNaA/Ge3	3	0.46	7	PNaA/PVA3	3	0.46
3	PNaA/Ge5	5	0.83	8	PNaA/PVA5	5	0.83
4	PNaA/Ge8	8	1.29	9	PNaA/PVA8	8	1.29
5	PNaA/Ge10	10	1.65	10	PNaA/PVA10	10	1.65

7.3 Results and Discussion

7.3.1 Synthesis and Characterization

Figure 7.3 depicts the ATR-FTIR spectrograph for a typical polymer synthesized of nanosilver. More details about the synthesized polymer chemical structure and nanocomposite formation and morphology are discussed elsewhere [32, 33].

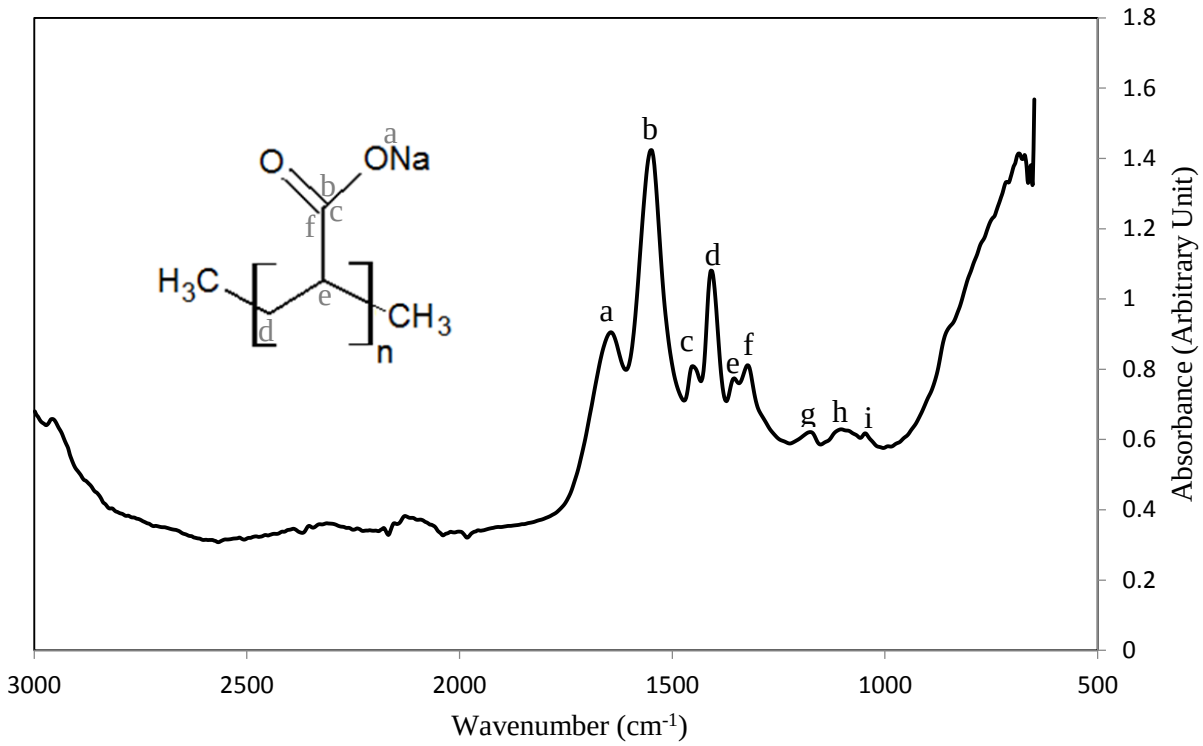

Figure 7.3 ATR-FTIR spectrum of the polymer synthesized.

7.3.2 Antibacterial Property

E. coli was selected as an indicator of bacterial growth in nanocomposites. Nutrient broth was used as the growing medium and all the activity was related to the silver nanoparticles. In order to measure the antibacterial activity of nanosilver in the liquid cultures, the reduction in the number of bacteria in the test sample compared to that of a control sample (i.e. a sample with no nanosilver in it) was calculated by Eq. (7.2) [18]:

$$\%reduction = \frac{N_{ref.} - N_{tst.}}{N_{ref.}} \times 100 \qquad (7.2)$$

where "$N_{ref.}$" represents the geometric mean of the number of bacteria recovered after the incubation period for the reference sample, and "N_{test}" represents that of the nanocomposite samples. The antibacterial activity can also be estimated according to by [18]:

$$Reduction\ log = log\ a\ - log\ b \tag{7.3}$$

A *Reduction log* around 0.026, 0.040, 1.355 and 1.385 was achieved for nanocomposites containing 0.5, 1, 2 and 3 wt.% nanosilver. These values reveal that the nanosilver was effective in preventing bacterial growth. At nanosilver loadings of 2 wt.% and higher, the effect was very strong. Figure 7.4 provides a visual illustration of the bacterial cultures in different nanocomposite samples before and after incubation. As shown in Figure 7.4, all of the samples were clear prior to incubation. After 24 h of incubation, bacterial growth is evident from the turbidity of selected samples. The samples containing 0, 0.5 and 1 wt.% nanosilver show differing degrees of turbidity. The samples PNaANS2 and PNaANS3 containing 2 and 3 wt% nanosilver, respectively, were still clear, implying low or no bacterial growth. Table 7.3 shows the quantitative assessment of bacterial growth where the number of bacteria recovered from the samples (pure polymer and the nanocomposites) after 24 h incubation are listed. Clearly, the addition of nanosilver led to the enhancement of antibacterial activity.

a)

b)

Figure 7.4 Visual illustration of sample vials of nanocomposites containing different nanosilver loadings a) before b) after the incubation.

Table 7.3 The number of bacteria, in cells/cm^3, after 24 h incubation.

Sample	**OD_{600}**	**Reduction log**	**%reduction**
PNaANS0	1.16±0.0035	-----	-----
PNaANS0.5	1.13±0.0030	0.026	5.88
PNaANS1	1.12±0.0005	0.040	8.82
PNaANS2	0.033±0.0012	1.355	95.58
PNaANS3	0.021±0.0010	1.385	95.88

7.3.3 Biocompatibility

Cell viability was calculated using the MTT assay as [35]:

$$\%\ Cell\ viability = \frac{test\ absorbance}{control\ absorbance} \times 100 \tag{7.4}$$

where control absorbance is the absorbance for cells grown in the presence of distilled water (without polymer or nanosilver). In this study, the absorbance for the control sample was 2.47±0.008. Table 7.4 summarizes the results of the MTT assay. The results indicate that cell viability decreases only slightly with increasing nanosilver loadings but is still within more than acceptable range for wound healing.

Table 7.4 Cell viability of samples containing different amounts of nanosilver.

Sample	Absorbance	Cell Viability (%)
PNaNS0	2.44±0.012	99.05±0.19
PNaANS0.5	2.42±0.013	98.11±0.19
PNaANS1	2.39±0.012	97.03±0.20
PNaANS2	2.37±0.013	96.08±0.20
PNaANS3	2.34±0.012	95.01±0.21

7.3.4 Bioadhesion

Figure 7.5 shows the stress strain relationship for a regular tissue sample as well as a sample joined with a nanocomposite bioadhesive (PNaANS2). The tissue sample failed at roughly 18% strain. The tissue sample bonded using the nanocomposite bioadhesive

failed at a slightly lower strain but for all intents and purposes, there is no appreciable difference. It should be noted however, that the failure of the bioadhesive bonded sample was at the bioadhesive joint. This implies that the bioadhesive is not as strong as the original tissue but given the results, it is not particularly less so. In addition, one should also consider that under normal conditions, the tissue would not be placed under such high stress.

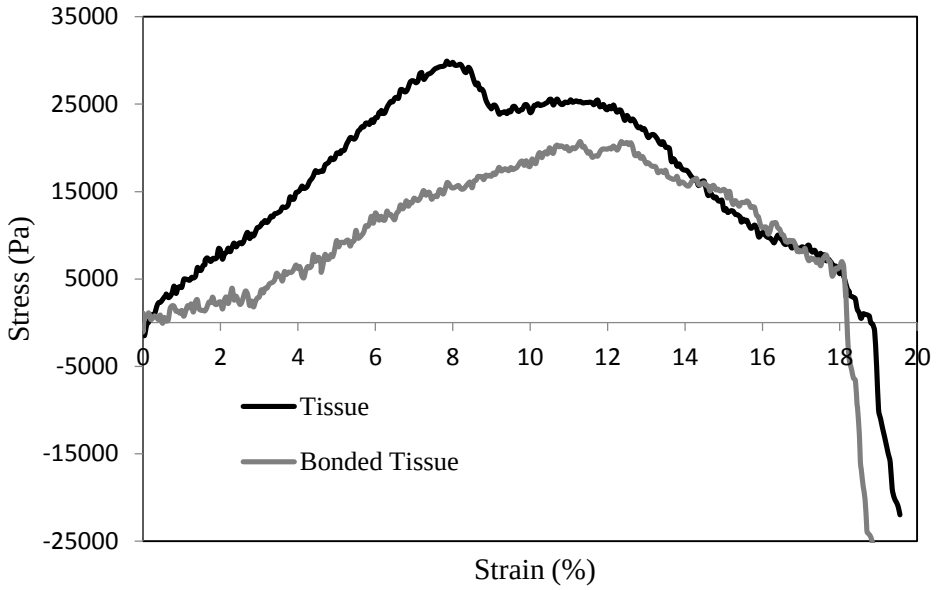

Figure 7.5 Stress-Strain relationships of tissue compare to that of bonded using PNaANS2 bioadhesive.

The presence of nanosilver in the bioadhesive results in an increase in polymer molecular weight on the one hand [32] and decreases cross-link density on the other hand [36]. These two factors may simultaneously increase and decrease the adhesion strength, respectively. Accordingly, no significant change is expected by varying the nanosilver loading.

7.3.5 Biodegradation

Figure 7.6 shows the contact angle of PNaA-based IPNs containing different amounts of a more hydrophilic polymer (i.e., PVA and Ge). The addition of 3 wt.% of the second, more hydrophilic polymer, decreased the contact angle notably. The addition of greater amounts of PVA or Ge had an insignificant effect on contact angle. The increased hydrophilicity after addition of either Ge or PVA as an IPN implies a higher degradation rate may be possible.

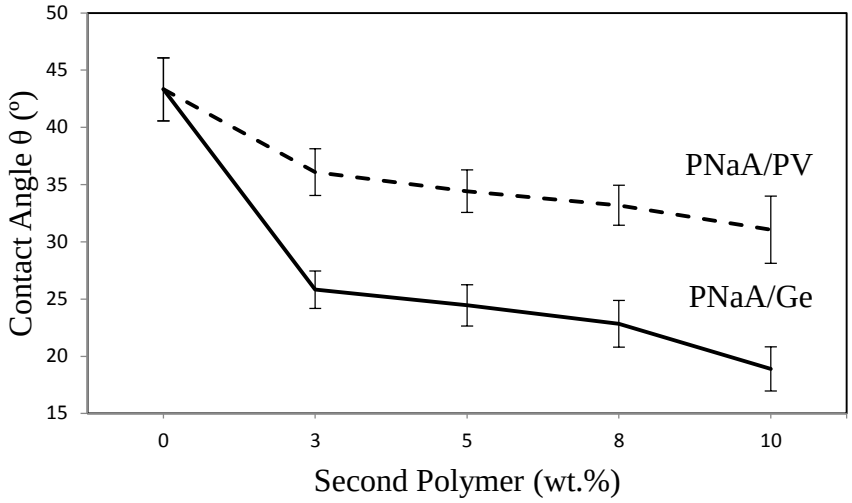

Figure 7.6 The effect of Ge and PVA on hydrophilicity.

Figure 7.7 shows the weight of PNaA and its IPNs in PBS solution. The presence of only 3 wt.% of the Ge or PVA increased the weight loss of the IPNs compared to the pure PNaA sample. This effect was less notable at the beginning of the degradation study period and as time elapsed, the difference in weight loss was significant. Thus, we can conclude that the presence of the more degradable polymer had a direct effect on the degradation rate in the IPN. Changes to the degradation rate were proportional to the

hydrophilic polymer concentration and this implies that the hydrophilic polymer (Ge or PVA) could be used to tune the degradation rate of the IPN.

a)

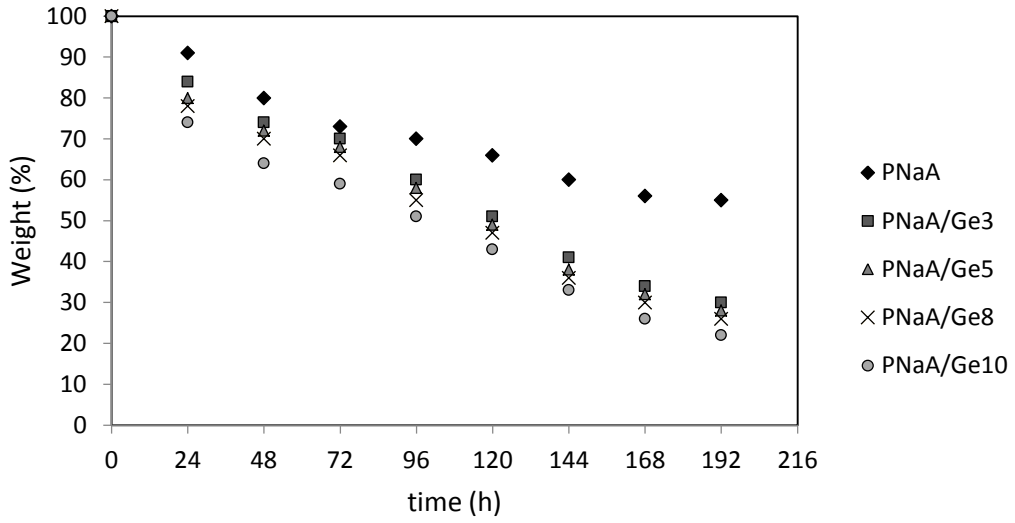

b)

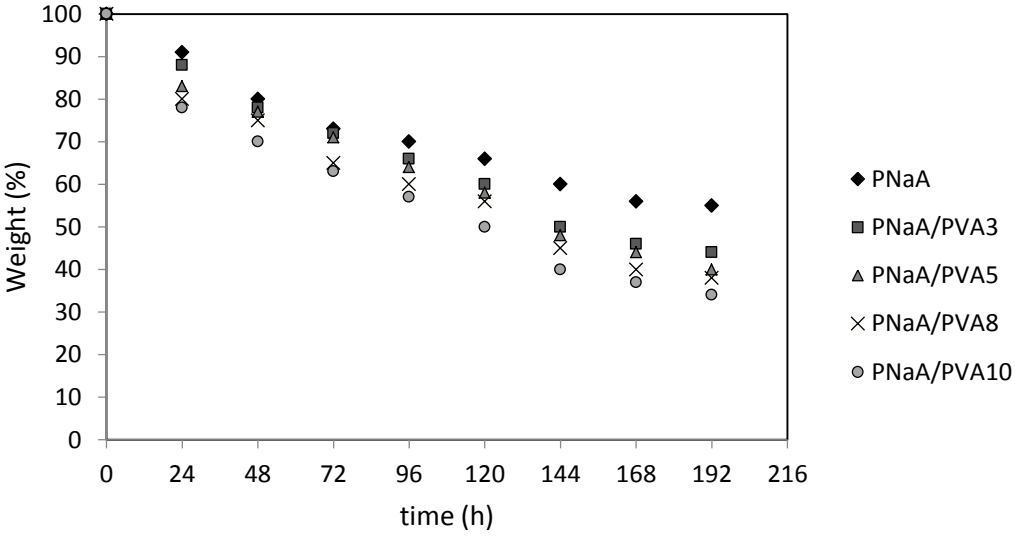

Figure 7.7 The effect of a) Ge and b) PVA incorporation on IPN degradations.

7.4 Conclusion

Poly (sodium acrylate)-based nanocomposites were synthesized via redox solution polymerization. The synthesized nanocomposites possess a significant antibacterial activity at very low loadings but this did not impede the biocompatibility of the nanocomposite material. Nanosilver is an effective antiseptic agent to be added to PNaA-based bioadhesives. Introducing a second, more degradable polymer, such as Ge or PVA, in the form of an IPN increases the hydrophilicity of the material and allows one to tune the degradation rate for application to specific medical demands. Cross-linked bioadhesives were shown to be within an acceptable range of bioadhesion; accordingly, this bioadhesive with antibacterial activity is a potential alternative for traditional suturing, especially in out-clinic aids e.g., in the aftermath of a natural disaster.

7.5 Acknowledgements

The authors would like to gratefully acknowledge Jamie Sivell for assistance with bacterial culture preparation and Shidan Cummings for help with tensile tests. We also acknowledge the financial support of the Natural Sciences and Engineering Research Council (NSERC) of Canada.

7.6 References

[1] J. Ambrosioni, D. Lew, and I. Uçkay, *Infectious Diseases and Infection Control After Natural Disasters,* International Journal of Infectious Diseases, **2010**, *14,* Supplement 1(0).

[2] S. Khanlari, and M. A. Dubé, *Bioadhesives: A Review,* Macromolecular Reaction Engineering, **2013**, *7(11)*: 573-587.

[3] P. Ferreira, J. F. Coelho, and M. H. Gil, *Development of a New Photocrosslinkable Biodegradable Bioadhesive,* International Journal of Pharmaceutics, **2008**, *352*: 172-181.

[4] S. K. Roy, and B. Prabhakar, *Bioadhesive Polymeric Platforms for Transmucosal Drug Delivery Systems – a Review,* Tropical Journal of Pharmaceutical Research, **2010**, *9(1)*: 91-104.

[5] J. D. Smart, *The Basics and Underlying Mechanisms of Mucoadhesion,* Advanced Drug Delivery Reviews, **2005**, *57*: 1556-1568.

[6] W. F. Lee, and Y. C. Chen, *Effect of Hydrotalcite on the Physical Properties and Drug-Release Behavior of Nanocomposite Hydrogels Based on Poly[Acrylic Acid-co-Poly(Ethylene Glycol) Methyl Ether Acrylate] Gels,* Journal of Applied Polymer Science, **2004**, *94*: 692-699.

[7] D. F. Aukerman, and W. J. Sebastianelli, *How Does Tissue Adhesive Compare with Suturing for Superficial Lacerations?* Journal of Family Practice, **2005**, *54*: 378-378.

[8] C. D. Hoemann, J. Sun, and A. Le´gare, M. D. Mckee, and M. D. Buschmann, *Tissue Engineering of Cartilage Using an Injectable and Adhesive Chitosan-based Cell-delivery Vehicle,* OsteoArthritis and Cartilage, **2005**, *13*: 318-329.

[9] M. Alexandre, and P. Dubois, *Polymer-Layered Silicate Nanocomposites: Preparation, Properties and Uses of a New Class of Materials,* Materials Science and Engineering: R: Reports, **2000**, *28*: 1-63.

[10] S. J. Ahn, S. J. Lee, J. K. Kook, and B. S. Lim, *Experimental Antimicrobial Orthodontic Adhesives Using Nanofillers and Silver Nanoparticles*, Dental Materials, **2009**, *25*: 206-213.

[11] W. Puntuwat, S. Wongas, J. Poonyawatpornkul, S. Punyanitya, and A. Raksujarit, *Processing and Characterization of Tissue Adhesive from Rice Starch Nanocomposites*, Advanced Materials Research, **2010**, *123-125*: 363-366.

[12] R. Koonawoot, S. Punyanitya, C. Tirapong, K. Boonchom, and A. Raksujarit, *Fabrication of Gelatin/Carbon Nanocomposite for Human Tissue Adhesive*, Advanced Materials Research, **2010**, *123-125*: 327-330.

[13] K. Chaloupka, Y. Malam, and A. M. Seifalian, *Nanosilver as a New Generation of Nanoproduct in Biomedical Applications*, Trends in Biotechnology, **2010**, *29*: 580-588.

[14] M. H. Youn, Y. M. Lim, H-J. Gwon, J. S. Park, S. J. An, and Y. C. Nho, *Characterization of an Antibacterial Silver Chloride/Poly(acrylic acid) Deodorant Prepared by a Gamma-Ray Irradiation*, Macromolecular Research, **2009**, *17(10)*: 813-816.

[15] P. A. Zapata , L. Tamayo, M. Páez, E. Cerda, I. Azócar, and F. M. Rabagliati, *Nanocomposites Based on Polyethylene and Nanosilver Particles Produced by Metallocenic ''In Situ'' Polymerization: Synthesis, Characterization, and Antimicrobial Behavior*, European Polymer Journal, **2011**, *47*: 1541-1549.

[16] D. C. Tien, C. Y. Liao, J. C. Huang, K. H. Tseng, J. K. Lung, T. T. Tsung, W. S. Kao, T. H. Tsai, T.W. Cheng, B. S. Yu, H. M. Lin, and L. Stobinski, *Novel Technique for Preparing a Nano-Silver Water Suspension by the Arc-discharge Method*, Reviews on Advanced Materials Science, **2008**, *18*: 750-756.

[17] H. J. Lee, S. Y. Yeo, and S. H. Jeong, *Antibacterial Effect of Nanosized Silver Colloidal Solution on Textile Fabrics,* Journal of Materials Science, **2003**, *38*: 2199-2204.

[18] M. Akbarian, M. E. Olya, M. Ataeefard and M. Mahdavian, *The Influence of nanosilver on Thermal and Antibacterial Properties of a 2 K Waterborne Polyurethane Coating*, Progress in Organic Coatings, **2012**, *75(4)*: 344-348.

[19] X. Chen, and H. J. Schluesener, *Nanosilver: A Nanoproduct in Medical Application,* Toxicology Letters, **2008**, *176(1)*: 1-12.

[20] Y. Huang, X. Li, Z. Liao, G. Zhang, Q. Liu, J. Tang, Y. Peng, X. Liu, and Q. Luo, *A Randomized Comparative Trial Between Acticoat and SD-Ag in the Treatment of Residual Burn Wounds, Including Safety Analysis,* Burns, **2007**, *33*: 161-166.

[21] S. Saxena, A. R. Ray, A. Kapil, G. Pavon-Djavid, D. Letourneur, B. Gupta, and A. M. Pelle, *Development of a New Polypropylene-Based Suture: Plasma Grafting, Surface Treatment, Characterization, and Biocompatibility Studies,* Macromolecular Bioscience, **2011**, *11*: 373-382.

[22] P. T. Sudheesh Kumar, S. Abhilash, K. Manzoor, S. V. Nair, H. Tamura, and R. Jayakumar, *Preparation and Characterization of Novel b-Chitin/Nanosilver Composite Scaffolds for Wound Dressing Applications,* Carbohydrate Polymers, **2010**, *80*: 761-767.

[23] V. Alt, T. Bechert, P. Steinrücke, M. Wagener, P. Seidel, E. Dingeldein ,E. Domann, R. Schnettler, *An in Vitro Assessment of the Antibacterial Properties and Cytotoxicity of Nanoparticulate Silver Bone Cement,* Biomaterials, **2004**, *25(18):* 4383-4391.

[24] R. Dastjerdi, M. Montazer, *A Review on the Application of Inorganic Nano-Structured Materials in the Modification of Textiles: Focus on Anti-Microbial Properties,* Colloids Surf. B: Biointerfaces, **2010**, *79*: 5-18.

[25] R. Kumar, H. Munstedt, *Silver Ion Release from Antimicrobial Polyamide/Silver Composites,* Biomaterials, **2005**, *26*: 2081-2088.

[26] L. Li, Y. Li, J. Li, L. Yao, A. F. T. Mak, F. Ko, and L. Qin, *Antibacterial Properties of Nanosilver PLLA FibrousMembranes.* J. Nanomaterials, **2009**(doi:10.1155/2009/168041): 1-5.

[27] T. G.Tihan, M. D. ionita, R. G. Popescu, and D. Iordachescu, *Effect of Hydrophilic–Hydrophobic Balance on Biocompatibility of Poly(methyl methacrylate) (PMMA)–Hydroxyapatite (HA) Composites,* Materials Chemistry and Physics, **2009**, *118(2–3)*: 265-269.

[28] S. Ekici, D. Saraydin, *Interpenetrating Polymeric Network Hydrogels for Potential Gastrointestinal Drug Release,* Polymer International, **2007**, *56*: 1371-1377.

[29] M. Changez, V. Koul, B. Krishna, A. K. Dinda, and V. Choudhary, *Studies on Biodegradation and Release of Gentamicin Sulphate from Interpenetrating Network Hydrogels Based on Poly(acrylic acid) and Gelatin: In vitro and In vivo,* Biomaterial, **2004**, *25*: 139-146.

[30] S. H. Baek , B. K. Kim, *Synthesis of Polyacrylamide/Polyurethane Hydrogels by Latex IPN and AB Crosslinked Polymers,* Colloids and Surfaces A: Physicochemical and Engineering Aspects, **2003**, *220*: 191-198.

[31] S. W. P. Wijnhoven, W. J. G. M. Peijnenburg, C. A. Herberts, W. I. Hagens, A. G. Oomen, E. H. W. Heugens, B. Roszek, J. Bisschops, I. Gosens, D. V. De Meent, S.

Dekkers, W. H. De Jong, M. V. Zijverden, A. N. J. A. M. Sips, R. E. Geertsma, *Nano-silver, a Review of Available Data and Knowledge Gaps in Human and Environmental Risk Assessment,* Nanotoxicology, **2009**, *3*: 109-138.

[32] S. Khanlari, and M. A. Dubé, *In situ Poly(sodium acrylate)-Based Nanocomposite Formation by Redox-Initiated Solution Polymerization*, Polymer Engineering and Science, **2015**, *55(6)*: 1230-1236.

[33] S. Khanlari, A. Gheibi, and M. A. Dubé, *Image Processing Techniques for Nanocomposite Distribution Quantification,* to be submitted, **2015**.

[34] W. F. Lee, K. T. Tsao, *Effect of Silver Nanoparticles Content on the Various Properties of Nanocomposite Hydrogels by in Situ Polymerization,* Journal of Materials Science, **2010**, *45*: 89-97.

[35] S. B. Subramanian, A. P. Francis, and T. Devasena, *Chitosan–Starch Nanocomposite Particles as a Drug Carrier for the Delivery of Bis-desmethoxy Curcumin Analog*, Carbohydrate Polymers, **2014**, *114(0)*: 170-178.

[36] S. Khanlari, and M. Kokabi, *Thermal Stability, Aging Properties, and Flame Resistance of NR-Based Nanocomposite,* Journal of Applied Polymer Science, **2011**, *119*: 855-862.

Chapter 8: General Discussion and Conclusion

8.1. General Discussion

In the past few years, bioadhesives have found increasing application, with a positive outlook for increasing future use. The first part of this study was dedicated to a comprehensive study about bioadhesives, their uses and potential in wound healing. Figure 8.1 depicts the total market share of bioadhesive use in 2012 and that predicted for 2017.

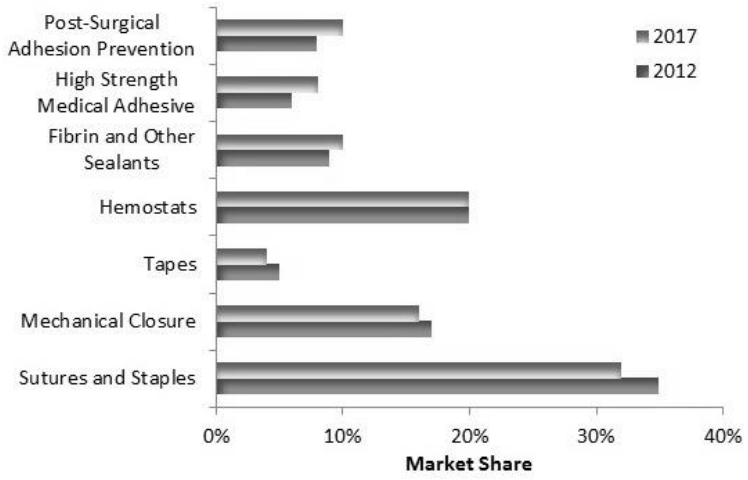

Figure 8.1 Global market share of bioadhesive and other wound closure methods (2012 vs. 2017).

Poly(acrylic acid) was found to be an appropriate polymer for bio-based applications given its favourable adhesive properties. There are no reports of antibacterial bioadhesives for sutureless surgery, to our knowledge; producing such materials was the main objective of this research.

The second part of this study was devoted to finding suitable reaction conditions for synthesizing poly(acrylic acid) with appropriate properties for application as a bioadhesive. Nonetheless we eventually decided to synthesize poly(sodium acrylate), which is similar to poly(acrylic acid), due to the positive effects of neutralization with sodium hydroxide. Figure 8.2 shows the chemical structure of poly(acrylic acid) (Fig. 8.2a) and poly(sodium acrylate) (Figure 8.2b) as well as the synthetic pathway (Figure 8.2c).

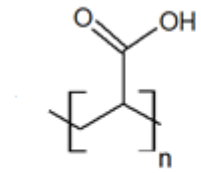

Poly(acrylic acid)

a)

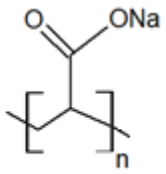

Poly(sodium acrylate)

b)

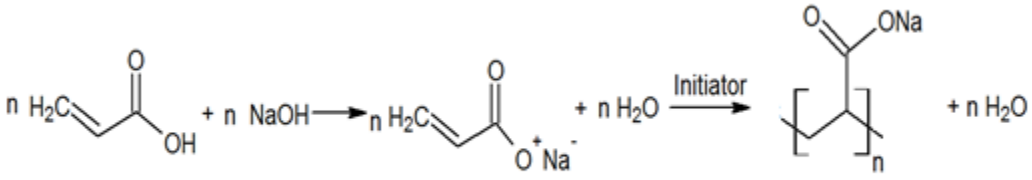

Acrylic acid | Sodium acrylate | Poly(sodium acrylate)

c)

Figure 8.2 Chemical structure of a) poly(acrylic acid) and b) poly(sodium acrylate); and c) synthetic pathway for poly(sodium acrylate).

It was shown that neutral pH is an appropriate reaction condition for polymerization of sodium acrylate in which the highest average molecular weight and the lowest residual monomers are achieved. Polymerizations occurring at lower degrees of

neutralization yielded poly(acrylic acid-*co*-sodium acrylate) copolymer. Performing the polymerization under normal atmosphere and at room temperature makes the method extremely straightforward and cost effective. Significant temperature rises of >60 ^{o}C were indicative of the high rate of polymerization. It is likely that these high reaction rates allowed the initiation system to overwhelm any radical consumption by atmospheric oxygen.

Figure 8.3 shows the ATR-FTIR scan of the polymer synthesized at pH = 7, where absorbance peaks at 1555 cm^{-1} and 1660 cm^{-1} are seen. The peak appearing at 1555 cm^{-1} is assigned to COO^- while the peak present at 1660 cm^{-1} is assigned to -ONa in poly(sodium acrylate). The peaks appeared at 1400 cm^{-1} are due to $–CH_2$ bending and the one at 1360 cm^{-1} is due to –CH bending of the poly(sodium acrylate). Therefore, a simple method for poly(sodium acrylate) synthesis was developed and ready for use in nanocomposite formation.

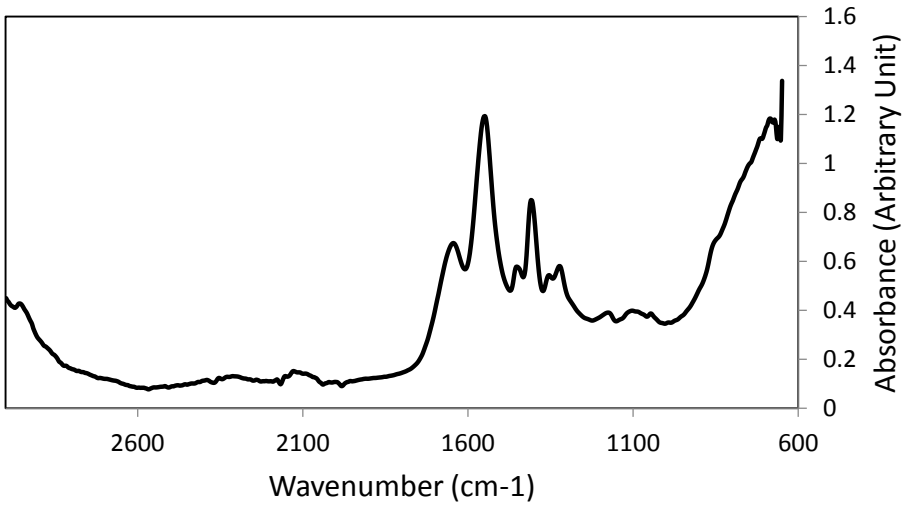

Figure 8.3 ATR-FTIR spectra of the polymer synthesized at pH = 7.

In the third part of this project, the incorporation of nanosilver in the poly(sodium acrylate) matrix was performed. The effect of nanosilver incorporation on the rate of polymerization, as well as the molecular weight, hydrophilicity, and thermal behaviour of the nanocomposites was studied. High conversion poly(sodium acrylate) was synthesized in the presence of nanosilver and the molecular weight greater than 100,000 g/mol was found to be suitable for bioadhesive applications.

Figure 8.4 depicts the morphology of the poly(sodium acrylate)-based nanocomposites synthesized using different nanosilver loadings.

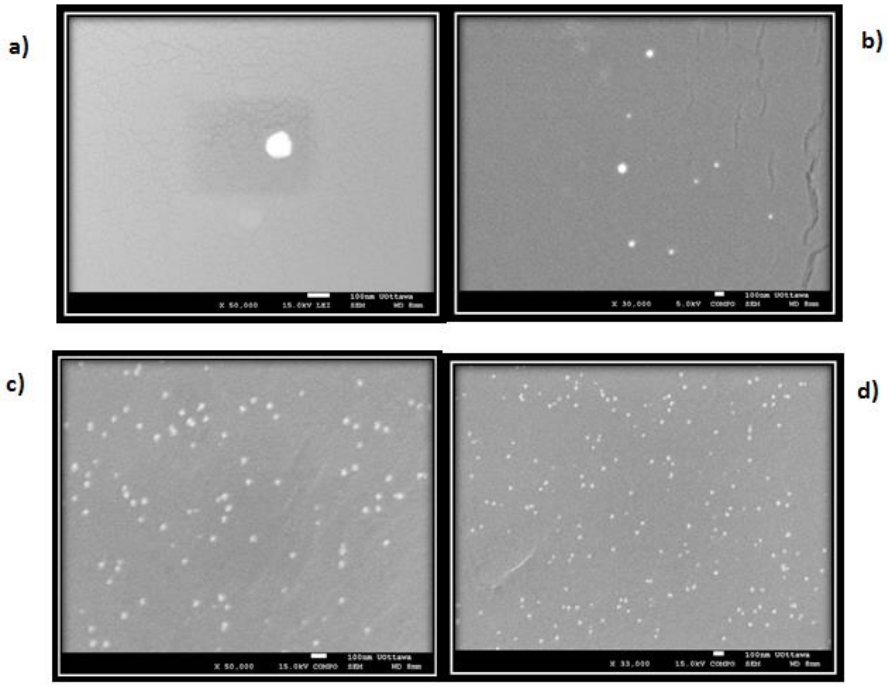

Figure 8.4 SEM images of poly(sodium acrylate) based nanocomposites containing 0.5, 1, 2 and 3 wt.% of nanosilver (scale bar is 100 nm).

The homogeneity of nanosilver distribution throughout the polymer matrix was examined using three different quantitative image processing methods: the Voronoi

diagram, the Euclidian minimum spanning tree (EMST) method and the pixel counting method. The distribution of nanoparticles was shown to be fairly homogeneous in the nanocomposite samples. Figure 8.5 shows two different quantitative methods applied for nanocomposite containing 2 wt.% of nanosilver. It should be noted that the value calculated from the pixel counting method for this sample was 2.09, which concurs with the amount originally added (i.e., 2 wt.%). In summary, it was observed that fairly homogeneous nanosilver loadings were achieved for all samples, which is crucial in biomedical applications such as for drug delivery when one requires an even dosage of a drug.

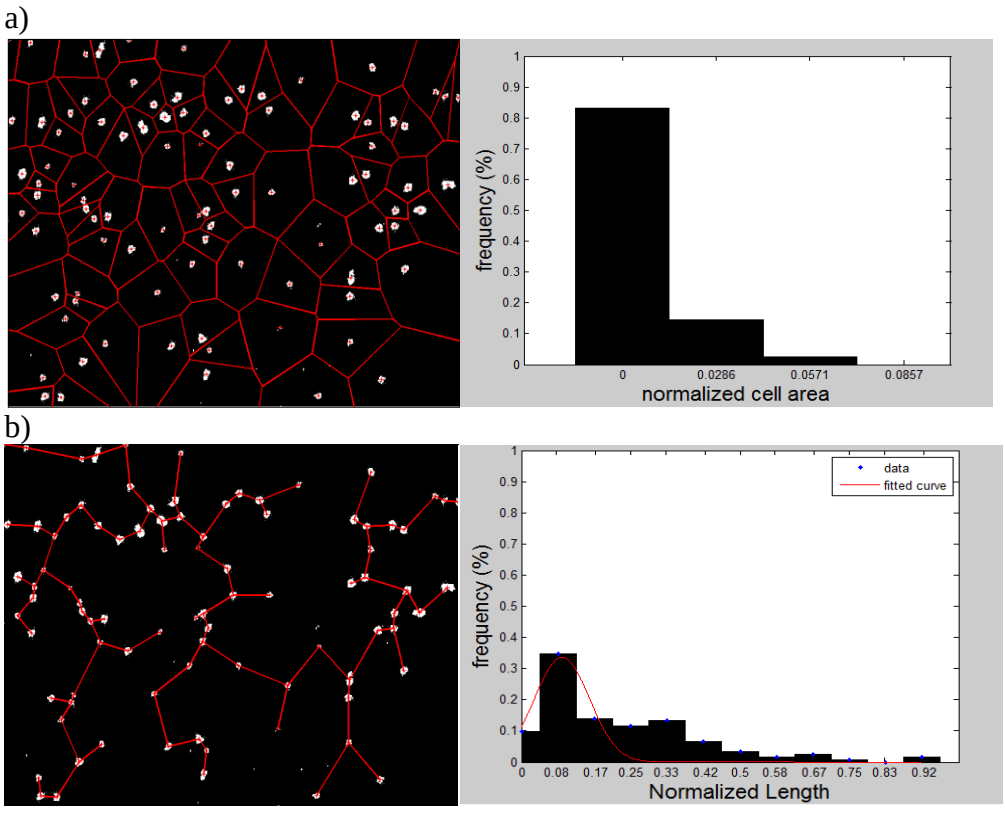

Figure 8.5 a) Voronoi diagram method and b) Euclidian minimum spanning tree applied on the nanocomposite containing 2 wt.% of nanosilver.

Throughout this project, an on-line sensor-based monitoring method using ATR-FTIR spectroscopy was used to monitor conversion of sodium acrylate to polymer. Calibration and confirmation of the efficacy of the technique was shown. Figure 8.6 shows the applicability of the multivariate model developed based on in-line data for the prediction of monomer conversion.

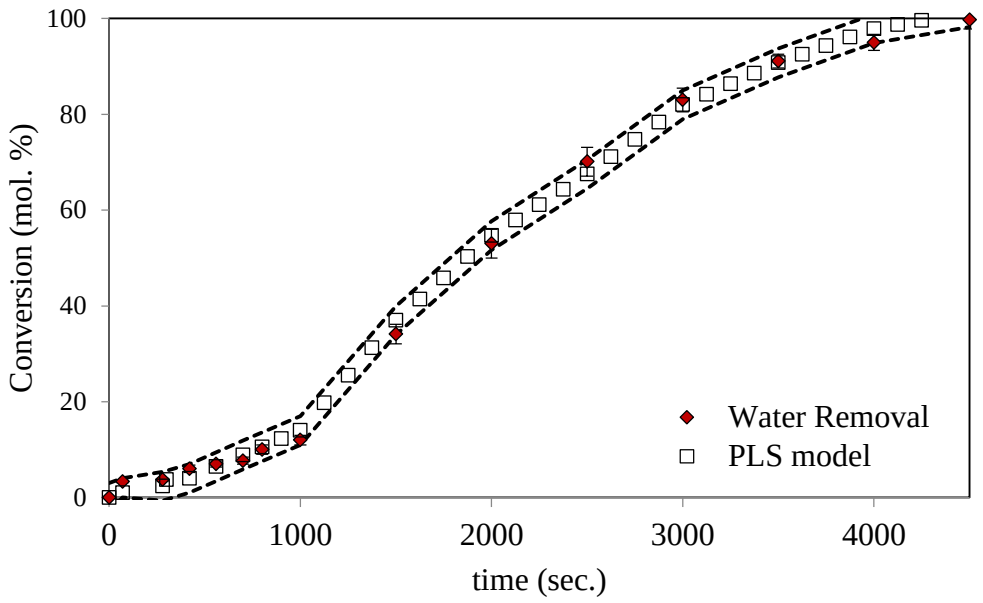

Figure 8.6 Predicted versus off-line conversion for sodium acrylate polymerization in the presence of 2 wt.% of nanosilver.

In the culmination of this study, the effect of interpenetrating polymer network (IPN) formation using two highly degradable polymers (PVA and Ge) on hydrophilicity and degradation rate of the IPN in phosphate buffer saline (PBS) solution was studied. Figure 8.7 depicts the effect of IPN formation on degradation rate and hydrophilicity of the systems.

a)

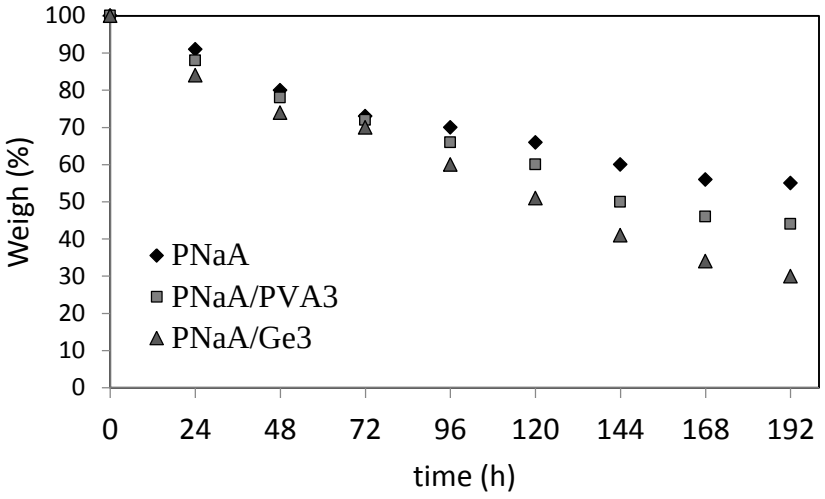

b)

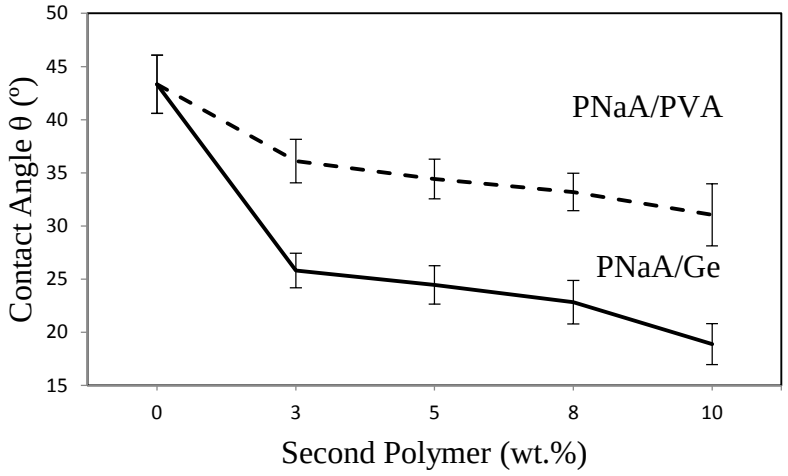

Figure 8.7 a) Degradation behavior of IPN formed using 3 wt.% of PVA and Ge b) The effect of IPN formation using a second, more degradable polymer on hydrophilicity of PNaA based bioadhesive.

The adhesive strength of the nanocomposite bioadhesives was studied as a function of nanofiller loading. Figure 8.8 shows the stress-strain diagram for adhesive strength tests.

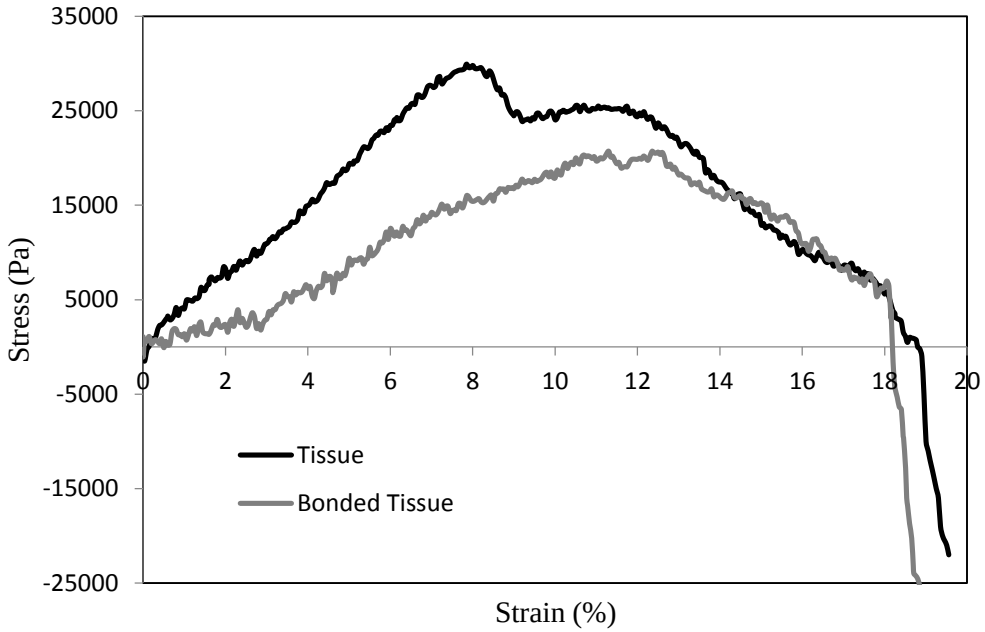

Figure 8.8 Stress-Strain relationships of tissue compare to that of bonded using PNaANS2 bioadhesive.

Finally, the antibacterial property and the biocompatibility of the synthesized nanocomposites were assessed as a function of nanosilver content. Results showed that the cell viability of the bioadhesives containing nanosilver decreased slightly with increasing nanosilver loading, but remained in an acceptable range. On the other hand, the antibacterial activity of the nanocomposites increased dramatically with nanosilver loading. IPN formation was shown to be an appropriate method for tuning the degradation rate of the bioadhesives. Altogether, the nanocomposite bioadhesive containing 2 wt.% nanosilver appears to be the best candidate for sutureless surgery.

Natural disasters inevitably leave a great many injured people, especially in instances of high population density. The chance of infection (e.g., tetanus) is very high after any natural disaster (e.g., earthquake, tsunami and volcanic eruption) where there is no choice but on site (i.e., out of clinic) treatment in the absence of a sterile environment. The range of injuries may also demand certain flexibility in terms of wound healing time. PNaA-nanosilver nanocomposite antibacterial bioadhesives can decrease infection and improve wound healing in the face of daunting circumstances. The ability to tune their degradation also makes them a flexible option.

8.2 Future Recommendations

Antibacterial nanocomposite bioadhesives provide an ideal alternative for traditional suturing in support of sutureless surgery. To our knowledge, there is no report of in situ polymerization of sodium acrylate in the presence of any antibacterial agent to molecular weights appropriate for applications in adhesives. Regarding its good biocompatibility and other probable application in pharmaceutical and biomedical industries (e.g. drug delivery and wound dressings) there are number of recommendations to extend the applicability of poly(sodium acrylate)-based biomaterials. What follows are various recommendations for future research according to each part of this study.

8.2.1 Recommendations for Parts 1 and 2

The rheology of synthesized polymers during polymerization should be studied further. The viscosity of the PNaA towards the end of synthesis was quite high. This posed some issues in terms of application of the bioadhesive to tissue. Polymer molecular weight

plays an important role in this instance. In addition, as was noted in Chapter 4, the nanosilver plays a role in molecular weight development. Thus, studying the effect of synthesis conditions and nanosilver content on molecular weight and ultimately on polymer rheology will be important.

8.2.2 Recommendations for Part 3

a) A comparative study between the Voronoi method and the Euclidian minimum spanning tree (EMST) method is necessary to determine which method is more precise. Although both methods were shown to be applicable and precise, further study could be used to discern which method is the best. Broadening the range of nanomaterial distributions would be useful in this regard.

b) Nowadays, 3-D images are finding important application in nanocomposite material studies. Thus, the use of a 3-D EMST method on 3-D images taken from nanofiller distributions in polymeric matrices may improve the method.

c) Extensions of the above methods to non-spherical nanofillers (e.g., clays, cellulose nanocrystals) may also be of interest.

d) Extensions of the method to larger fillers in composite materials are also obvious. Examples include rubber compounding and plastic processing applications.

8.2.3 Recommendations for Part 4

Extending the multivariate calibration model for the ATR-FTIR monitoring to other reaction conditions can be used to further reinforce the usefulness of this technique.

8.2.4 Recommendations for Part 5

a) Although *E-coli* is one of the most common infectious microorganisms, it is not the only one. A study of the antibacterial activity of the nanocomposite bioadhesives against other microorganisms (e.g., *Staphylococcus aureus* and *Clostridium tetani*), fungi and viruses, may also broaden the scope of these materials.

b) Because the healing period of most tissues is often greater than 200 h, it is recommended to study the degradation of the bioadhesives over longer time periods.

c) An obvious next step in terms of biocompatibility and biodegradability would involve a comprehensive in vivo evaluation of the bioadhesives.

d) A number of parameters potentially affecting degradation rate were not studied here. These include initiator and crosslinker concentration, UV curing time, and cross-link density. Manipulating the aforementioned parameters may lead further tissue specific bioadhesives to cover a broader range of tissue types.

e) Continuing on the topic of degradation, further study on the products of degradation is likely necessary. An important question is what is the molecular weight of the final degradation products and how might they affect the host tissue.

f) In this study, the adhesive strength of the bioadhesive alone was tested. Given that an IPN may be used, extending the adhesive testing to IPNs is clearly necessary.

g) Extending testing to different tissues would also expand the applicability of the bioadhesive.

h) It is recommended to synthesize of PNaA-based *haemostatic* bioadhesives for sutureless surgery. Bleeding is another important cause of mortality after natural disasters. Therefore, it is recommended to synthesize haemostatic bioadhesives.

Appendices

Appendix A: Publications

A1) Journal Contributions

This research project contributed several peer-reviewed publications and conference papers listed below:

1. **Bioadhesive, A review**, S. Khanlari and M. A. Dubé, *Macromolecular Reaction Engineering*, 2013, *7(11)*: 573–587.

2. ***In situ* Poly(sodium acrylate)-Based Nanocomposite Formation by Redox-Initiated Solution Polymerization**, S. Khanlari and M. A. Dubé, *Polymer Engineering and Science*, 2015, *55(6)*: 1230–1236.

3. **Effect of pH on Poly(acrylic acid) Solution Polymerization**, S. Khanlari and M. A. Dubé, *Macromolecular Science, Part A: Pure and Applied Chemistry*, 2015, *52*, 587–592.

4. **Reaction Monitoring of in-situ Formation of Poly(sodium acrylate) Based Nanocomposites Using ATR-FTIR Spectroscopy**, S. Khanlari and M. A. Dubé, *Industrial and Engineering Chemistry Research*, 2015, *54*, 5598−5603.

5. **Poly(sodium acrylate)-based Nanocomposite Bioadhesives for Sutureless Surgery**, S. Khanlari and M. A. Dubé, submitted (2015).

6. **Image Processing Techniques for Nanofiller Distribution Quantification**, S. Khanlari, A. Gheibi and M. A. Dubé, to be submitted (2015).

7. **Bioactivity of Nanocomposites Synthesized as Bioadhesives**, S. Khanlari, M. A. Dubé, J. Tang, K. Kirkwood, to be submitted (2015).

A2) Conference Contributions

Six conference papers were submitted to national and international conferences as below:

1- Polyacrylic Acid/Nanosilver Nanocomposite: The Effect of Nanoparticles on the Rate of Polymerization, S. Khanlari, Marc A. Dubé, 63rd Canadian Chemical Engineering Conference, October 20-23 2013, Fredericton NB, Canada.

2- The Effect of IPN Formation on Hydrophilicity of Polyacrylic Bioadhesive, S. Khanlari, M. A. Dubé, First Annual Conference of the International Society for Biomedical Polymers and Polymeric Biomaterials (ISBPPB 2014) 9-12 July 2014, Washington DC, USA.

3- SEM Image Processing Techniques to Examine the Morphology of Polyacrylic Acid Based Nanocomposites, S. Khanlari, A. Gheibi, M. A. Dubé, First Annual Conference of the International Society for Biomedical Polymers and Polymeric Biomaterials (ISBPPB 2014), 9-12 July 2014, Washington DC, USA.

4- Image Processing Technique to Quantify Nanofiller Loading Accuracy in Nanocomposites, S. Khanlari, A. Gheibi, M. A. Dubé, The 4th International Conference on Composites Characterization, Fabrication and Application (CCFA-4) December 16-17, 2014, Tehran, Iran.

5- In-Line Conversion Monitoring of Poly(sodium acrylate)/Nanosilver Nanocomposites, S. Khanlari, M. A. Dubé, Polymer Reaction Engineering IX (PRE 9) May 10-15, 2015, Cancun, Mexico.

6- The Effect of pH on the Polymerization and Properties of Poly(acrylic acid) Synthesized via Redox Polymerization, S. Khanlari, M. A. Dubé, Polymer Reaction Engineering IX (PRE 9) May 10-15, 2015, Cancun, Mexico.

Appendix B: Kinetics of Acrylic Acid and Sodium Acrylate polymerization

B1) Linear

The kinetics of polymerization of acrylic acid at different pHs was studied. In principle, the rate of propagation in radical polymerization can be controlled by changing the initiator concentration. Mathematically, this is illustrated by the first-order rate equation for radical propagation as below:

$$R_p = -\frac{d[M]}{dt} = k_p \left(\frac{k_d f[I]}{k_t}\right)^{1/2} [M] \qquad \text{(B1.1)}$$

where, f is the efficiency of an initiator I, k_d is the rate constant of initiator decomposition, k_p is the rate constant for propagation for a monomer M, and k_t is the rate constant for termination[1]. In this experiment, we have examined the validity of this rate equation for the redox solution polymerization of acrylic acids polymerized at different extents of neutralization. In particular, we have used Equation 1 to verify that propagation is first-order in acrylic acid concentration, and to calculate the propagation rate constant k_p for the polymerization.

In case of redox initiation systems equation B1.1 is rewritten as bellow:

$$R_p = -\frac{d[M]}{dt} = k_p \left(\frac{k_d f[red][ox]}{2k_t}\right)^{1/2} [M] \quad \text{(B1.2)}$$

$$ln\frac{[M]_0}{[M]} = k_p \left(\frac{k_d f[red][ox]}{2k_t}\right)^{1/2} t \quad \text{(B1.3)}$$

By substitution of equation 4.3 in B1.3 the equation B1.3 will be shortened in form of B1.4:

$$\ln\frac{1}{1-x} = k_p[P^0]t = k_p^{app}t \quad \text{(B1.4)}$$

where $[P^0]$ is the stationary concentration of radicals and k_p^{app} is the apparent propagation rate constant of the reaction. One can simplify equation 12 and drop the term of time as below[2]:

$$R_p = -\frac{d[M]}{dt} = k_p[P^0][M] = k_p^{app}[M] \quad (B1.5)$$

Figure B1.1 depicts the kinetic of different polymerizations introduced in table 3.1.

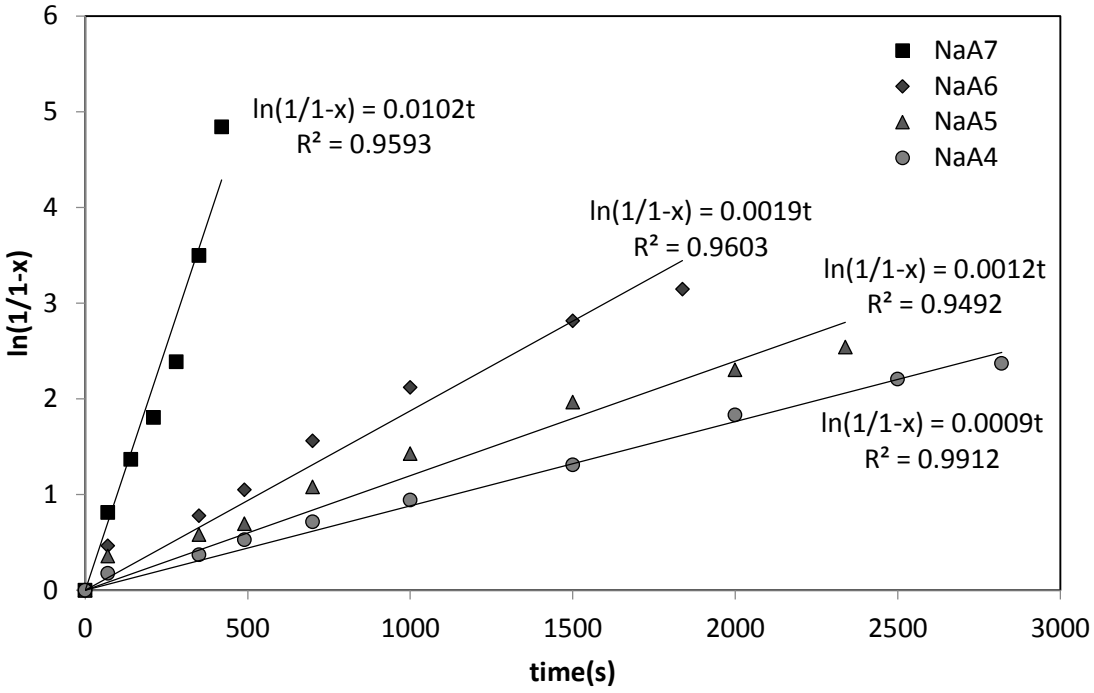

Figure B1.1 Semi-logarithmic kinetic plot of polymerization of acrylic acid via redox solution polymerization at different extents of neutralization.

Figure B1.1 depicts the dependency of ln(1/1-x) to time. It shows that the increase in the extent of neutralization had a significant effect on reaction rate (N.B. rate is proportional to the slope of the conversion vs. time curve).

The linear fit indicated constant concentration of propagating radical species and radical termination reactions are not significant on the time scale of this reaction. This is reported further with linear increase of molecular weights with conversion, indicating that the number of chains is constant during the reaction. The correlation coefficient (R^2) for these linear regressions are 0.9593, 0.9603, 0.9492 and 0.9912 for NaA7, NaA6, NaA5 and NaA4 respectively. The linear fit indicates constant concentration of propagating radical species during the polymerization.

B2) Polynomial

Another approach for kinetic data measurement is the polynomial approach. The rate equation can be considered as seen in Equation (B1.5) [3]:

$$\frac{d[M]}{dt} = -k[M]^n \qquad \text{(B1.5)}$$

where *[M]* is the monomer concentration, *t* is the reaction time, *k* is the rate constant and *n* is the reaction order. Figure B2.1 depicts $\frac{d[M]}{dt}$ dependence to time and Table B2.1 summarizes the kinetic data of different runs.

a)

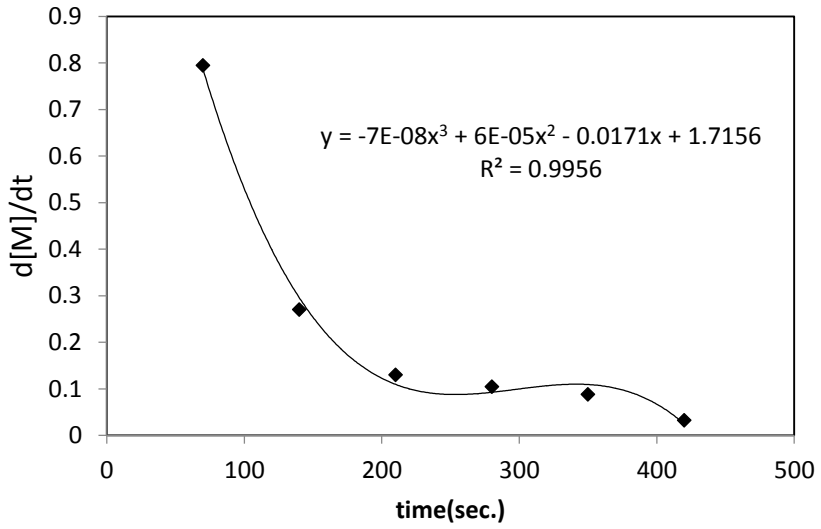

b)

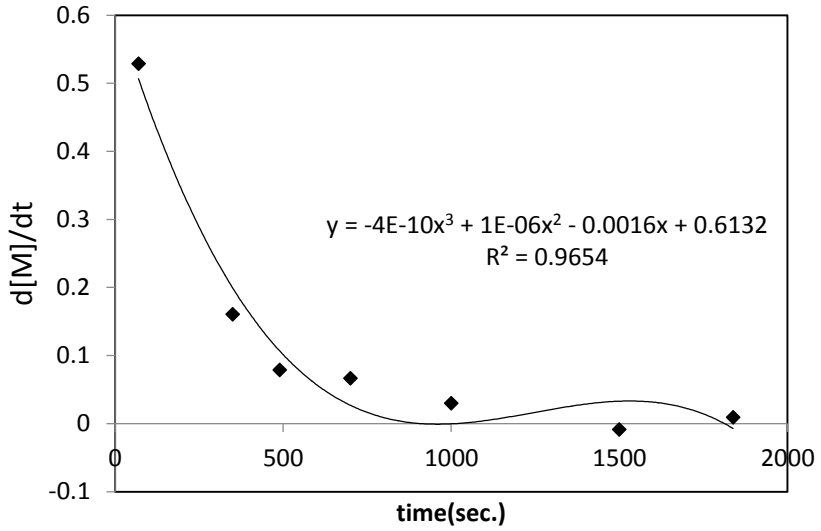
0.6
0.5
0.4
0.3
0.2
0.1
0
-0.1
d[M]/dt
y = -4E-10x³ + 1E-06x² - 0.0016x + 0.6132
R² = 0.9654
0
500
1000
1500
2000
time(sec.)

c)

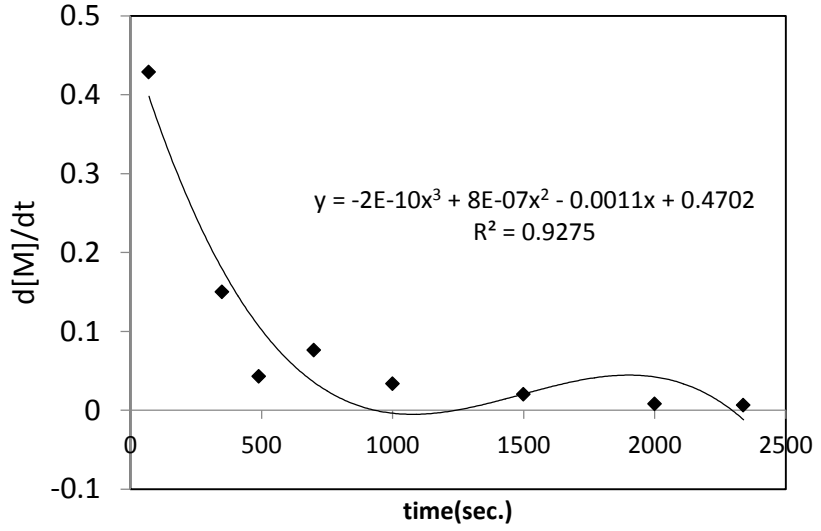
0.5
0.4
0.3
0.2
0.1
0
-0.1
d[M]/dt
y = -2E-10x³ + 8E-07x² - 0.0011x + 0.4702
R² = 0.9275
0
500
1000
1500
2000
2500
time(sec.)

d)

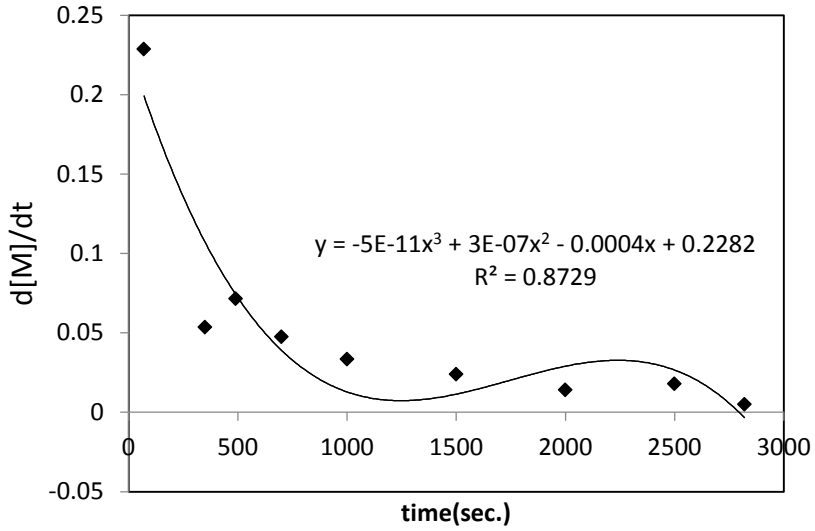

Figure B2.1 *d[M]/dt* vs. time for polymers synthesized at a) pH=7, b) pH=6, c) pH=5 and d) pH=4.

Table B2.1 Kinetic data for different polymerizations.

Sample	Reaction Order	Rate Constant (k)	Regression Coefficient (R^2)
NaA7	3	7×10^{-8}	0.9956
NAA6	3	4×10^{-10}	0.9654
NAA5	3	2×10^{-10}	0.9275
NaA4	3	5×10^{-11}	0.8729

References:

[1] G. Odian, *Principles of Polymerization*, 3rd ed.; Wiley: New York, 1991, 206.

[2] J. Guo, Z. Han, and P. Wu, *A New Complex Catalytic System CuX/bpy/Al(OR)$_3$ for Atom Transfer Radical Polymerization.* Journal of Molecular Catalysis A: Chemical, 2000, *159(1)*: 77-83.

[3] H. Madra, S. B. Tantekin-Ersolmaz, and F. S. Guner, *Monitoring of Oil-based Polyurethane Synthesis by FTIR-ATR.* Polymer Testing, 2009, *28(7)*: 773-779.

Appendix C: Matlab™ Codes

C1) Matlab™ Code for VORONOI method

```
%%%%%%%%%%%%%%%%%%%%%%%%%%%%%%%%%%%%%%%%%%%%%%%%%%%%%%%%%%%%%%%%%%%%%%%
% Voronoi Section
% The purpose is to first find the center of the pixles that are
%clustered
% together. Then we find the center of mass of these clusters. then
% we calculate the Voronoi of the centers.
%%%%%%%%%%%%%%%%%%%%%%%%%%%%%%%%%%%%%%%%%%%%%%%%%%%%%%%%%%%%%%%%%%%%%%%
close all;
clear;
%Load a figure
%mainFigure=imread('results\3darsad\2.92.jpg');
mainFigure=imread('results\2darsad\2.0947.jpg');
%mainFigure=imread('grid points.jpg');
%mainFigure=imread('random points.jpg');
%mainFigure=imread('non-even points2.jpg');
%mainFigure=imcomplement(mainFigure);
%for picNo=2:6
%picNo=5;
%picName=strcat('Slide',int2str(picNo),'.jpg');
%mainFigure=imread(picName);
mainFigure=im2bw(mainFigure,0.1);
figSize=size(mainFigure);
%numberOfPixels=figSize(1)*figSize(2);
imshow(mainFigure);
%Detect Connected Components
CC=bwconncomp(mainFigure);
%Measure the stats
stats=regionprops(CC,'centroid','area');
centroids=[0,0];
%counter=1;
for cellNo=1:CC.NumObjects
```

```
    if(stats(cellNo,1).Area>10)
        centroids=cat(1, centroids,stats(cellNo,1).Centroid);
        CC_areas(cellNo,1)=stats(cellNo,1).Area;
    end
   % centroids=cat(1,stats.Centroid);
end
ccno=1;
for i=1:size(CC_areas)
    if(CC_areas(i,1)>0)
        CC_area(ccno)=CC_areas(i,1);
        ccno=ccno+1;
    end
end
centroids=centroids(2:end,:); %we need to remove the [0,0] initial
value
hold on
plot(centroids(:,1),centroids(:,2),'r+');

%%Run voronoi of the centroids, this function just plot voronoi
voronoi(centroids(:,1),centroids(:,2),'-r');
%%If you want to have the information about Voronoi cells use voronoin
hold off
%  V contains the Voronoi vertices,
%  C contains indices of Voronoi vertices that form the (finite sides
of the)
%  Voronoi cells.
%
[n,dim]=size(centroids);
[V,C]=voronoin(centroids);
%
% Two nodes are neighbors if they share an edge, that is, two Voronoi
%  vertices.
%
%  vn = zeros ( n, n );
%  distances=zeros(n,n);
%  for i = 1 : n
%    for j = i + 1 : n
%      s = size ( intersect ( C{i}, C{j} ) );
%      if ( 1 < s(2) )
%        vn(i,j) = 1;
%        vn(j,i) = 1;
%        %measure the distances
%        distances(i,j)=sqrt(power(centroids(i,1)-
centroids(j,1),2)+power(centroids(i,2)-centroids(j,2),2));
%     end
%    end
%  end
%%%%%%%%%%%%%%%%%%%% For distances
 % k=1;
```

```
 % for i = 1 : n
  %  for j = i + 1 : n
  %      if(distances(i,j)>0)
  %         data(k)= distances(i,j);
  %         k=k+1;
  %      end
   % end
  %end

  %Histogram function
  %for bin=5:3:100
  %    figure;
  %    hist(data,bin);
  %end

  %m=mean(data);
  %st=std(data);
%%%%%%%%%%%%%%%%%%% For areas
max_x=-Inf;
max_y=-Inf;
min_x=Inf;
min_y=Inf;

for i=1:size(V,1)
    if(V(i,1)~=Inf)
        if(V(i,1)>max_x)
            max_x=V(i,1);
        elseif(V(i,1)<min_x)
            min_x=V(i,1);
        end
    end
    if(V(i,2)~=Inf)
        if(V(i,2)>max_y)
            max_y=V(i,2);
        elseif(V(i,2)<min_y)
            min_y=V(i,2);
        end
    end
end
%   convexhull=convhull(centroids(:,1),centroids(:,2));
%  numberOfPixels=
polyarea(centroids(convexhull,1),centroids(convexhull,2));

 hold on
 %plot(centroids(convexhull,1),centroids(convexhull,2),'-w');
 hold off
%numberOfPixels=(max_x-min_x)*(max_y-min_y);
  for i = 1 : size(C ,1)
      ind = C{i}';
```

```
      if ind~=1
          tess_area(i,1) = polyarea( V(ind,1) , V(ind,2) );
          %tess_area(i,1)=tess_area(i,1)/numberOfPixels;
      end
  end
numberOfPixels=max(tess_area(:,1));
tess_area(:,1)=tess_area(:,1)/numberOfPixels;


  %sort areas
  tess_area(:,1)= sort(tess_area(:,1));
  %remove top 5 percent
  cutPercentage=ceil(5*size(tess_area(:,1),1)/100);
  tess_area_after_noise=tess_area(1:end-cutPercentage,1)

  %if you want to determine the number of bins uncomment the following
code
  %for bin=5:3:100
  %    figure;
  %    [elements,centers]=hist(tess_area_after_noise,bin);
  %    bar(centers,elements/sum(elements));
  %end
  for range=20:3:40
      figure;

      xvlaues=0.0001:(1/range):0.999;
      [elements,centers]=hist(tess_area_after_noise,xvlaues);
      bar(centers,elements/sum(elements),'r');
      [maxElement,i]=max(elements);
      title(num2str(centers(i)));
      axis([0,0.2,0,1]);
      xlabel('normalized cell area', 'FontSize',16 );
      ylabel('frequency (%)','FontSize',16);
  end
%end
```

C2) Matlab™ code for EMST method

```
function [G,dist] = graph_EMST(data,options)
% GRAPH_EMST finds the Euclidean Minimum Spanning Tree graph among
points
% in P dimensions.
% Usage: [G,dist,connect] = graph_EMST(data,options)
% ---------------------------------------------------------------------
----
% INPUTS:
% data          : [n x p] matrix of point coordinates.
% options.show  : if 0, plot of the graph is not shown [default=0]
```

```
% ------------------------------------------------------------------------
----
% OUTPUTS:
% G             : [n x n] sparse matrix that represents a graph.
Nonzero
%                 entries in matrix G represent the weights of the
edges.
% dist          : corresponding edge lengths (Euclidean distances);
%                 non-connected edge distances are given as zero.
% connect       : [n x n] boolean adjacency matrix.
%------------------------------------------------------------------------
----
% Copyright (C) 2014, Sama
%------------------------------------------------------------------------
----
% Add the toolboxes
%addpath('C:\Users\Khanlari\Dropbox\Matlab
codes\Sama\toolboxes\GrTheory');

if nargin < 2
    options.show=[];
end

if isempty(options)
    options.show=0;
end
% [N,D]=size(data);

% compute Delaunay triangulation

% 2-D and 3-D case
% if D < 4
%   DT=DelaunayTri(data);
% else
%   DT=delaunayn(data);
% end

%E = edges(DT);
%nEdges=size(E,1);
dist = dist_euclidean(data,data);

%create sparse matrix-graph representation
%C=sparse(E(:,1),E(:,2),ones(nEdges,1),N,N,nEdges);
%connect=C;
%G= C+C';
% weight graph by distances
%G=G.*dist;
```

```
% graph is undirected, so we can forget half of edges
%G=tril(G);

% compute minimal spanning tree on graph

%This part is edited by Amin to use the new MST function
%nMST=grMinSpanTree(E)
[G] = mst_prim(dist,0);

hold on;
gplot(G,data,'-r');
plot(data(:,1),data(:,2),'.r');
%axis('equal');
```

C3) Matlab™ code for Pixel counting method

```
%The purpose of this code is to find the loading percentage of
%nanosilver in the
%nanocomposites from SEM images
%for any question contact s.khanlari@gmail.com
%load the picture
mainFigure=imread('after noise removal\1-8.tif');
imshow(mainFigure);

%delete the footer of the image
figure;
cutFigure=mainFigure;
%If the figure has footer uncomment the following line
%cutFigure=mainFigure(1:end-65,1:end,1);
imshow(cutFigure);

for i=0.75:0.01:0.8
    bwFigure=im2bw(cutFigure,i); %make a binary file
     fig1=figure;

    %Wiener Filter for 2D image

    bwFigureFilter=wiener2(bwFigure,[5 5]);
    imshow(bwFigureFilter);

    %Median Filter; a kind of spatial filter
    fig2=figure;
    bwFigureFilter2=medFilt2(bwFigure);
    imshow(bwFigureFilter2);

    %Median Filter on the Wiener filter result
```

```
fig3=figure;
bwFigureFilter3=medFilt2(bwFigureFilter);
imshow(bwFigureFilter3);

%Morphological openning and closing
fig4=figure;
%openFigure=bwmorph(bwFigureFilter2,'open');
closedFigure=bwmorph(bwFigureFilter2,'fill');
closedFigure=bwmorph(closedFigure,'dilate');
closedFigure=bwmorph(closedFigure,'thicken',2);

imshow(closedFigure);

%calculating the percentage of loading
whitePixels=0;
blackPixels=0;
for r=1:size(bwFigureFilter,1)
    for c=1:size(bwFigureFilter,2)
        if (bwFigureFilter(r,c)==true)
            whitePixels=whitePixels+1;
        else
            blackPixels=blackPixels+1;
        end
    end
end
percentage1=whitePixels/(whitePixels+blackPixels)*100
set(fig1,'Name',num2str(percentage1))

whitePixels=0;
blackPixels=0;
for r=1:size(bwFigureFilter2,1)
    for c=1:size(bwFigureFilter2,2)
        if (bwFigureFilter2(r,c)==true)
            whitePixels=whitePixels+1;
        else
            blackPixels=blackPixels+1;
        end
    end
end
percentage2=whitePixels/(whitePixels+blackPixels)*100
set(fig2,'Name',num2str(percentage2))

whitePixels=0;
blackPixels=0;
for r=1:size(bwFigureFilter3,1)
    for c=1:size(bwFigureFilter3,2)
        if (bwFigureFilter3(r,c)==true)
            whitePixels=whitePixels+1;
```

```
            else
                blackPixels=blackPixels+1;
            end
        end
    end
    percentage3=whitePixels/(whitePixels+blackPixels)*100
    set(fig3,'Name',num2str(percentage3))

    whitePixels=0;
    blackPixels=0;
    for r=1:size(closedFigure,1)
        for c=1:size(closedFigure,2)
            if (closedFigure(r,c)==true)
                whitePixels=whitePixels+1;
            else
                blackPixels=blackPixels+1;
            end
        end
    end
    percentage4=whitePixels/(whitePixels+blackPixels)*100
    set(fig4,'Name',num2str(percentage4))
end
%show the image
```